Computer Aided Medical Procedures
Prof. Dr. Nassir Navab

Dissertation

Challenges in Deployment of Advanced Radioguided Surgery Solutions

Aslı Okur Kuru

Fakultät für Informatik
Technische Universität München

TECHNISCHE UNIVERSITÄT MÜNCHEN

Fakultät für Informatik
I16 / Computer-Aided Medical Procedures

Challenges in Deployment of Advanced Radioguided Surgery Solutions

Aslı Okur Kuru

Vollständiger Abdruck der von der Fakultät für Informatik der Technischen Universität München zur Erlangung des akademischen Grades eines

Doktors der Naturwissenschaften (Dr. rer. nat.)

genehmigten Dissertation.

Vorsitzender: Prof. Dr. Hans Michael Gerndt

Prüfer der Dissertation:

1. Prof. Dr. Nassir Navab
2. Assoc. Prof. Fijs van Leeuwen

Die Dissertation wurde am 14.05.2019 bei der Technischen Universität München eingereicht und durch die Fakultät für Informatik am 21.10.2019 angenommen.

Abstract

Radioguided surgery made it possible for the first time to functionally differentiate radioactively labeled target structures from the surroundings intraoperatively, which in most cases could not be previously achieved based only on the anatomical differences. The technique is based on the utilization of handheld radiation detectors to identify radiotracers injected into the patient, thus providing real-time guidance and feedback to the surgeon and opening a new era for minimally invasive surgery for the treatment or staging of numerous malignancies.

This thesis addresses several challenges associated with the deployment of new technologies in different clinical scenarios within the well-established radioguided surgery discipline, where the available systems are not necessarily optimized for the target clinical use case. It includes the analysis of the clinical workflow, definition of the supporting functions of the technology and its modification towards integrated applications on the concrete example of Freehand SPECT.

Freehand SPECT is a novel 3D nuclear functional imaging and navigation system suited for intraoperative usage, which was initially tailored to fulfill the surgical and technological requirements of the radioguided sentinel lymph node biopsy technique. Therefore, it needs alterations to be applicable for a new clinical use case having different requirements in terms of radiation detection, accuracy, performance, acquisition, visualization or real-time feedback. Furthermore, its overall success and its intraoperative acceptance is highly dependent on the particular human operator due to the freehand nature.

Retrospective analysis of automatic logging provided by Freehand SPECT system provides a basis for pinpointing the challenges associated with its utilization inside the operating room and allows us to learn from experience within the initial clinical use case. This enables not only the identification of potential usage problems, but also the detection of surgical phase transitions as well as usage characteristics for different users or user groups.

Building on top of this, we explore two new possible clinical use cases for Freehand SPECT. First, we propose the adaptation of Freehand SPECT imaging for recurring head and neck squamous cell carcinoma patients by the integration of a high energy gamma probe instead of the conventional (low energy) gamma probe due to the utilization of a

positron emitting radiotracer. Secondly, we propose the first fully 3D Freehand SPECT - ultrasound fusion with the clinical motivation of non-surgical core needle biopsies of axillary sentinel lymph nodes for breast cancer.

Results of our experiments and evaluations demonstrate both the capabilities as well as the limitations of the proposed methods, which can be considered as initial steps towards advanced radioguided interventions. Especially the fusion of Freehand SPECT and ultrasound has the potential to revolutionize the nodal staging of early stage breast cancer by providing a less invasive alternative to the state-of-the-art radioguided sentinel lymph node biopsy technique.

Acknowledgments

First and foremost, I would like to thank Prof. Dr. Nassir Navab for offering me the opportunity to do the research for my doctoral thesis at the CAMP chair at Technical University of Munich. It was a great experience for me, especially thanks to his guidance, encouragement and support over the last years. I also wish to express my gratitude to Prof. Dr. Markus Schwaiger and Prof. Dr. Marion Kiechle, who together with Prof. Dr. Nassir Navab funded my research with a scholarship over four years.

Moreover, I would like to thank Prof. Dr. Klemens Scheidhauer, Prof. Dr. Markus Essler, Prof. Dr. Matthias Eiber, Dr. Ingo Einspieler, Dr. Carlos Gerngross and Dr. Christina Blümel from nuclear medicine; Dr. Stefan Paepke, PD Dr. Andreas Schnelzer and Dr. Alexandra Ehlerding from gynecology; Prof. Dr. Marc Martignoni, Dr. Andreas Rieger, Dr. Jacob Saeckl and Prof. Dr. Hubertus Feussner from surgery; PD Dr. Tobias Maurer from urology as well as all other surgeons and physicians I had the privilige to collaborate and to publish together. Not to forget their teams including the operating room staff in the surgical departments and the technical assistants in nuclear medicine; without their support and patience, this interdisciplinary scientific outcome would not be achievable.

Along with all my colleagues at CAMP, I would like to thank especially José Gardiazabal, Philipp Matthies, Christoph Hennersperger, Benjamin Frisch, Ralf Stauder, Dzhoshkun Shakir, Tobias Lasser and Thomas Wendler for our great collaboration and teamwork resulting in numerous publications as well as the friendship we built over the course of our scientific work. Furthermore, special thanks to all students I (co-)supervised during my time at CAMP for their successful projects supporting my research activities. In addition, I would like to thank John-Michael Fischer, Stefan Wiesner, Martin Horn, Matthias Keicher, Jörg Traub and SurgicEye GmbH for our great cooperation throughout the years.

Finally, I would like to thank my friends and my family, especially my mother Nevin and my brother Asım for supporting me, believing in me and always being there for me. İsmail, my husband, my friend, my companion, my reason, my peace in life... I do not know how to begin with saying thank you. We took this path together, and without your presence, your trust and support, it simply would not have been possible.

...Hasan, my father, my past;
Hasan Efe, my son, my future...

Contents

List of Figures

List of Tables

CHAPTER 1

Introduction

The discovery of radiation and the invention of radiation detectors has opened new doors for inspiration and innovation in various disciplines including medicine. Development of small handheld radiation detectors allowed intra-operative detection and identification of radioisotopes that has been injected to the patient previously and consequently provided real-time guidance and feedback to the surgeon. Since its first utilization in the middle of the twentieth century, radioguided surgery has evolved enormously and has become a well-established branch within the surgical practice. By the use of appropriate radiotracers and suited radiation detectors, radioguided surgery allows the surgeon to localize and differentiate otherwise invisible structures and therefore to minimize the degree of surgical invasiveness.

Even though radioguided surgery has been investigated and successfully applied for numerous malignancies, up until now it achieved the most significant impact on the surgical treatment of breast cancer and melanoma. With advancements in radiation detector technology as well as introduction and development of tracking and navigation, new radioguided surgery systems such as Freehand SPECT (fhSPECT) have been developed and found its way into the operating room. Freehand SPECT is a novel intraoperative nuclear imaging and navigation system which was initially developed at our institution, the chair for Computer Aided Medical Procedures at the Technische Universität München, and first introduced by Wendler et al. in year 2007 at the Medical Image Computing and Computer-Assisted Intervention (MICCAI) conference [119]. After the proof of concept and the success of the initial research prototype via clinical pilot studies, it is commercialized by the spin-off start-up company SurgicEye GmbH and marketed and sold under the product name *declipseSPECT* around the world.

The Freehand SPECT concept is based on the idea of bringing SPECT-like imaging capabilities into the operating room by tracking of the conventional gamma radiation detection probes which are commonly used for radioguided surgery and by reconstruction of a 3D radiation distribution in the volume of interest out of the non-uniform scan coverage of this tracked gamma detector which is moved by the surgeon over the patient. This non-uniformity brings additional challenges along for the mathematical modeling and computation of the reconstruction so that the initial research was more focused on this part. Freehand SPECT technology uses iterative reconstruction algorithms to generate a 3D image of the radiation distribution inside the scanned anatomy, but in contrast to SPECT imaging, in a relatively small reconstruction volume and using a comparably small set of measurements in a non-uniform geometry, in order to be able to reconstruct the image in less than a couple of minutes to comply with the requirements of the operating room.

The first reported clinical use cases and clinical studies for Freehand SPECT imaging were sentinel lymph node biopsy procedures for breast cancer and melanoma patients. The high number of cases of sentinel lymph node surgery procedures for breast cancer and melanoma patients per year in our university hospital laid a perfect basis for technical and clinical studies to improve and evaluate this new technology. Furthermore, the reconstruction of superficial small hot spots with almost no background radiation in close proximity -as it is commonly the case for sentinel lymph node biopsy- is mathematically and computationally less complex and therefore more advantageous as a first direction for Freehand SPECT compared to the reconstruction of cold spots in tissue with high radioactive uptake or deep-seated hot spots as well as hot spots in a region with high background radioactivity. Another advantage is the minimal alteration of the surgical workflow caused by the introduction of Freehand SPECT since the gamma probe is already a fundamental component for these well established radioguided surgical procedures. Because of all these reasons, the Freehand SPECT technology was initially tailored to fulfill the surgical and technological requirements of sentinel lymph node biopsy technique.

Since its introduction, Freehand SPECT imaging is often compared with SPECT imaging, which it is named after and closest to in terms of the reconstruction problem. However, such a quantitative comparison may be biased without taking into account the trade off required for its intraoperative utilization and acceptance by the surgeons. SPECT images can serve as a ground truth for comparing the Freehand SPECT quality against it, but expecting it to achieve and even outcome the SPECT imaging quality would be unreasonable. Available time and computational resources as well as the dependency on the human operator are the main limiting factors for Freehand SPECT, in contrast to SPECT imaging. In the operating room, the additional overhead for the scanning and the reconstruction

time needs to be in an acceptable range so that the intraoperative utilization of the Freehand SPECT technology can be justified. Furthermore, the workstation needs to be small enough to be easily incorporated into the housing as well as powerful enough to compute the reconstruction in a fast manner with highest possible resolution. And of course most importantly, the surgeon needs to be well trained about the best practices for scanning the anatomy as well as the technology itself in terms of handling and clinical interpretation of resulting 3D reconstructions. Because of this, the overall success and acceptance of the Freehand SPECT technology is highly dependent on the *human*.

1.1. Objective

The main objective of our research is deriving models for specific adaptation of the intraoperative nuclear imaging and guidance technology Freehand SPECT in respect to different clinical domains as well as its evaluation by conduction of appropriate experiments and/or studies. In the following our objectives are briefly highlighted:

- Identification of new surgical procedures where the Freehand SPECT technology can be applied as it is or with some adaptations/modifications.
- Observation of the clinical/surgical workflow of the procedure in detail for finding the minimum alteration required so that the surgeons can accept the system easier.
- Modification and calibration of the Freehand SPECT system for this new clinical application.
- Definition of proper scanning protocols based on the anatomy to be scanned.
- Conduction of experiments or studies which measure the effectiveness of the system in terms of technology, imaging, guidance or handling.

1.2. Outline

This thesis is structured in three parts and seven chapters.
Part I contains the background information serving as a basis for the subsequent chapters:

- **Chapter 2** introduces radioguided surgery in general, provides information about radionuclides, radiotracers and radiation detectors used in radioguided surgery and furthermore describes briefly different radioguided surgery techniques in literature.

- **Chapter 3** describes Freehand SPECT imaging and its components in detail.

Part II contains the scientific contributions of this thesis:

- **Chapter 4** investigates the importance of *human* component in Freehand SPECT imaging via postoperative *user* driven analysis and evaluations, especially in respect to the medical augmented reality. The methodology is based on the analysis of the automatically generated device and performance log files by the system during the actual surgical procedure.
- **Chapter 5** deals with the applicability of Freehand SPECT imaging for head and neck cancer by administration of positron emitting radiotracer ^{18}F-FDG and integration of a high energy gamma probe instead of the conventional gamma detection probe.
- **Chapter 6** presents the first feasibility study for fully 3D Freehand SPECT - ultrasound fusion with the motivation of *non-surgical* core needle biopsies of axillary *sentinel* lymph nodes for breast cancer.

Finally, **Part III, Chapter 7** concludes by providing a summary of the contributions as well as giving an outlook on future work and potential improvements. The **Appendix** contains the bibliography, a glossary of terms and a list of acronyms used throughout the thesis and the list of publications contributed to the scientific community.

Part I.

Background

CHAPTER 2

Radioguided Surgery

With the technological and methodological advancements in medicine, surgical procedures became less and less invasive over the course of time. It is beneficial and also desired to apply minimally invasive surgical techniques, where applicable, since they result in more tissue preservation, less side effects and morbidity and comparably shorter recovery times. The radioguided surgery concept can be seen as a result of this trend. It leads to minimally invasiveness by the utilization of a radiation detection device inside the operating room to identify in real-time the tissue with significant radioactive uptake due to the administration of an ad-hoc radiotracer to the patient beforehand. Since its first introduction in mid twentieth century, radioguided surgery has evolved to a well established surgical discipline for the treatment or staging of numerous malignancies [91, 90].

This chapter is organized as follows: Section 2.1 gives a brief historical background on radioguided surgery. Thereafter, main concepts of radioguided surgery are presented, varying from the physical fundamentals of radionuclides (section 2.2) to their medical administration as radiotracers (section 2.3); from principles of radiation detection (section 2.4) to radiation safety and dosimetry (section 2.5). Finally, different radioguided surgery techniques in literature are described in section 2.6 and an overview of their various clinical application domains is given in section 2.7.

2.1. A Brief History

The first application of the concept of radioguided surgery dates back to the year 1949, when Selverstone et al. [94] for the first time used a radiation detection device inside the operating room. In this work, the patients were injected with the pure β radiation

emitter Phosphorus-32 (^{32}P) prior surgery and a handheld Geiger-Müller counter was used intraoperatively for the detection of the radiation inside the tissue during brain surgery.

Geiger-Müller counters are relatively simple and easy to produce radiation detector devices so they are even now commonly used as general purpose radiation detectors for dosimetry. However, they are not really well suited for the intraoperative usage. Especially since they cannot measure the incident radiation energy and since there is no discrimination between radiation types, better radiation detection devices were essential for more precise application of radioguided surgery. In addition to that, introduction of new radiotracers into the community over time also has a major influence on the successful application of radioguided surgery in various clinical domains.

The first intraoperative usage of a gamma radiation detecting probe -devices which are still commonly used for radioguided surgery- is reported in literature not much after the work of Selverstone and colleagues. Harris et al. [42] described in 1956 the specifications of their handheld gamma scintillation detection probe and reported on the radioguided resection of residual thyroid tissue during a revision surgery of a thyroid patient using Iodine-131 (^{131}I). Since then, radioguided surgery has been investigated for numerous clinical applications using different detector technologies as well as different radiotracers. Nowadays, radioguided surgery is a well established surgical discipline for the surgical treatment of various malignancies thanks to the technological advancements in radiation detection as well as radionuclide and radiotracer production. Table 2.1 shows a classification of the major historical milestones in radioguided surgery as described in [91, 90] based on the radionuclide and corresponding radiation types (section 2.2), the applied radiation detector technology (section 2.4), and the clinical application (section 2.7).

2.2. Radionuclides

A radionuclide or radioisotope is an artificial or natural nuclide with an unstable neutron to proton ratio, which tends toward radioactive decay to achieve nuclear stability (or at least a more stable nuclear status), with the emission of energy that may be measurable with a dedicated detector. The processes of radioactive decay mainly includes alpha particle emission (a helium nucleus composed of two neutrons and protons), negative beta particle emission (electron decay), positive beta particle emission (positron decay), electron capture and gamma radiation. In medical research and nuclear medicine practice positron-emitting radionuclides are very important in positron emission tomography (PET). Radionuclides which emit gamma rays are mainly relevant for scintigraphy and single-photon emission computed tomography (SPECT) imaging, while radionuclides emitting α and β^-

Year	Group	Detector	Radionuclide	Radiation	Clinical Application
1949	Selverstone et al. [94]	G-M	^{32}P	β^-	Brain surgery
1956	Harris et al. [42]	CsI(Tl)	^{131}I	β^-, γ	Thyroid surgery
1981	Harvey et al. [45]	NaI(Tl)	^{99m}Tc	γ	Biopsy of bone lesions
1981	Ghelman et al. [39]	NaI(Tl)	^{99m}Tc	γ	Resection of bone lesions
1984	Aitken et al. [4]	CdTe	^{131}I	β^-, γ	Colorectal cancer
1984	Ubhi et al. [109]	CdTe	^{201}Tl	γ	Parathyroid adenoma
1993	Krag et al. [61]	NaI(PMT)	^{99m}Tc	γ	Breast cancer (SLNB)
1993	Alex et al. [7]	NaI(PMT)	^{99m}Tc	γ	Malignant melanoma (SLNB)
1995	Martinez et al. [67]	CdZnTe	^{99m}Tc	γ	Parathyroid gland pathology
1997	Norman & Chheda [82]	CdZnTe	^{99m}Tc	γ	Primary hyperparathyroidism
2000	Desai et al. [24]	CdZnTe	^{18}F	β^+ (γ)	Colorectal cancer
2001	Gray et al. [41]	GP	^{125}I	γ	Breast cancer (RSL)
2008	Strong et al. [103]	BP	^{124}I	β^+ (γ)	Clear cell renal cell cancer

G-M: Geiger-Müller counter, CsI(Tl): gamma probe with scintillation crystal thallium-activated cesium iodide, NaI(Tl): gamma probe with scintillation crystal thallium-activated sodium iodide, NaI(PMT): gamma probe with scintillation crystal sodium iodide coupled to a photomultiplier tube, CdTe: gamma probe with semiconductor crystal cadmium telluride, CdZnTe: gamma probe with semiconductor crystal cadmium zinc telluride, GP: gamma probe (unspecified), BP: beta probe with plastic scintillator

Table 2.1.: Historical milestones for radioguided surgery

are mainly used for therapy.

Radionuclides are characterized by their atomic number (number of protons) and mass number (sum of protons and neutrons), their physical half-life (the time required for half of the entities to decay on average), their decay mode and the energy and probability of the emission per decay. The applicability of a radionuclide for radioguided surgery depends very much on its decay types and probabilities as well as the energy of the emitted particles. The review paper of Povoski et al. [91] published in 2009 summarizes physical properties radionuclides which are gamma emitters (or generate 511 keV gamma photons from positron-electron annihilation) and have been used in radioguided surgery in combination with gamma detection probes. Furthermore, [19] gives more detail as it also involves more radiotracers including beta emitters which have been at least once clinically applied in radioguided surgery and cites for each radionuclide one example of its use in literature to date. Another recent summary of the most frequently used radionuclides in radioguided surgery for intraoperative detection, calibration and/or therapy is given in [117]. Table 2.2 combines all these information in one table.

In the following subsections the most important radionuclides in the scope of this doctoral thesis will be introduced.

Radionuclide	Half-life	Decay	Energy	Probability	Use
Carbon-11 (^{11}C)	20.4 min	β^+	960 keV	100%	PET
Fluorine-18 (^{18}F)	109.7 min	β^+	634 keV	97%	PET
Phosphorus-32 (^{32}P)	14.3 days	β^-	690 keV	100%	Historical [94]
Natrium-22 (^{22}Na)	2.6 years	EC(γ)	1.27 MeV	100%	None
		β^+	546 keV	90%	Calibration/QC
Cobalt-57 (^{57}Co)	271.8 days	EC(γ)	122 keV	86%	Calibration/QC
		EC(γ)	136 keV	11%	Calibration/QC
		EC(γ), β^-	14 keV	9%	None
Gallium-67 (^{67}Ga)	3.26 days	EC(γ)	93 keV	38%	SPECT
		EC(γ)	184 keV	20%	SPECT
		EC(γ)	300 keV	17%	SPECT
		β^-	84 keV	28%	None
Gallium-68 (^{68}Ga)	67.6 min	β^+	1.90 MeV	88%	PET
		β^+	2.92 MeV	9%	PET
Zirconium-89 (^{89}Zr)	78.4 h	EC(γ)	909 keV	100%	None
		β^+	902 keV	23%	PET
Yttrium-90 (^{90}Y)	64 h	β^-	2.3 MeV	100%	Therapy
Technetium-99m (^{99m}Tc)	6.01 h	IT	141 keV	89%	SPECT
Indium-111 (^{111}In)	2.8 days	EC(γ)	171 keV	90%	SPECT
		EC(γ)	245 keV	94%	SPECT
Iodine-123 (^{123}I)	13.3 h	EC(γ)	158 keV	83%	SPECT
		EC(X)	27 keV	72%	None
		EC(X)	31 keV	12%	None
Iodine-124 (^{124}I)	4.18 days	EC(γ)	602 keV	63%	None
		EC(γ)	722 keV	10%	None
		EC(γ)	1.69 MeV	11%	None
		β^+	1.53 MeV	12%	PET
		β^+	2.14 MeV	11%	PET
Iodine-125 (^{125}I)	59.4 days	EC(γ)	35 keV	7%	Marker
		EC(X)	27 keV	100%	Marker
		EC(X)	31 keV	20%	Marker
Iodine-131 (^{131}I)	8.02 days	IT	364 keV	82%	SPECT
		IT	637 keV	7%	None
		β^-	333 keV	7%	Therapy
		β^-	606 keV	90%	Therapy
Thallium-201 (^{201}Tl)	73 h	EC(γ)	167 keV	10%	Historical [109]

Emissions >10 keV and probabilities >5% are included in the table.
PET nuclides are used for direct β^+ detection or detection of annihilation photons. SPECT nuclides are used for γ detection. In particular I-125 is used for solid markers implanted in tissue interventionally to guide surgical resection.
QC: quality control, EC: electron capture, IT: isomeric transition

Table 2.2.: Properties of radionuclides used in radioguided surgery

2.2.1. Technetium-99m

Technetium-99m is a nuclear isomer of Technetium-99 (^{99}Tc), which is itself an radioactive isotope of Technetium. Technetium is a chemical element with symbol Tc and atomic number 43. It is named after the Greek word "τεχνητός", meaning "artificial", since it was the first element to be artificially produced before its discovery in nature [54]. Interestingly, all of its isotopes are radioactive; none stable.

Technetium-99m (^{99m}Tc) is a perfect example for gamma decay via *isomeric transition*[1], in which a nucleus emits energy without changing its number of protons or neutrons. ^{99m}Tc is a *metastable* radionuclide (as denoted by an "m" after its mass number 99), whose nucleus is an excited state lasting longer than typical and resulting in a rather delayed gamma emission instead of an immediate emmision [117] (cp. its physical half-life of about 6 hours). The nucleus de-excites to its ground state mainly (89%) through the emission of gamma rays (141 keV):

$$^{99m}Tc \rightarrow {}^{99}Tc$$

Technetium-99m is without a doubt the most commonly used radionuclide in nuclear medicine practice for diagnostic imaging and radioguided surgery. Technetium-99m decays mainly by gamma emission with a photon energy of about 141 keV which can be detected with almost all commercially available gamma detectors as it is in the ideal range (100-200 keV) for gamma detection [19]. Its medium energy gamma radiation and its relatively short physical half-life of about 6 hours, makes it a perfect candidate for diagnostic purposes, allowing fast scanning procedures, but keeping total patient and personnel radiation dose relatively low. Same reasons apply for its common use in radioguided surgery.

Technetium-99m is widely used in various different radiotracers (section 2.3) and in various radioguided surgery techniques (section 2.6 and table 2.3). For radioguided surgery procedures, depending on the targeted anatomy and depending on the characteristics of the tracer material, it can be injected either locally (subsection 2.3.1) or intravenously (subsection 2.3.2). For more details about different ^{99m}Tc-based radiotracers and their use, please refer to [19].

[1] Another type of isomeric transition can be via internal conversion, wherein the energy is used to excite and emit one of the atom's orbital electrons. Please note that this is not a beta decay, since the emitted electron is not generated from the nucleus.

2.2.2. Fluorine-18

Fluorine-18 is a radioisotope of Fluorine which is a chemical element with symbol F and atomic number 9. Its physical half-life is 109.7 minutes and it decays by *positron emission (β^+ decay)* 97% of the time converting into a negatively charged oxygen-18 (a neutrino is also emitted):

$$^{18}F \rightarrow {}^{18}O^- + e^+ + \nu$$

In the other 3% of the time it decays via *electron capture*, where the nuclei captures an electron from inner orbits and makes one of its protons a neutron, so that the atom becomes a stable oxygen-18 (a neutrino is also emitted):

$$^{18}F \rightarrow {}^{18}O + \nu$$

Following this, the loss in energy of the nucleus is either emitted in form of X rays or passed to an electron.

Fluorine-18 (^{18}F) is a major radionuclide used in nuclear medicine, especially in form of fluorodeoxyglucose (^{18}F-FDG), as it is perfectly suited for PET imaging due to the fact that it predominantly decays via positron emission. These positrons have max. 634 keV energy and travel only a short distance (typically 1-2 mm) within human tissue before hitting an electron, which is its anti-matter. This results in an *electron-positron annihilation* which generates two high energy 511 keV gamma photons in (almost) opposite directions. In contrast to the positrons, these simultaneously emitted annihilation photons can travel long distances within human tissue and can be detected with commercial PET scanners using a technique called *coincidence detection*, which localizes an annihilation event somewhere along the line joining the two detectors detecting each of the photons. More details about PET imaging can be seen in [98] and [23].

Fluorine-18 can be used in radioguided surgery in combination with two different type of detectors: (1) so-called beta probes which can directly detect positrons; (2) high energy gamma probes (also called "PET" probes) which can detect 511 keV annihilation photons [91].

2.2.3. Iodine-125

Iodine-125 (^{125}I) is a radioisotope of the chemical element Iodine with symbol I and atomic number 53. It is a low-energy gamma emitter with a physical half-life of 59.4 days. It decays 100% by *electron capture* to an excited state of Tellurium-125 (denoted with an asterisks after the element symbol). This state is not the metastable Te-125m, but

rather a lower energy state that decays immediately:

$$^{125}I \rightarrow {}^{125}Te^{*} + \nu \rightarrow {}^{125}Te + \nu$$

The excited nucleus reaches its ground state via numerous radioactive emissions which can occur in form of gamma decay with a maximum energy of 35 keV (7%) or internal conversion (93%), the latter resulting in additional X-ray radiation of similar energies (27 keV and 31 keV) due to several orbital electron transitions. The gamma ray as well as these X-rays are in the low-energy window, which are useful in radioguided surgery as they can be detected with dedicated gamma probes or cameras.

There are two different approaches presented in literature for radioguided surgery using Iodine-125 as radionuclide. First approach is intravenous administration of ^{125}I-labeled radiotracers, which can be in form of small molecules, peptides or antibodies [19]. Second approach is local placement of ^{125}I-labeled closed titanium seeds, similar to the ones used in brachytherapy. The most wellknown use case for this is the radioguided seed localization (RSL) procedure (subsection 2.6.3) as an alternative to wire-guided localization (WGL) of impalpable breast tumors.

2.2.4. Indium-111

Indium-111 (^{111}In) is a radioisotope of the chemical element Indium with symbol In and atomic number 49. It is a gamma emitter with a physical half-life of 2.8 days. It decays 99.99% by *electron capture* in a stepwise fashion first to excited state Cadmium-111 (denoted with an asterisks after the element symbol) and finally to ground state Cadmium-111 with associated gamma ray emissions at 171 keV (90%) and 245 keV (94%):

$$^{111}In \rightarrow {}^{111}Cd^{*} + \nu \rightarrow {}^{111}Cd + \nu$$

Indium-111 is the only radioisotope of Indium, which is used in medicine. Indium-111 is suited for labeling of peptide-based tracers and antibodies (section 2.3). Compared to Technetium-99m, the radiation energy of Indium-111 is higher but it is still in the detection range of commercial gamma probes and cameras. Furthermore, the physical half-life is longer so the radiation burden is higher for both patients and for personnel compared to Technetium-99m. Although it sounds like a limitation for its use in nuclear medicine and radioguided surgery, these characteristics of Indium-111 may be even beneficial in some cases depending on the tracer material and the targeted anatomy. Radiolabeled antibodies for example are more specific and have longer circulation times inside the body until they reach the lesion of interest (slow biological uptake). After intravenous radiotracer

injection, several days may be required so that the lesion can be imaged or intraoperatively localized via radioguidance. In this regard, radioisotopes such as Indium-111 may be better suited than Technetium-99m due to their longer physical half-lives [19].

2.3. Radiotracers

A radioactive tracer (radiotracer) is a chemical compound in which one or more atoms have been replaced by a radionuclide. This process is often called radioactive labeling.

The radiotracers applied in radioguided surgery can roughly be categorized into four general classes: (a) radiocolloids, (b) small molecules, (c) peptides and (d) antibodies and antibody fragments [19]. Furthermore, they can be differentiated by their method of administration: local injection and intravenous injection. Please note that in diagnostic nuclear imaging practice, radiotracers may be administered in other ways as well, such as inhalation as a gas or aerosol or ingestion while combined with food, however hereby the focus is set on only the methods relevant for radioguided surgery. Table 2.3 shows such a classification of commonly used radiotracers by their administration method and associated radioguided surgery techniques [59, 19]. Details about radioguided surgery techniques mentioned in the table will be given in section 2.6.

Class	Radiotracer	Injection	RGS Techniques
	^{125}I-seeds	Local	RSL
(a)	^{99m}Tc-labeled radiocolloids	Local	RGSLNB,ROLL,SNOLL,RULL
(a)	^{99m}Tc-tilmanocept (Lymphoseek)	Local	RGSLNB
(b)	^{99m}Tc-MIBI	Intravenous	RIME
(b)	^{18}F-FDG	Intravenous	RIME, FDGDS
(b)	^{124}I and ^{131}I	Intravenous	RIME
(b)	^{124}I- and ^{131}I-MIBG	Intravenous	RIME
(c)	^{111}In- and ^{99m}Tc-octreotide analoges	Intravenous	RIME
(d)	^{124}I, ^{131}I, ^{125}I, ^{111}In, ^{99m}Tc-labeled antibodies	Intravenous	RIGS

(a) radiocolloids, (b) small molecules, (c) peptides, (d) antibodies and antibody fragments
RSL: radioguided seed localization; RGSLNB: radioguided sentinel lymph node biopsy; ROLL: radioguided occult lesion localisation; SNOLL: sentinel node occult lesion localization; RULL: radioguided ultrasound lymph node localization; RIME: radioguided intraoperative margins evaluation; FDGDS: ^{18}F-FDG directed surgery; RIGS: radioimmunoguided surgery.

Table 2.3.: Radiotracers and their injection methods used for different radioguided surgery techniques

2.3.1. Radiotracers for Local Injection

Radionuclides which are attached to big molecules such as radiolabeled colloid particles (radiocolloids) are well suited for local administration. There is a large variety of radiocolloids used in nuclear medicine. Although many of the radiocolloids are administered locally (table 2.3), some (comparably smaller) radiocolloids may be injected intravenously depending on the organ/tissue targeted. For example, ^{99m}Tc-sulfur colloid can be injected locally for lymphatic mapping or it can also be injected intravenously for diagnostic imaging of liver/spleen, where however the radiocolloid works as systemic tracer instead (cf. subsection 2.3.2). The main parameter here is the particle size: if the molecule is too small (<5nm), it penetrates to the intravascular system which does not enable local accumulation; if the molecule is too big (>200nm), it basically remains at the injection site. Particles between 5nm to 10nm in size enter the lymphatic system but are easily distributed to numerous lymph nodes [22]. In case a mapping of the first draining lymph nodes of a region is desired (particle size between 10nm and 200nm), the majority of the radioactive material injected stays at the injection site and only a small portion drains via the lymphatic system to the closest lymph note or lymph notes.

If injected directly or close to the primary tumor, the radioactivity accumulated in these lymph nodes, called sentinel lymph nodes (SLNs), can be measured intraoperatively using a handheld radiation detector (Figure 2.1). The SLNs can be identified and removed surgically under radioguidance and examined pathologically to determine the metastatic status of the cancer diagnosis. This procedure is called sentinel lymph node biopsy (SLNB) and is a well-established radioguided surgery technique, which is applied in various clinical indications using ^{99m}Tc-labeled radiocolloids (subsection 2.6.1).

If injected directly into the primary tumor under ultrasound (US) or X-ray guidance, these radiotracers can be applied for marking of non-palpable tumors and their radioguided surgical removal using a dedicated handheld radiation detector. An example here would be radioguided occult lesion localisation (ROLL) (subsection 2.6.4) or sentinel node and occult lesion localization (SNOLL: a combination of SLNB and ROLL) (subsection 2.6.5) technique applied for breast cancer patients using ^{99m}Tc-labeled radiocolloids as radiotracers.

Besides radiocolloids, titanium seeds which encapsulate radionuclides (similar as the ones used in brachytherapy) can be administered locally for primary tumor marking. Radioguided seed localization (subsection 2.6.3) has been introduced to mark primary breast tumors where ^{125}I-seeds are injected into the tumor directly as an alternative to wire guidance as commonly used for non-palpable breast tumor marking.

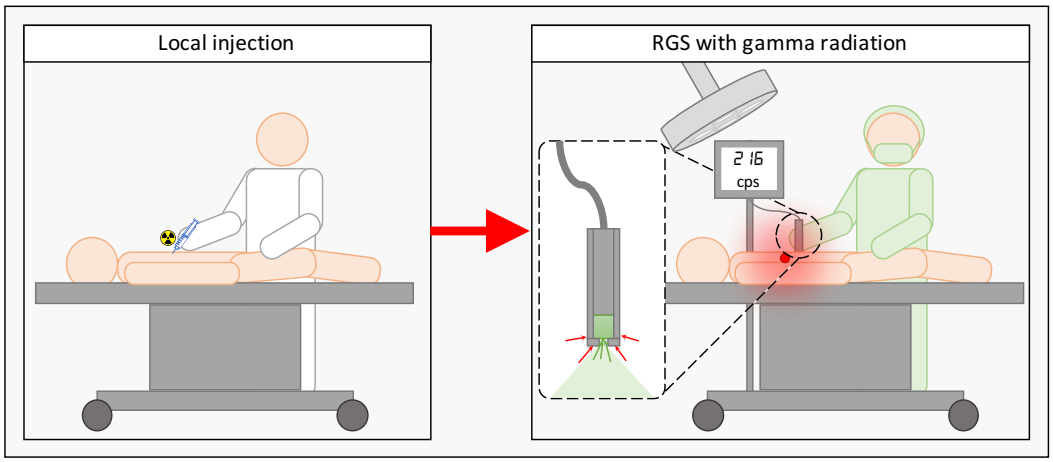

Figure 2.1.: Technetium-99m guided surgery with local injection and a regular gamma radiation detection probe. A typical clinical use case is radioguided sentinel lymph node biopsy technique.

2.3.2. Radiotracers for Intravenous Injection

Bunschoten et al. [19] lists three main classes of radiotracers for intravenous injection: small molecules, peptides and antibodies/antibody fragments. However, some radiocolloids may also be administered intravenously (cp. ^{99m}Tc-sulfur colloid for liver/spleen screening). As these radiotracers are injected directly into the intravascular system, they are easily distributed inside the body. Here the main paramater is not the particle size, but active sites of the tracer itself: it matters to which molecule the radionuclide is attached to so that it properly accumulates at the targeted organ or tissue. For example, fluorodeoxyglucose (FDG), radiolabeled with Fluorine-18 (^{18}F-FDG) is a commonly used radiotracer, which is intravenously administered. As malignant tumors have an increased glucose metabolism than healthy tissue, radiotracers such ^{18}F-FDG mimicking glucose have an increased uptake in malignant areas [59]. It is mainly used for PET imaging but it also can be used for radioguided surgery. However, due to its decay mode and energy (Table 2.2), its intraoperative detection is very challenging due to the requirement of more advanced detector technology (Figure 2.2).

Of course it is desired that a radiotracer is specific enough that it only accumulates in diseased areas. That would allow perfect diagnostic imaging and eventually perfect intraoperative detection. Unfortunately, this is most of the time not the case. The major example for this is again ^{18}F-FDG. It allows visualization of glucose metabolism. There-

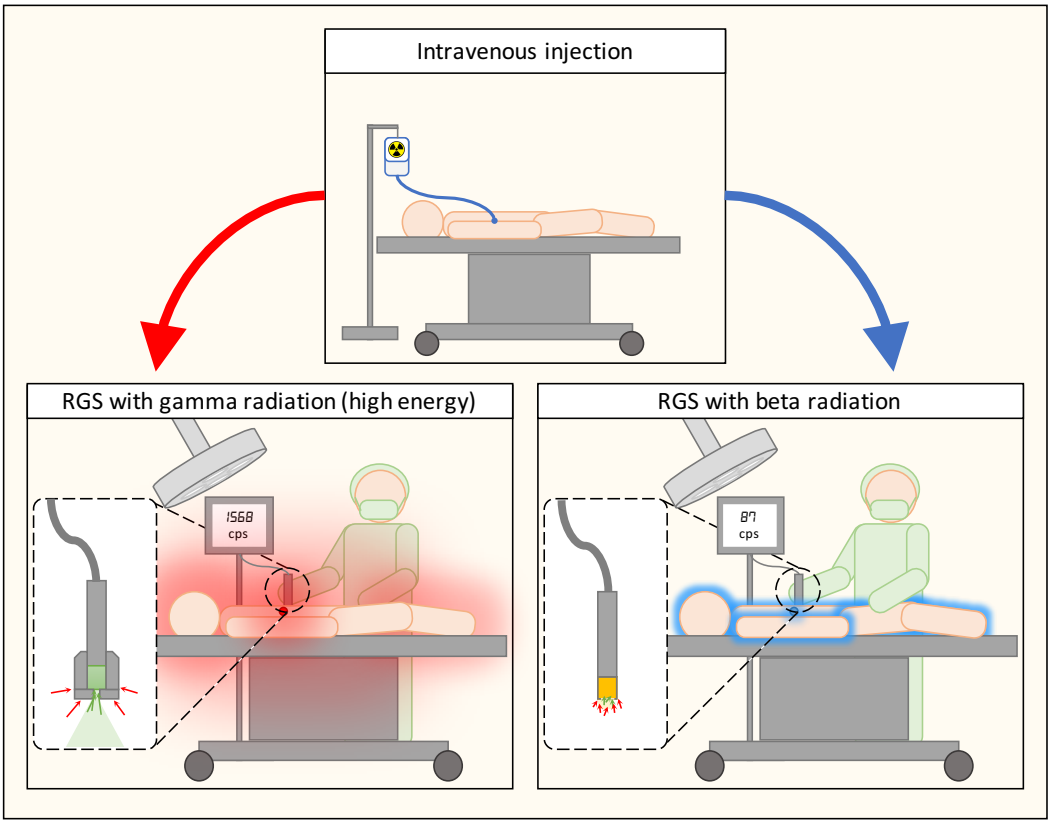

Figure 2.2.: FDG guided surgery with intravenous injection and high background uptake. Here, due to high energy of the gammas emitted (511 keV), better shielding is required which results in bulkier gamma detectors. Beta radiation (positron) detecting probes can also be used instead, however these are only effective in very short distances (1-2 mm).

fore it is not cancer specific, so it is also expected to have a higher uptake in regions with higher metabolism such as sites of muscular hyperactivity, infection, tissue repair, etc. Furthermore, some organs show always high uptake in a ^{18}F-FDG PET scan such as the brain, the heart, the liver and the bladder [30], so lesions in or close to these anatomies can be overseen or misinterpreted.

Compared to small molecule based tracers mimicking hormones (e.g. MIBG), amino-acids (e.g. DOPA) or glucose (e.g. FDG), peptide tracers and antibodies are more specific as they target a disease specific receptor [19]. With increased specificity the production cost/effort of radiotracers also increase: small molecule based tracers are easiest to produce whereas peptide based ones are more complex. However they are still much easier

to produce compared to radiolabeled antibodies or antibody fragments, which are used for radioimmunoguided surgery (RIGS) (subsection 2.6.2). Please note that the long circulation time of antibodies inside the body is a major challenge in radioimmunoguided surgery [59], therefore radionuclides with longer physical half-life such as Indium-111 are more suited here compared to Technetium-99m.

2.3.3. Hybrid Tracers

Radioguided surgery is a concept fundamentally relying on the intraoperative utilization of radiation detection systems. Depending on the target anatomy and the characteristics of the utilized *radiotracer*, the intraoperative localization of the lesion of interest can be extremely challenging due to background activity in close proximity, influencing the detection significantly. In such clinical application areas, the combination of radioguidance with other intraoperative guidance methods such as *fluorescence imaging* can be also considered to improve the success of the surgical procedure.

Hybrid tracers are required, having both a *radioactive* as well as a *fluorescent* component, in order to benefit from the advantages of both modalities. Even though the idea of hybrid tracer dates back to the mid twentieth century [19], the introduction of indocyanine green (ICG)-^{99m}Tc-nanocolloid, the state-of-the-art hybrid tracer in clinical practice, was not until the year 2011 [110]. The addition of the fluorescent component extends the applicability of clinically widely used radiotracer ^{99m}Tc-nanocolloid even further, because the fluorescence imaging does not suffer from background signals originating from injection site or other organs with high accumulation of tracer material.

Of course, fluorescence imaging brings also some additional technical overhead to the operating room, due to the utilization of a fluorescence camera. The lights in the operating room may also interfere with the near infrared fluorescence acquisition, which may be a limiting factor in some use cases requiring additional measures.

First clinical application area of the hybrid tracer ICG-^{99m}Tc-nanocolloid was the sentinel lymph node biopsy technique for prostate cancer [110]. Since then it achieved a significant impact on the community and has been applied for various other clinical domains, especially for sentinel lymph node biopsy technique where radioguidance via the radiotracer ^{99m}Tc-nanocolloid is the standard clinical practice [36]. More details about the fluorescent and hybrid tracers and their clinical application areas can be found in [78, 19].

2.4. Radiation Detectors

Nowadays, various different radionuclides have been used in at least preliminary radioguided surgery scenarios due to the advancements in radiation detector technology. Small handheld gamma radiation detectors such as gamma probes or mini gamma cameras are available. Depending on the energy level of the radiotracer applied different detector technologies may be better suited; additionally proper calibration and/or collimation may be required.

In order to quantify and detect the radiation, it needs to be converted to electrical pulses which then can be counted using a pulse reader. For this purpose two main approaches are available for the detectors used in radioguided surgery: *light detection via scintillators* and *direct radiation detection via semiconductors*.

2.4.1. Light Detection via Scintillators

A scintillation detector is a sensitive crystal that converts ionizing radiation to flashes of light which in turn are sensed by an optically coupled photon detector converting these to electrical pulses. Commonly used scintillators for intraoperative radiation detection include thallium-activated sodium iodide (NaI(Tl)), thallium-activated cesium iodide (CsI(Tl)) and sodium-activated cesium iodide (CsI(Na)). In addition to these inorganic scintillators, plastic scintillators -solutions of organic scintillation compounds dissolved in an organic solvent that is subsequently polymerized to form a solid- are well-suited for intraoperative beta radiation detection, particularly for positron detection probes [47]. Scintillators can be coupled with photomultiplier tubes (PMT), which amplify the photoelectron by the use of a strong electric field and several dynodes (Figure 2.3), or with silicon photomultipliers (SiPM), which combine several photodiodes (PD) in arrays for linear light amplification. The advantages of the latter over PMTs are higher speed, reduced size, immunity to electronic fields and need for significantly lower voltages [117].

2.4.2. Direct Radiation Detection via Semiconductors

A semiconductor is a substance, usually a solid chemical element or compound, that can conduct electricity under some conditions but not others, making it a good medium for the control of electrical current. Its conductance varies depending on the current or voltage applied to a control electrode, or on the intensity of irradiation by infrared (IR), visible light, ultraviolet (UV), gamma (γ) or X rays. Therefore semiconductors are very well suited for radiation detection. Typical semiconductor crystals used in gamma detection

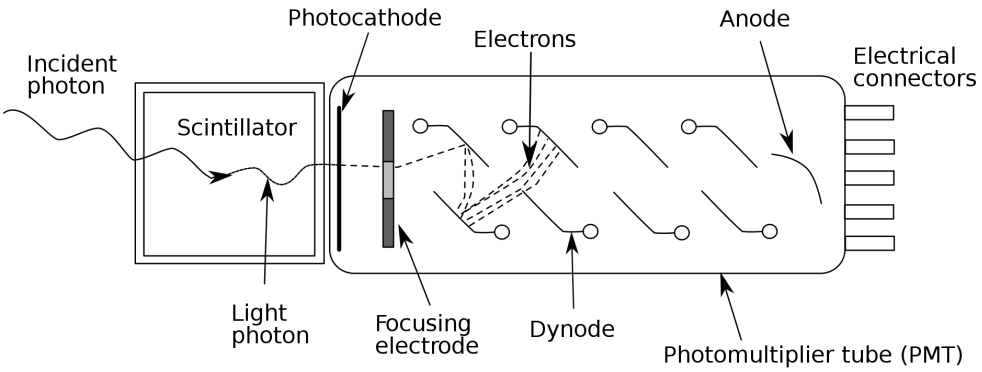

Figure 2.3.: Radiation detection using scintillator and photomultipliertube (PMT) [29].

systems are cadmium telluride (CdTe) and cadmium zinc telluride (CdZnTe). In contrast to scintillating crystals, the detection here is direct, there is no light conversion in between. The incident gamma-ray interacts with the semiconductor and excites electron-hole pairs, that are proportional to the deposited energy and drifts apart under the applied electric field. Electrons flow towards the anode and holes towards the cathode, which results in an electrical pulse.

2.4.3. Further Characteristics

Both technologies mentioned above have their advantages and disadvantages and therefore are alternatively used in different commercial gamma detection systems used in radioguided surgery. In general, scintillation based systems are cheaper to produce compared to the ones based on semiconductors. Furthermore, semiconductor based systems have a better energy resolution than most of the scintillator based systems, whereas scintillator based systems have a higher sensitivity [48]. In detectors with high energy resolution, the pulses have a proportionality to the energy of the radiation, which is a very useful feature for detection of a specific energy window. This allows for instance the usage of the same gamma probes or gamma cameras for different types of radionuclides by only adjusting the electronics via the control unit of the detector. In detectors with high sensitivity, the pulses are proportional to the amount of incident photons, which can be detected simultaneously [117]. Scintillators coupled with silicon photomultipliers composed of photodiodes can offer the advantages of both scintillator and semiconductors based technology: high energy resolution and high sensitivity [48].

Depending on the requirements of the clinical use case, a well suited radiation detection system needs to be chosen carefully. Besides the detection technology and its capabilities, the size and weight as well as the collimation and shielding of the system are very important factors for its acceptance by the end users e.g. surgeons. The field of view (FOV) of the detector depends on the type of the collimator and the detector dimensions. It is a trade-off between sensitivity and spatial resolution. Small field of view collimators allow better spatial resolution, whereas large field of view collimators allow detection of more photons and therefore result in higher sensitivity. Some radiation detection systems offer interchangeable collimators, so that the user can choose a better suited collimator for a specific clinical use case (Figure 2.4).

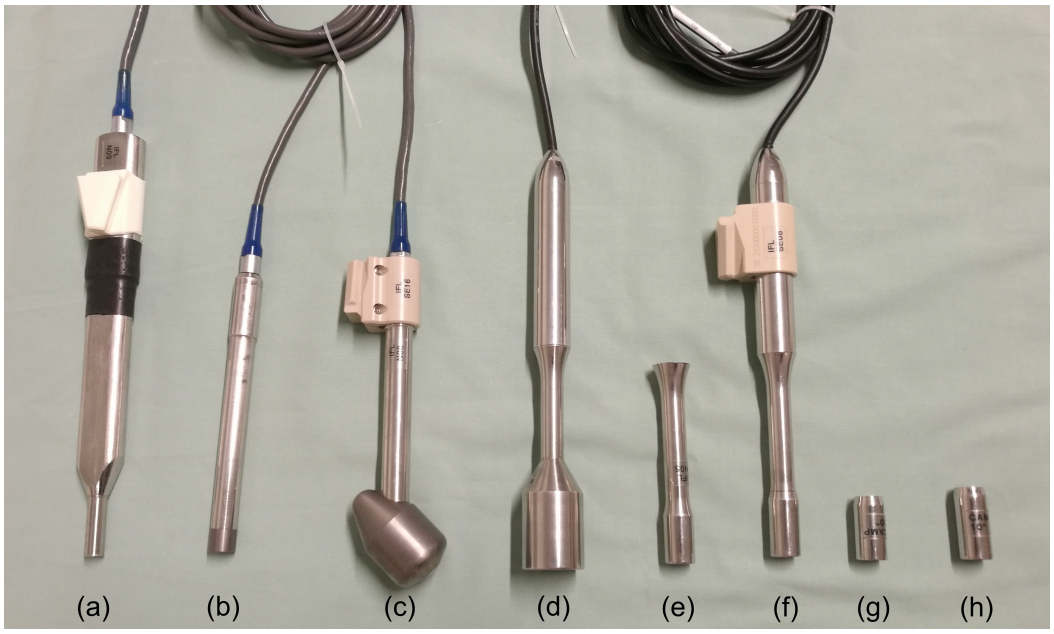

Figure 2.4.: Different types of radiation detection probes available in our interdisciplinary research lab at Klinikum rechts der Isar: Beta (a), gamma (b) and high-energy gamma (c) probes of NodeSeeker 800 system (Intra Medical Imaging LLC, USA); high-energy gamma probe (d) and regular gamma probe (f) of Crystal Probe radiation detection system (Crystal Photonics, Germany) with additional interchangeable collimators (e,g,h).

Another parameter which can be tuned to achieve better radiation detection, is the number of detector crystals incorporated in the gamma radiation detection system. Typical gamma probes, as commonly used in radioguided surgery, consist only one single detector

crystal. In contrast to this, incorporation of multiple small detector crystals in a gamma camera system may lead to better spatial resolution, better sensitivity and a larger field of view. In addition, the placement of these crystals on a small 2D grid allows the generation of intraoperative scintigraphic images.

The first prototype of such a gamma camera was introduced and patented by Soluri et al. [100] in 1997 and was called the *imaging probe*. Please note that even though it is actually the name of a product, the term *imaging probe* is commonly used as a synonym for a handheld mini gamma camera in the literature [93]. Since then, several different prototypes and also commercially available portable[2] or handheld gamma camera systems are introduced for radioguided surgery. An extensive comparison of the characteristics and the clinical application areas of such gamma cameras can be found in [48].

Minimally invasive radioguided interventions, such as laparoscopic radioguided surgery or robot-assisted radioguided surgery (e.g. da Vinci, Intuitive Surgical Inc.), require utilization of gamma detection systems in special forms. Laparoscopic gamma probes - gamma probes straight and very long in form- are available, which can be placed through one trocar, when needed. Furthermore, very small gamma probes (so-called drop-in probes) are also introduced for laparoscopic interventions [34], which can be inserted into the patient and can be picked up using regular laparoscopic tools or forceps, with improved handling due to higher degrees of freedom and flexibility and without fully blocking one of the access ports during its usage. The first patient studies utilizing drop-in gamma probes for robotic sentinel lymph node biopsy of prostate cancer patients are also recently reported in literature [73]. Such drop-in probes for radioguided surgery can be advantageous both in a robotic or non-robotic minimal invasive clinical scenario, where the limited collimation and detection of the single pixel detector is still sufficient for the laparoscopic radiation detection and guidance. The combination with fluorescence imaging via hybrid tracers as reported in [73] or inclusion of tracking and reconstruction algorithms of Freehand SPECT technology as reported in [34] may be considered to further extend the capability of the drop-in gamma probes.

2.5. Radiation Safety

Numerous radiotracers with different physical and physiological characteristics are used in nuclear medicine practice and in particular in radioguided surgery. Due to the usage of radioisotopes for radioguided surgery, several people are exposed to radiation: the pa-

[2] with mechanical support to compensate for its comparably heavy weight

tient, nuclear medicine physicians and technicians, surgeons, operating room personnel and pathologists.

Of course the person who is exposed to radiation the most is the patient himself/herself, as the radioactive material is directly injected to his/her body. Therefore the nuclear medicine experts take into account various parameters for finding the optimal dose required which would allow imaging or radioguidance during surgery while trying to keep the total dose as low as possible to avoid further damage due to radiation exposure. For sure there needs to be more gain than loss for the patient. Radioisotopes which have shorter physical half-lives and lower emission energies result commonly in less radiation burden for the patient compared to radioisotopes with longer half-lives and higher emission energies. In addition to this, tracer material and its characteristics also play an important role here: it has an effect on how the radioisotope is injected to the patient, how it is distributed inside the body, how and when it is accumulated on the lesion of interest, which further organs are exposed to radiation and finally how the radioactivity is cleared out via the metabolism of the patient.

2.5.1. Definitions

In this subsection, an overview of some of the important terms for radiation protection and dosimetry will be given. Definitions given here are mainly from the 2007 recommendations of the International Commission on Radiological Protection (ICRP) [1].

In context of radiation protection, three different definitions for the commonly used term *dose* are relevant: *absorbed dose*, *equivalent dose* and *effective dose*.

Absorbed dose: The fundamental dose quantity D given by

$$D = \frac{d\varepsilon}{dm}$$

where $d\varepsilon$ is the mean energy imparted to matter of mass dm by ionising radiation. The SI unit for absorbed dose is joule per kilogram (J/kg) and its special name is Gray (Gy) [1]. Radiation measuring instruments indicate strictly absorbed dose [106].

Equivalent dose: The dose H_T in a tissue or organ T given by:

$$H_T = \sum_R w_R D_{T,R}$$

where $D_{T,R}$ is the mean absorbed dose from radiation R in a tissue or organ T, and w_R is the radiation weighting factor (Table 2.4). Since w_R is dimensionless, the unit for the

equivalent dose is the same as for absorbed dose, J/kg, and its special name is Sievert (Sv) [1].

Radiation type	Radiation weighting factor, w_R
Photons	1
Electrons	1
Protons	2
Alpha particles, fission fragments, heavy ions	20
Neutrons	A continous function of neutron energy

Table 2.4.: Radiation weighting factors recommended by ICRP [1]

.

Effective dose: The tissue-weighted sum E of the equivalent doses in all specified tissues and organs of the body, given by the expression:

$$E = \sum_T w_T \sum_R w_R D_{T,R} \quad \text{or} \quad E = \sum_T w_T H_T$$

where H_T or $w_R D_{T,R}$ is the equivalent dose in a tissue or organ T, and w_T is the tissue weighting factor (Table 2.5). The unit for the effective dose is the same as for absorbed dose, J/kg, and its special name is Sievert (Sv) [1].

Tissue	w_T	$\sum_T w_T$
Bone marrow (red), colon, lung, stomach, breast, remainder tissues	0.12	0.72
Gonads	0.08	0.08
Bladder, esophagus, liver, thyroid	0.04	0.16
Bone surface, brain, salivary glands, skin	0.01	0.04
Total		1.00
Remainder tissues: adrenals, axtrathoracic (ET) region, gall bladder, heart, kidneys, lymphatic nodes, muscle, oral mucosa, pancreas, prostate (male), small intestine, spleen, thymus, uterus/cervix (female)		

Table 2.5.: Tissue weighting factors recommended by ICRP for an average human [1]

.

2.5.2. Dosimetry

ICRP differentiates between three categories of radiation exposure: *occupational exposure*, *public exposure* and *medical exposure of patients* [1]. Occupational exposure is defined as all radiation exposure of workers incurred as a result of their work. Medical

exposure of patients compromises all radiation exposures occurring in diagnostic, interventional and therapeutic procedures, which is intentional and for the direct benefit of the patient. Public exposure involves all exposures of the public other than occupational exposures and medical exposures of the patients. The most significant component of public exposure is of course radiation due to natural sources, however, radiation from artificial sources due to human actions such as the Chernobyl or the Fukushima accidents or atmospheric nuclear testing also have a share.

To monitor the radiation a person is exposed to over a certain amount of time, devices called dosimeters are available. As nuclear medicine experts and technicians are routinely exposed to higher doses of radiation due to their occupation, they have to follow strict guidelines by doing their daily job, they work in controlled areas and they are obligated to wear dosimeters. Commonly, the radiation exposure to nuclear medicine personnel is monitored via film badge dosimeters. The badge is typically worn on the outside of clothing, around the chest or torso to represent dose to the "whole body". This location monitors exposure of most vital organs and represents the bulk of body mass. Additional dosimeters can be worn to assess dose to extremities, for example nuclear medicine technicians working in the hot lab may be obligated to wear additional ring dosimeters on their hands, while they are preparing the required radiotracer proportions. These dosimeters are *passive*, so there is a photographic film inside sensitive to radiation, which needs to be developed. The more radiation the film absorbs, the darker it becomes when it is developed. Badges are checked periodically, and the degree of exposure of the film indicates the cumulative amount of radiation to which the wearer has been exposed. Such film dosimeters are advantageous for monitoring nuclear medicine staff due to the fact they may contain several films of different sensitivities in order to determine a more accurate measure of the dose received. There are also technologically more sophisticated *active* personal dosimeters available for further situations where monitoring via passive film dosimeters would not be adequate. Such electronic personal dosimeters allow real-time acoustic alarm warnings at preset levels and live readout of the accumulated dose. These dosimeters are especially useful in high dose areas where residence time of the wearer is limited due to dose constraints or for monitoring pregnant personnel (Table 2.6).

In contrast to nuclear medicine staff, operating room and pathology personnel involved in a radioguided surgical procedure are not routinely exposed to higher doses of radiation and therefore are not routinely monitored for occupational radiation exposure. Depending on the type of the surgery and the tracer used, different measures may be required. Sentinel Lymph Node Biopsy (subsection 2.6.1) with ^{99m}Tc-based radiotracers (subsection 2.2.1) is the most known and established radioguided surgery technique applied throughout the

Type of limit	Occupational, per year	Public, per year
Effective dose	20 mSv*, averaged over 5 years, with no more than 50 mSv in any year	1 mSv (exceptionally, a higher value of effective dose could be allowed in a year provided that the average over 5 years does not exceed 1 mSv in a year)
Equivalent dose to lens of the eye	20 mSv, averaged over 5 years, with no more than 50 mSv in any year	15 mSv
Equivalent dose to skin	500 mSv	50 mSv
Equivalent dose to hands and feet	500 mSv	-

*Additional restrictions apply to the occupational exposure of pregnant women. Exposures of the embryo and fetus of pregnant workers are considered and regulated as public exposures.

Table 2.6.: Dose limits in planned exposure situations recommended by ICRP [1, 17]

world, therefore, the largest case numbers and consequently the most reliable dosimetric considerations and guidelines are available in the literature. Limitation of performed case numbers as well as additional shielding and monitoring of radiation exposure to operating room and pathology staff is not required for sentinel lymph node biopsy procedures performed with ^{99m}Tc-based tracers [63]. However, for radioguided surgical procedures performed with radiotracers with longer half-lives and/or with higher emission energies, routine intra- and post-operative monitoring of the staff exposure and contamination may be necessary for large patient numbers [63].

2.6. Radioguided Surgery Techniques

In the following, major radioguided surgery techniques described in the literature will be presented briefly.

2.6.1. Sentinel Lymph Note Biopsy

Lymph nodes are small organs of the lymphatic system and the immune system. They are linked by the lymphatic vessels as a part of the circulatory system and are widely distributed throughout the human body. Bigger groups of lymph nodes are found in the neck, underarms, chest, abdomen, and groin. Lymph nodes may become inflamed or enlarged due to various reasons including cancer. The spread of some forms of cancer usually follows an orderly progression, spreading first to regional lymph nodes and then to other nearby group of lymph nodes, since the flow of lymph is directional. This means that

some cancers spread in a predictable fashion from a primary tumor. The first lymph node to which the cancer is likely to spread is called sentinel lymph node (SLN). Since several lymph nodes may receive direct drainage from the primary tumor, there can be more than one sentinel lymph node.

Sentinel Lymph Node Biopsy (SLNB) is a surgical procedure in which the sentinel lymph node(s) are removed and examined pathologically to determine whether cancer cells are present. If the sentinel lymph node(s) do(es) not contain cancer, then there is a high likelihood that the cancer has not spread to any other area of the body and therefore the rest of the regional lymph nodes may be spared and the patient can be treated rather in a less aggressive way. On the other hand if the sentinel nodes are infected by tumor cells, regional lymph nodes commonly need to be removed as well and an aggressive treatment is indicated to the patient, e.g. chemo- or radiotherapy.

Sentinel lymph node biopsy is a widely accepted surgical procedure for the treatment of some cancers like malignant melanoma or early breast carcinoma. Its high diagnostic accuracy has led to a rapid acceptance of the method, and it is widely used in routine clinical practice [77]. It is an accurate and reliable way of determining the nodal stage of the cancer disease where the patient benefits from a significantly less invasive operation compared to standard lymph node removal procedures -like radical axillary lymph node dissection (ALND) for breast carcinoma-, since it usually results in a smaller scar, less pain, faster recovery and fewer long-term side effects.

The sentinel lymph node concept was first introduced in 1992 by Morton and colleagues [76], who performed lymphatic mapping and sentinel lymph node biopsy using vital blue dye in early stage melanoma. Not much after that, in 1993, first use of radioisotopes and gamma probes for intraoperative mapping and detection of sentinel lymph nodes is described by Alex et al. for melanoma patients [7]. Again in 1993, Krag and colleagues introduced the radioguided sentinel lymph node biopsy for breast cancer, using Technetium-99m sulfur colloid and a hand-held gamma probe [61]. In this technique, a hand-held gamma detector guides the surgeon to radioactive lymph nodes (SLNs), which are then removed and sent to pathology for further analysis. Furthermore, complete excision of sentinel lymph nodes can be verified by measuring residual radioactivity in the region of interest using the gamma detector. The radioguided sentinel lymph node biopsy concept relies heavily upon the local administration of relatively large sized radiocolloids which accumulate in closest lymph nodes, as previously described in subsection 2.3.1.

Throughout the years, several new methods or approaches have been introduced to improve the sentinel lymph node biopsy procedure. Albertini et al.[6] first reported the successful use of lymphatic mapping with both blue dye and radioisotopes. Several authors

later have also demonstrated that the combination of radioisotope and blue dye for lymphatic mapping improves the sentinel lymph node identification rate. Usage of fluorescent dyes is also a valid alternative for the intraoperative lymphatic mapping and detection of the sentinels. The indocyanine green (ICG) is the most widely used fluorescent dye in clinical practice [36]. An advantage over blue dye is that ICG does not stain the surgical field because it is not directly visible to the human eye, but only via near infrared fluorescence cameras and only when excited with near infrared light, so the visualization can be controlled by the operator directly.

The usage of dye alone, radioisotopes alone and their combination are still very common methods throughout the world for SLN detection and removal. Technological and computational advancements in the recent years allowed the development of more complex and sensitive handheld radiation detectors such as 2D mini gamma cameras and the introduction of tracking and navigation capabilities inside the operating room (OR) for radioguided sentinel lymph node biopsy. Furthermore, the introduction of hybrid tracers (subsection 2.3.3) also extended the impact of the sentinel lymph node biopsy technique even more, especially in more complex clinical use cases such as (minimally invasive) radioguided sentinel lymph node biopsy for prostate cancer [110], vulvar cancer or penile cancer [36].

For more details about various different clinical domains where radioguided sentinel lymph node mapping and biopsy has been applied until now please refer to [91] and [50]. More details on the intraoperative SPECT-like imaging and navigation technique Freehand SPECT [119, 120] will be given in chapter 3.

2.6.2. Radioimmunoguided Surgery

Radioimmunoguided surgery (RIGS) is a technique applied in tumor localization, which combines the intravenous injection of radiolabeled monoclonal antibodies, that target antigens expressed on tumor cells or in the tumor stroma, and gamma probes for the intraoperative detection of the cancer.

The concept of radioimmunodetection using gamma probes was first introduced in 1984 by Aitken et al. [5], where they used ^{131}I-labeled antibodies as radiotracer and reported the results of their study on mice [5] and also reported the very first clinical application of RIGS in a case study of a patient with rectal cancer [4]. After that many studies have been reported in literature involving RIGS on different malignancies using different radiotracers [91] (table 2.7), however the majority of them still address colorectal cancer using ^{125}I-labeled antibodies as radiotracer due to its lower energy window. These radiotracers can be

used for both diagnostic imaging and for the surgical localization of tumors. Depending on the gamma radiation energy window of the used radiotracer a suitable gamma probe technology needs to be chosen.

For more detailed information about different types of antibodies or radionuclides used for RIGS in various clinical applications please refer to [91].

2.6.3. Radioguided Seed Localization

If a patient is diagnosed with an impalpable breast cancer, its complete surgical removal requires a preoperative marking of the tumor. As surgeons cannot differentiate intraoperatively by the look or the touch of the tissue if it is healthy or suspicious, they can only identify and resect the tumorous tissue using such a marking as a guidance. The common practice is the use of wire-guided localization (WGL) technology, where the tumor is marked preoperatively using a hooked wire with the help of an imaging technique such as mammography or ultrasound. Although being still the most widely used technique for this purpose, the WGL still has many disadvantages, which may influence the timing, handling and success of the surgical procedure.

Radioguided seed localization (RSL) is introduced in 2001 by Gray et al. [41] as an alternative to wire-guided localization which overcomes many of its disadvantages. One issue is the timing of the marking: wire placement needs to take place shortly before the surgical operation which results in logistics and scheduling challenges [40]. Insertion of the titanium seeds filled with Iodine-125 (subsection 2.2.3) on the other hand can happen even days, weeks or even months (e.g. in a neoadjuvant setup) before the surgical procedure which eases the scheduling of the surgery. Furthermore the placement of the wire may happen via a route suited best for the imaging modality used for guidance. However, there may be a much shorter route to the tumorous tissue which is suited for the surgical setting. If the surgeon follows the wire for the incision and localization, he/she may end up damaging more healthy tissue than actually needed. Using radioguidance, the surgeon may approach the tumor from various angles and decide for the shortest way to the tumor or the way resulting in the best aesthetic outcome and resulting in less tissue damage. RSL also overcomes some of the disadvantages of ROLL technique (subsection 2.6.4) as the titanium seeds are point sources and are also detectable in mammography [88]. For marking of extended or multifocal tumors, several seeds can be used. Furthermore, it can be also applied for marking of suspicious non-palpable lymph nodes [46] or tumor-positive axillary lymph nodes prior neoadjuvant therapy (so-called MARI procedure) to determine the pathological response of the treatment making axilla-conserving surgery possible [25].

Iodine-125 emits low energy photons (35 keV), therefore this procedure can even be combined with a radioguided sentinel lymph node biopsy, as it is not interfering with Technetium-99m gamma emission (141 keV). In this case, a dual-isotope gamma detector system with dedicated probes/collimators, or two different gamma detector systems adjusted for each of the energy windows of the two different tracers should be present.

2.6.4. Radioguided Occult Lesion Localization

Similar to radioguided seed localization (subsection 2.6.3), radioguided occult lesion localization (ROLL) technique also provides an alternative to wire-guided localization (WGL). As this method is used to mark non-palpable breast lesions, the intratumoral injection of the radiotracer, commonly ^{99m}Tc macroaggregate albumin (MAA) or ^{99m}Tc albumin nanocolloid, takes place under image guidance, such as ultrasound [89]. Since both radiotracers are Technetium-99m derivates, the suspicious lesion can easily be detected intraoperatively using a gamma detection system such as gamma probe. An advantage of the method is that the gamma detector can be used after the excision to search for remaining major radioactive uptake in the surgical cavity and to check the resection margins directly during the surgery. Of course this also needs to be verified via frozen section analysis or standard postoperative histopathological analysis.

Radioguided occult lesion localization method was first described in 1998 by Luini et al. [65]. After this initial success, the technique received global attention and has been applied in various hospitals throughout the world. Nowadays, it is one of the two alternatives to the gold standard wire-guided surgery technique for removal of non-palpable breast lesions, together with radioguided seed localization [27, 89].

2.6.5. Sentinel Node Occult Lesion Localization

The radioguided occult lesion localization technique (subsection 2.6.4) can easily be combined with radioguided sentinel lymph node biopsy (subsection 2.6.1), which is then called Sentinel Node Occult Lesion Localization (SNOLL).

If lesions resected in a ROLL surgery are histologically tumorous, a SLNB procedure may be indicated for further diagnosis and cancer staging. However, after the ROLL surgery, the drainage from the tumor to the lymph nodes is damaged so the localization of the sentinel lymph node may not be possible in a follow up SLNB surgery. Therefore it may be advantageous to combine ROLL and SLNB in one session (even if SLNB is redundant after pathology results of the suspicious breast tissue). This is possible due to the fact that in both surgery techniques same radionuclides and same kind of radiation detectors.

In the literature two different approaches are presented for the SNOLL technique: First approach favors the use of two different ^{99m}Tc-based radiotracers, ^{99m}Tc MAA (microaggregated albumin) injected directly into the breast tumor and ^{99m}Tc albumin nanocolloid injected subdermally for the mapping of the sentinel lymph node. The second approach combines these two into one intratumoral injection using a single tracer, ^{99m}Tc albumin nanocolloid [89]. In any case, the intraoperative localization of both the tumor and the sentinel lymph node is possible via a conventional gamma detector, which is calibrated to detect 141 keV photons of ^{99m}Tc gamma decay.

2.6.6. Radioguided Ultrasound Lymph Node Localization

In Radioguided Ultrasound Lymph Node Localization (RULL) technique ^{99m}Tc is used as radionuclide as in SLNB or ROLL/SNOLL techniques (table 2.3), however the major difference here is that the radiotracer (human albumin macroaggregates labeled with radioactive ^{99m}Tc) is injected directly into the suspicious lymph node under ultrasound guidance. Preoperative scintigraphy is performed to assure that the lymph node is marked properly. Later, the marked lymph node is excised intraoperatively under gamma probe guidance similar to sentinel lymph node biopsy.

The term RULL was introduced by Testori et al. in 2010 [105], where they applied this method successfully to melanoma patients with non-palpable lymph nodes which are suspicious in ultrasound examination. Although it is an interesting and promising concept and could be applied in other clinical indications than melanoma, the literature search reveals that the definition of RULL is not well known and perceived in the community. However similar approaches have been denoted as derivations of RULL technique such as the study of Martino et al. in 2014 [68] for thyroid patients. Radioguided seed localization (RSL) uses cases for lymph nodes, such as the MARI procedure -marking the axillary lymph node with radioactive iodine seeds- [25], can also be counted for radioguided ultrasound lymph node localization (RULL) applications.

2.6.7. Radioguided Intraoperative Margin Evaluation

As the name clearly states, Radioguided Intraoperative Margin Evaluation (RIME) technique is applied to resect the primary tumor as well as to assess intraoperatively whether the resection margins of the tumorous tissue are negative. In this technique, the systemic (intravenous) administered radiotracer would accumulate in the tumor itself or on its surface and may be detected with a dedicated gamma probe. The acoustic feedback of the gamma probe or the numeric output shown on its display may help the surgeon intraoper-

atively to detect the extent of the tumor. If any major residual activity is determined in the resection cavity, the surgeon may decide to extend the resection margins and excise more tissue.

Duarte et al. first mentioned the term RIME in 2007 [28], where they reported on their experience on breast cancer patients using ^{99m}Tc-sestamibi as the radiotracer and a conventional gamma probe for tumor resection and margin evaluation. This is possible due to the fact that ^{99m}Tc-sestamibi has a higher affinity for tumor cells than healthy breast tissue, which allows the intraoperative differentiation between breast carcinoma and healthy adjacent tissue using a gamma probe. As the radionuclide used here is the same one as the one used in SLNB procedures (^{99m}Tc), the same gamma probe can be used intraoperatively, however also because of that this technique cannot be combined with SLNB. One should also note that the ^{99m}Tc-sestamibi is injected intravenously and mainly used for cardiac imaging in nuclear medicine, so during a RIME procedure the background radiation coming from the heart may affect the success of the surgery. These may be the reasons why the RIME technique for breast cancer is described in literature in a limited manner, even though there are numerous publications reporting on the use of ^{99m}Tc-sestamibi for diagnostic preoperative nuclear imaging for breast cancer patients (e.g. breast-specific gamma imaging (BSGI) also known as scintimammography) [104].

2.7. Clinical Applications

Although most of the techniques above are mainly applied on breast cancer cases, there is a huge variety of clinical applications where radioguided surgery techniques are presented in literature. Povoski et al. [91] gives a nice summary of the clinical applications where RGS techniques are applied as of 2009. Table 2.7 follows the same structure and presents an updated summary to best of our knowledge. For more detailed information about the clinical applications and the RGS techniques, please refer to the book “Radioguided Surgery - Current Applications and Innovative Directions in Clinical Practice” [50].

Clinical applications	Specific type(s) of radioguided surgery applications
Breast Cancer*	RGSLNB, RIGS, ROLL, RIME, FDGDS, RSL, SNOLL
Cutaneous malignancies	
Malignant melanoma*	RGSLNB, FDGDS, RULL
Merkel cell carcinoma*	RGSLNB
Other cutaneous malignancies	RGSLNB
Gastrointestinal malignancies	
Colorectal cancer	RIGS, RGSLNB, FDGDS
Anal cancer	RGSLNB
Esophageal cancer	RGSLNB
Gastric cancer	RGSLNB, RIGS, FDGDS
Pancreatic cancer	RIGS
Gastrointestinal stromal tumor	FDGDS
Head and neck malignancies	
Squamous cell cancer*	RGSLNB, RIGS, FDGDS
Parathyroid disease	RGS
Thyroid cancer	RGS, FDGDS, RGSLNB, ROLL
Parotid gland cancer	RGSLNB
Gynecologic malignancies	
Vulvar cancer*	RGSLNB
Vaginal carcinoma	RGSLNB
Cervical cancer*	RGSLNB
Endometrial cancer*	RGSLNB
Ovarian cancer	RIGS, FDGDS
Urologic malignancies	
Penile cancer*	RGSLNB
Prostate cancer*	RGSLNB, RIGS
Testicular cancer*	RGSLNB, FDGDS
Bladder cancer	RGSLNB
Renal cell cancer	RIGS
Thoracic malignancies	
Lung cancer	RGSLNB, RIGS, RGS, FDGDS
Pulmonary nodules	RGS, ROLL, RSL
Neuroendocrine tumors	
Gastroenteropancreatic neuroendocrine tumors	RGS
Bronchial carcinoids	RGS
Neuroblastoma	RGS
Pheochromocytoma	RGS
Adenocortical carcinoma	FDGDS
Sarcoma	RGSLNB
Brain tumors	RGS
Bone lesions	RGS
Lymphoma	RGS
Monitoring of isolated limb perfusion	RGS

RGS: radioguided surgery; RIGS: radioimmunoguided surgery; RGSLNB: radioguided sentinel lymph node biopsy; ROLL: radioguided occult lesion localisation; RIME: radioguided intraoperative margins evaluation; FDGDS: ^{18}F-FDG directed surgery; RSL: radioguided seed localization; SNOLL: sentinel node occult lesion localization; RULL: radioguided ultrasound lymph node localization.
* Clinical use cases with hybrid tracers also reported in literature (ICG-^{99m}Tc-nanocolloid).

Table 2.7.: Clinical applications of radioguided surgery using gamma detection technology

CHAPTER 3

Freehand SPECT

Due to the advancements in radiopharmacology and radiation detection, nuclear medicine has become an important player in medical diagnostics. Physicians inject radiolabeled tracers, that target specific body parts of the patient; radiation detectors then use the radiation emitted from these tracers to create signals and images. These radiation detectors are available in form of complex nuclear imaging systems containing several detectors on big gantries as well as in form of small and comparably simple handheld radiation counters. Most 3D nuclear imaging systems such as SPECT (Single-Photon Emission Computed Tomography) are not suited for intraoperative use due to their size as well as operating room time constraints, so they are used only for diagnosis, planning or monitoring. For intraoperative detection of the radiation, handheld radiation counters such as gamma probes or mini gamma cameras are available, but these devices often fail in more complicated clinical cases because they only provide acoustic/numeric information or only two dimensional scintigraphic images without any anatomical or spatial relevance in three dimensional space.

Freehand SPECT offers a compromise: The addition of tracking to the handheld radiation counter makes it possible to reconstruct 3D SPECT-like images during surgery with minimal alteration of the surgical workflow. Since its first introduction in year 2007 by Wendler et al. [119], Freehand SPECT has evolved from a research prototype to a commercial product, the *declipseSPECT* cart system manufactured by SurgicEye GmbH, which has received a European conformity (CE) marking and has been certified and approved by the United States Food and Drug Administration (FDA) [79].

Currently, Freehand SPECT technology is being used in several centers throughout the world for sentinel lymph node biopsies (SLNB) in various malignancies such as breast

cancer and melanoma. However, the clinical usage of Freehand SPECT is not limited to SLNB, it can be applied in most of the clinical cases in which radioactive tracers are injected prior or during surgery and detected intra-operatively using a dedicated radiation counter. Utilization of Freehand SPECT extends the conventional radiation counter's functionality, making it possible for users (e.g. surgeons) to visually and spatially distinguish among different hotspots. An extensive expert review on the Freehand SPECT technology and on its clinical use cases is given by Bluemel et al. [14] in year 2016.

This chapter is organized as follows: Section 3.1 describes individual components required for Freehand SPECT imaging in general. Thereafter, tracking and radiation detection technologies incorporated in Freehand SPECT and the declipseSPECT cart system in particular are presented in sections 3.2 and 3.3, respectively. Following that, information about synchronization of the readings provided by the components are given in section 3.4. Section 3.5 emphasizes the importance of the acquisition step to obtain Freehand SPECT reconstructions of good quality in relatively short times. Finally, mathematical details about Freehand SPECT reconstruction itself are given in section 3.6 and different variations for its visualization to the users as well as different visual scan guidance approaches in the declipseSPECT cart system are presented in section 3.7.

3.1. System Overview

Freehand SPECT technology compromises multiple components. Figure 3.1 shows the declipseSPECT cart system incorporating Freehand SPECT technology in an actual surgical sentinel lymph node biopsy procedure in the gynecology department at Klinikum rechts der Isar. The system includes a handheld gamma radiation detector (either a gamma probe or a mini gamma camera) and an optical infrared tracking system for spatial positioning, which requires two sterile tracking attachments ("targets") with retroreflective markers. One target is attached to the handheld radiation detector, in Figure 3.2 a gamma probe covered in a sterile foil, and another target is placed on the patient to serve as a reference coordinate system for all the calculations as well as to compensate for repositioning of the camera arm or for the slight patient movements such as breathing. For data acquisition, synchronization, computation of the 3D reconstruction and visualization, a PC is integrated into the housing. For enabling augmented reality (AR) visualization and providing an anatomical/visual reference for the resulting 3D reconstruction, a video camera is also mounted and calibrated accordingly. A touchscreen monitor provides visualization to the end user and supports user interaction. Commonly, an OR nurse (e.g. "circulator") or a Freehand SPECT technician operates the system based on the commands of the main

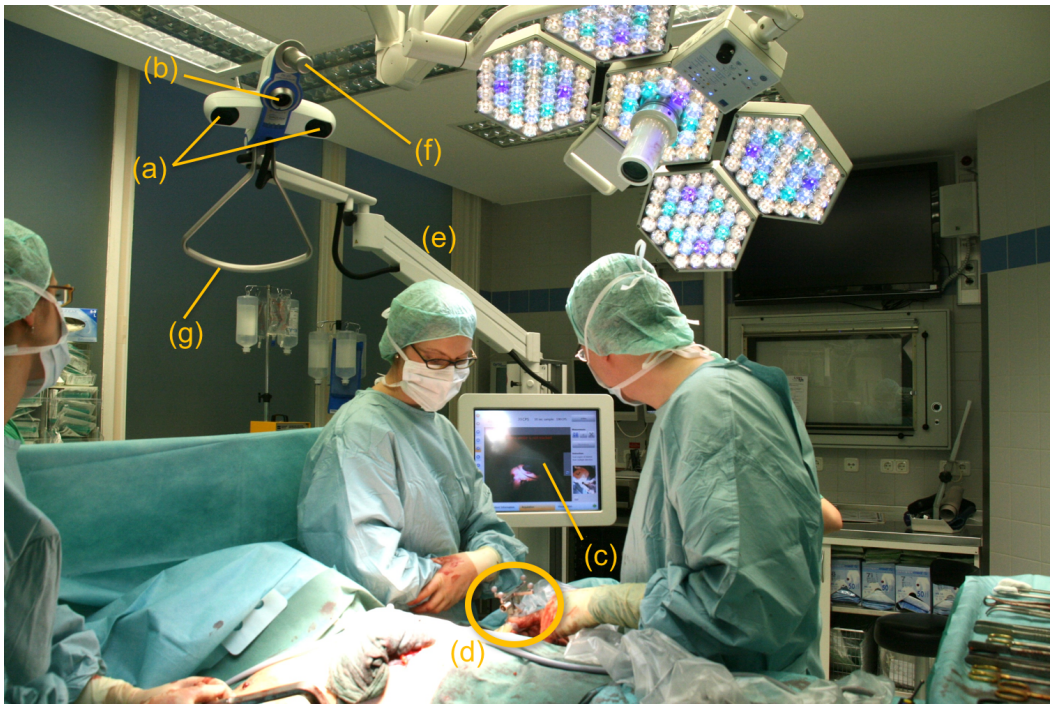

Figure 3.1.: Freehand SPECT device in the operating room. (a) Infrared tracking cameras. (b) video camera for AR visualization. (c) Touch-screen monitor for visualization and user interaction. (d) Gamma probe in a sterile foil and sterile tracking target attached. (e) Positioning arm. (f) Sterile handle. (g) Unsterile handle.

surgeon, however, if the surgeon wants to take full control of the system, the touchscreen monitor as well as one of the handles of the head of the system can be made accessible via appropriate single use sterile covers.

For many clinically relevant use cases, the Freehand SPECT system can reconstruct the volume of interest in less than one minute after scanning the targeted body region with the tracked radiation detector from at least two directions for about one to two minutes. That is why Freehand SPECT is well-suited for the operating room since it is much faster and needs fewer computational resources than conventional SPECT imaging, which requires longer time for image acquisition as well as computation of the final 3D volume. However, there is a trade off here, as the quality and accuracy of the resulting 3D reconstruction is of course much lower compared to the ones coming from a conventional SPECT/CT system, but still sufficient for many intraoperative clinical use cases where exact spatial correlation is not as important as the presence of major hot spots in reconstructed image indicating

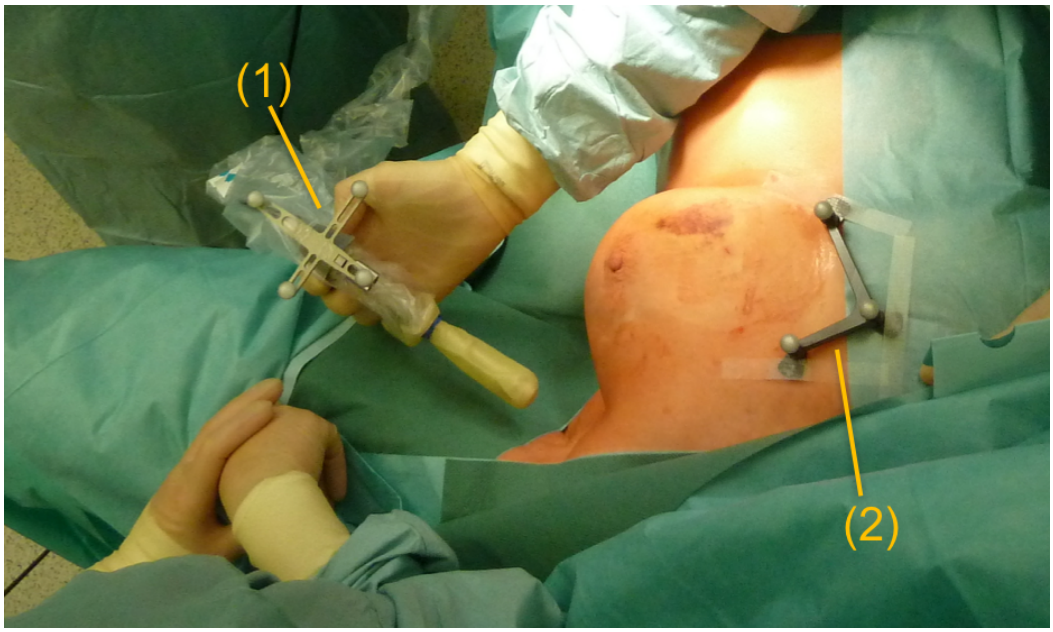

Figure 3.2.: Tracking targets of the Freehand SPECT system. (1) Sterile probe target attached to the gamma probe in sterile covering for tracking the position and orientation of the probe throughout the surgery. (2) Sterile patient target serving as a reference coordinate system for displaying the 3D Freehand SPECT reconstruction relative to the patient.

remaining radioactivity in tissue. The short distances between the detector and the target anatomy also work in favor of Freehand SPECT imaging.

3.2. Tracking

Generation of 3D reconstructions from the signals of a handheld radiation detector requires the usage of a suitable tracking technology. In contrast to SPECT imaging, where the radiation detectors are mounted inside a rotating gantry around the patient, in Freehand SPECT imaging, the surgeon moves the radiation detector in a freehand fashion and scans the targeted area as close as possible while covering multiple angles. Based on the radiation detectors's positions and orientations determined by the tracker, Freehand SPECT system can use iterative image reconstruction techniques to generate 3D images showing the radiation distribution in the scanned volume of interest.

Two tracking technologies are relevant for tracking tools or objects in an non-robotic

intraoperative surgical setting: Electromagnetic tracking and optical tracking. They both are commonly used in various surgical navigation systems [12, 31]. Please note that are also some commercial and non-commercial intraoperative navigation solutions available which are based on mechanical or robotic tracking technology, however, for the initial development of Freehand SPECT this approach was ruled out, most probably because it would make the final system bulkier and more cost intensive. Furthermore, it would complicate its handling and acceptance by the end users and it is against the "freehand" nature.

Both optical and electromagnetic tracking technologies are evaluated repeatedly in literature and are reported having comparable technical accuracies under optimal experimental setups. However, due to their advantages and disadvantages in different scenarios, the selection of the suited tracking technology very much depends on the working environment itself and the additional tools and devices present and further requirements of the actual clinical use case [12, 60]. A perfect example for this is Freehand SPECT. Incorporation of electromagnetic tracking instead of optical tracking could be considered to overcome the line-of-sight problem, which may occur during surgery due to bad positioning or occlusions. Nevertheless, during the development of Freehand SPECT, electromagnetic tracking was also tested but was considered as not suited due to high tracking errors for gamma probe positioning encountered. The presence of metallic materials can be the cause of the distortions in the magnetic field. Furthermore, magnetic fields generated by photomultiplier tube based gamma radiation detectors may also interfere with the electromagnetic tracking. In contrast to this, this would not be an issue for optical tracking, regardless which kind of gamma detector is being used for the Freehand SPECT imaging. [121].

Due to its satisfying tracking performance (20 Hz update rate, 0.25 RMS volumetric error) inside the tracking volume (Tracking area of 491 x 392 mm2 at minimal operating distance: 557 mm, maximal operating distance: 1336 mm), also due to its comparably small size (273 mm x 69 mm x 69 mm) and light weight (0.80 kg), *Polaris Vicra*® (manufactured by Northern Digital Inc.) is perfectly suited as the tracking camera for Freehand SPECT imaging and is incorporated in the commercial product *declipseSPECT* of SurgicEye GmbH since its launch. In the scientific community, robotic tracking is also used instead optical tracking for Freehand SPECT modality in experimental setups [38, 113, 34], but yet without any transition into patient studies.

3.3. Radiation Detection

Previously in section 2.4 the technical background for gamma radiation detection is introduced and discussed. Theoretically speaking, every handheld radiation detector system which is certified and clinically approved for intraoperative usage, can be considered for Freehand SPECT imaging. For the introduction of Freehand SPECT imaging in a new operating theatre, of course it is best to utilize the same gamma radiation detector system, which is already available und is being used for radioguided surgery, especially for better acceptance by the surgeons and minimal alteration of the surgical workflow. However, this may not be straightforward or sometimes not even possible. In order to be able to utilize a handheld gamma probe or gamma camera system for Freehand SPECT imaging, the device needs to provide an output for real-time reading of the detected counts, which are then processed by the workstation directly to compute the 3D reconstruction. As handheld gamma radiation detection systems are commonly sold as standalone products for the intraoperative use only, they do not necessarily come along with such an interface as standard. Because of that, during the initial development of Freehand SPECT imaging, Wendler et al. investigated several different gamma probes on the market and collaborated with some manufacturers for customizations in their product either to provide a gateway for detected counts per second as processed by the controlling unit directly or to provide a direct access to the raw readings in real-time [121]. For the former, Node Seeker® gamma probe system (NodeSeeker 800, Intra Medical Imaging LLC, Los Angeles, CA, USA) is an example. Here, the energy calibration has to be done directly at the controlling unit since the readings provided to the workstation of Freehand SPECT are preprocessed and depend on these calibration settings. However, if the raw signals can be read from the controlling unit of the gamma detection system directly, then the energy calibration needs to be done at the workstation of the Freehand SPECT system. For this, a data acquisition card needs to be integrated into the system to sample the analog signal provided by the controlling unit of the gamma detector. [121].

At the commercialization of the Freehand SPECT technology, SurgicEye GmbH followed the latter approach and signed an agreement with the gamma detector manufacturer Crystal Photonics GmbH in Berlin, Germany. The controlling unit in both version SG03 and SG04 of the Crystal Probe gamma detection system (Figure 3.3) provide an output for the analog signal which then is processed via a PicoScope® (Pico Technology Ltd., Cambridgeshire, United Kingdom) prior passing it to the reconstruction algorithm. As standard, sampling time is set to 1 μs, sampling range is set from -5V to 5V and the trigger threshold is set to 1V. Before applying for Freehand SPECT imaging, the gamma

probe needs to be calibrated by setting a low and a high threshold for the energy window of the targeted radionuclide for assuring a good energy resolution and for eliminating scattered gamma rays. This is done by pointing the probe to a radiation source and measuring over some time. At the calibration routine of the commercial software of declipseSPECT cart system, a real-time visualization of a histogram of the detected counts for different energy channels allows the end user to set these thresholds easily when expected energy peaks of the radionuclide become clearly visible. Furthermore, the sampling and trigger parameters can be fine-tuned as well, if needed.

Figure 3.3.: Crystal Probe gamma radiation detection system in declipseSPECT. Left: Controlling unit SG03. Right: High-energy and standard straight gamma detection probes with interchangeable collimators.

The partnership with Crystal Photonics also allowed SurgicEye to have access to an early prototype of the CrystalCam handheld gamma camera to contribute to its development as well as to improve the acquisition process and the reconstruction algorithm for the FreehandSPECT imaging (Figure 3.4). In contrast to the gamma probes of Crystal Photonics, which are based on thallium-activated cesium iodide (CsI(Tl)) scintillation crystals, the CrystalCam is based on cadmium zinc telluride (CdZnTe) semiconductor technology. Because of that, the camera does not need a controlling unit as their gamma probes and has a USB connector for digital data transfer. This is beneficial since it eliminates the need of an oscilloscope component such as PicoScope® for digitalization of the signal. For the visualization of the 2D camera image alone, Crystal Photonics provides simply a regular laptop with preinstalled software to which the camera is attached via the USB

port, if sold as standalone product. The CrystalCam has 256 pixels on a 16x16 grid, with a combined area of 40x40mm^2 and only weighs about 800 grams including the shielding and the $11mm$ low energy high sensitivity (LEHS) collimator. Furthermore, it has a energy range of 40 keV to 250 keV and is perfectly suited for the detection of 141 keV gammas of Technetium-99m (^{99m}Tc), the most commonly used radionuclide for radioguided surgery. In addition, the camera comes along with two interchangeable parallel hole tungsten collimators, one with $11mm$ (LEHS) and one with $22mm$ depth (LEHR: low energy high resolution). For energy calibration of individual pixels of the camera, a flat field calibration phantom is also provided by the manufacturer, which can be filled up with radioactive fluid such as ^{99m}Tc with known activity and volume to produce a homogenous flat radiation source.

Figure 3.4.: CrystalCam handheld gamma camera in declipseSPECT Imaging Probe.

Due to advantages above and increased detector field of view, the latest version of the declipseSPECT system includes CrystalCam handheld gamma camera as the radiation detector and is called the *declipseSPECT Imaging Probe*.

3.4. Synchronization

Proper synchronization of the spatial information acquired by the tracking camera and radiation counts measured by the radiation detector is very important for the success of the

Freehand SPECT technology. An improper synchronization, an unknown offset between the signals from these two sources or a wrong calibration could result in artifacts in the reconstructed image which could easily be clinically misinterpreted by the end users. Signals coming from different sources may have different speeds / refresh rates which also needs to be taken into account.

The synchronization of the signals for Freehand SPECT imaging is achieved by ring buffers and timestamp matching [121]. Upon arrival and parsing of packages, a timestamp is added before storing the information in a ring buffer. If one source (e.g. tracking system) sends packages faster than the other (e.g. gamma probe), then the closest timestamp of the faster signals is matched to the latest timestamp of the slower source. Via timestamps, fixed known delays in any of the signals can also be easily compensated by subtraction.

Addition of timestamps is not only useful for synchronization of the data for reconstruction of the Freehand SPECT image right after the acquisition or during the surgery, but it also allows an offline mode for loading previous patient acquisitions for further evaluations using different reconstruction parameters and settings.

3.5. Acquisition

Acquisition is the most crucial step for the success of Freehand SPECT imaging. Better hardware components to increase computational power, better radiation detectors, better shielding and better models may all be considered for achieving increased reconstruction quality and increased usability for Freehand SPECT. But this would be no use if the acquisition itself is not good enough and does not cover the region of interest from various angles to provide enough angular information for the reconstruction of a 3D image. In case of laparoscopic Freehand SPECT, there is an additional physical constraint due to the pivot point at the trocar limiting the range of motion significantly. Because of all that, acquisition is the part which is very much dependent on the knowledge and experience of the user. The acquisition quality may differ from a novice to an expert user remarkably. In clinical usage of Freehand SPECT, it is almost impossible to compare acquisitions of different users among each other under exact same circumstances, since time is limited and every patient can only be scanned by one single operator.

Optimization of scan trajectories to obtain good reconstructions with the minimum set of measurements is a hot topic of research. In order to define scanning protocols for different clinical indications, researchers first replicate a typical clinical use case by phantoms and do repeated experiments with different operators and different scanning patterns. Only after evaluation of these experiments, scanning guidelines are defined for the clinical usage

and human operators (surgeons or nuclear medicine physicians) are instructed accordingly during their initial trainings. By such phantom experiments, the impact of the operator experience can also be directly observed, such as in our study published in [37], where one expert and two novice operators scan the same phantom under same conditions and the expert scans result in significantly better Freehand SPECT reconstructions.

Trajectory optimization problem can also be addressed mathematically on the underlying iterative reconstruction problem and can be validated by computer simulations and robotic experiments [113]. This involves however much more effort, resources and computational power and the resulting trajectories may be even very complex scanning patterns which are not really suited for usage by human operators inside the operating room.

3.6. Reconstruction

After the completion of the acquisition, the measurements are processed by an iterative solver, since we are dealing with an inverse problem, which cannot be solved directly. Here we need an algorithm to approximate the solution first and then improving it via multiple iteration steps as it is typical in various imaging modalities such as SPECT or PET. Of course, compared to analytical (direct) solvers, iterative solution techniques require higher computational resources, but can be applied in a wider context since they allow reconstructions with even small set of non-uniform and sparse projections. Also, it takes into account the probabilistic nature of the problem.

This is the case for the Freehand SPECT imaging. The first step is the discretization of the problem. The isotropic voxelsize and the size of the volume of interest (VOI) -the actual reconstruction volume in voxels- needs to be specified at first. The voxelsize is set to $5mm$ per default for each dimension in the *declipseSPECT* cart system but depending on the maximum tolerable reconstruction duration for the actual clinical use case and available computational resources, this setting can be fine-tuned.

After the discretization, we assume there is a linear relation between the reconstructed volume and the projections (measured count rates of individual gamma detectors at their synchronized position and orientation), so that the problem of reconstructing an image from projections can be stated as the problem of solving a linear equation system as below

$$A\vec{x} = \vec{y}$$

where $\vec{x}$ is the vector representation of the discretized reconstruction volume in n isotropic voxels and $\vec{y}$ is the vector of m measurements. The mapping between them is the so-called *system matrix* A of dimension $m \times n$, where each row corresponds to one projection and

each column corresponds to one voxel of the reconstruction volume. The rows of the system matrix are calculated for each measurement by using the known *model* of the gamma detector and the synchronized position and orientation of the detector. Each element A_{ji} of the system matrix A describes the linear contribution of each volume element x_i to each projection element y_j.

The creation of a more accurate model of the gamma radiation detector or the usage of a even better gamma radiation detector is expected to influence the iterative reconstruction process positively and is therefore another topic of research interest. If the specifications of the used gamma detector are known beforehand, then an analytical model based on the shielding, geometry and physical properties of the detector can be obtained [44, 43, 96]. This can be applicable for relatively simple detectors such as a (straight) gamma probe with a single detector (crystal) and symmetrical shielding around it.

In more sophisticated gamma detector systems, computer simulations can be used to generate a simulated model instead. These are so-called Monte Carlo simulations, which rely on repeated random sampling to solve deterministic problems [69]. Another approach to generate such a model is directly measuring the response of the gamma detector in 3D space in respect to a known radioactive point source. This can be achieved by placing the gamma detector and the point source on a positioning table, moving them systematically in respect to each other in 3D space and measuring the radiation counts in each spatial configuration for a predefined exposure time [43, 70, 38].

For Freehand SPECT, mini gamma cameras can also be used as radiation detector systems, which can be considered as a 2D array of individual detectors. A gamma camera is so to say k gamma probes placed on a 2D grid working simultaneously. Every pixel value of the 2D gamma camera image represents the counts detected of that particular detector pixel k. When using tracked mini gamma cameras for Freehand SPECT imaging, an appropriate model is required for *each* detector pixel k to generate the system matrix accordingly. At every acquired gamma camera image, every pixel value is then considered as individual projections with different detector models for the linear equation system $A\vec{x} = \vec{y}$. It is simpler in case of imaging with gamma probes since there is only one radiation detector to be modeled ($k = 1$).

Look up tables (LUT) can be used to speed up the generation of the system matrix and are the only possibility for reconstructions with complex detectors which can only be modeled via simulations or direct measurements. Each row of the system matrix is then calculated by interpolation of the closest entries in the look up table of the detector k corresponding to the relative position of the voxel x_i to the gamma detector k during that particular measurement.

After creation of the system matrix, it is filtered before starting with the iterative algorithm. The rows which are completely zero are removed as they represent measurements outside the reconstruction volume and therefore not relevant. Furthermore, rows with row sums below a predefined small threshold $t_r > 0$ representing measurements with little relevance as well as columns with column sums below a predefined small threshold $t_c > 0$ representing voxels in the reconstruction volume with little scan coverage are also removed to improve the numerical stability of the solution and the quality of the final reconstructed image [38]. In addition to these, a carving inside the reconstruction volume can also be applied by removing any voxels intersecting with the gamma detector itself during the acquisition, as these voxels cannot be inside the object of interest (patient or phantom) [121]. For notational simplicity, the filtered versions of A, $\vec{x}$ and $\vec{y}$ are still called the same along with their respective sizes n, m [62].

The particular reconstruction algorithm employed in Freehand SPECT imaging is Maximum Likelihood Expectation Maximization (MLEM), which is first introduced by L.A. Shepp and Y. Vardi in year 1982 [97]. This statistical method includes the randomness of radioactive decay in the reconstruction pipeline by assuming each voxel in the volume to be an emitter according to a Poisson distribution. The process of projection j detecting emissions from voxel i is modeled using a Poisson process, denoting the detection probability as

$$p(i,j) = P[\text{detected in projection } j | \text{emitted from voxel } i].$$

These $p(i,j)$ are so to say just another representation for the the entries a_{ji} of the system matrix A.

An approximated solution is computed iteratively for iteration index $q \in \mathbb{N}$ and all voxels $i \in \{1, \ldots, n\}$ of the reconstruction volume

$$x_i^{q+1} = x_i^q \cdot \frac{1}{\sum_j p(i,j)} \sum_j \frac{y_j \cdot p(i,j)}{\sum_i x_i^q \cdot p(i,j)}.$$

For the first iteration, the reconstruction volume is considered as a matrix of ones so that its vector representation $\vec{x}^0$ is defined as $\vec{1} \in \mathbb{R}^n$ for Freehand SPECT reconstructions [70, 38].

As mentioned previously in section 3.5, the quality of the Freehand SPECT reconstruction very much depends on the quality of the acquisition. For example, if an inexperienced operator scans the volume of interest only from one direction, it is expected that the final reconstruction would have a large deviation from the exact solution of the reconstruction problem, leading to artifacts or inaccurately reconstructed hotspots in the final 3D

Freehand SPECT image. Therefore, proper angular coverage is essential to improve the numerical stability of the problem.

Further details about iterative reconstruction techniques in general and the reasons behind the selection of MLEM as the reconstruction method for Freehand SPECT patient studies can be seen in [62]. For research purposes, other reconstruction strategies such as List-Mode Expectation-Maximization (LMEM) are also considered for Freehand SPECT imaging recently especially for addressing the reconstruction problem by more challenging clinical use cases such as the precise reconstruction of the cold and hold hotspots in a realistic thyroid phantom [38]. However for all real patient scans up until now, the commercial product *declipseSPECT* is used which employs MLEM since its introduction regardless if gamma probes or gamma cameras are used as the tracked radiation detector.

3.7. Visualization

Besides the capability of generating 3D SPECT-like images from 1D or 2D signals coming from tracked handheld radiation detectors, another major advantage over other comparable intraoperative nuclear imaging devices is the addition of an optical video camera allowing an Augmented Reality (AR) visualization (Figure 3.1). The head of the declipseSPECT cart system, which is the commercial product by SurgicEye GmbH facilitating Freehand SPECT technology, is designed and constructed in a way so that the optical video camera required for the AR visualization and the optical infrared stereo camera required for tracking are rigidly mounted together and only a one-time calibration after the assembly of the cart is sufficient for assuring precise augmentation [79].

Since the beginning of the initiation and development of Freehand SPECT concept, AR was an essential component, even though the main objective of the research was the mathematical modeling and solution of the 3D reconstruction problem based on radiation readings of tracked gamma probes. In contrast to displaying only section images (2D planes of the 3D volume) and scrolling through them as it is typical 3D volumetric medical data visualization, AR allows the end users e.g. physicians to have a direct spatial reference, as the reconstructed volume is directly overlaid on the patient. Another reason for integration of augmented reality can be the fact that Prof. Navab himself and his group CAMP at TUM bring along considerable prior experience for AR in industrial and medical applications, which they easily could adapt into this new research area.

Until the commercialization of the technology by SurgicEye GmbH under the product name of *declipseSPECT*, augmented reality was the only choice for visualization of the reconstructed 3D volume of radiation distribution in the scanned area. As seen in Figure 3.5,

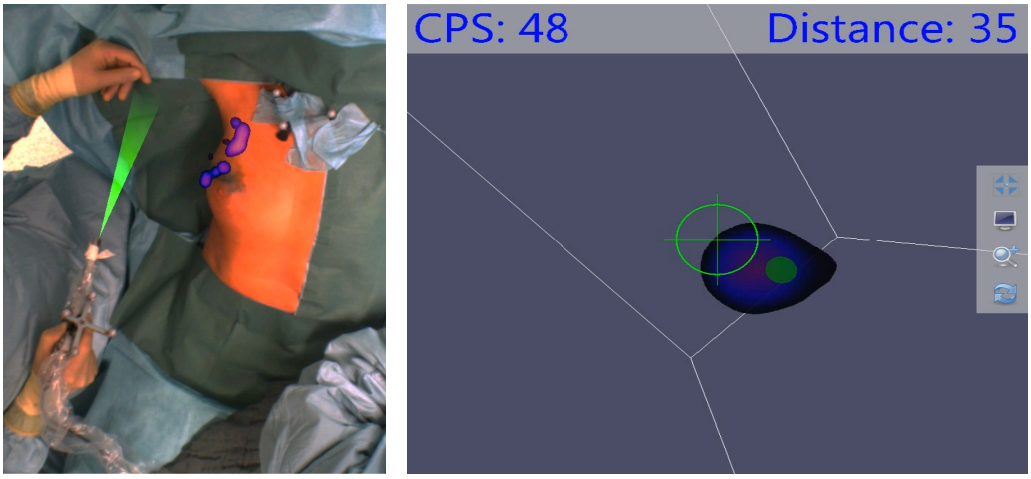

Figure 3.5.: Visualization of a 3D Freehand SPECT reconstruction. AR mode (left): The reconstruction is overlaid on the patient. The surgeon can distinguish between the lymph nodes and the injection site based on their anatomical locations. VR mode (right): The surgeon sees the reconstruction from the radiation detectors's view and moves the detector around to navigate inside the volume.

this viewing mode allows the users to relate to the anatomy of the patient and distinguish hot spots from injection site, background radiation or artifacts depending on the clinical indication and targeted anatomy. However, it is highly dependent on the position of the camera and therefore it can be confusing to the user in some circumstances. Furthermore, it does not reveal the full benefit of 3D imaging as it does give exact depth information.

To compensate for these deficiencies, an alternate viewing mode is included in declipseSPECT: a pure virtual reality (VR) visualization of the 3D reconstruction as seen from the radiation detector's view. Using this so-called *3D-view mode*, users can see the 3D volume from different angles and distances simply by moving the radiation counter around. Furthermore, it allows depth measurements. For example, the surgeon can measure the distance to a reconstructed hotspot from different positions and can plan the incision on the skin based on these findings. The availability of two viewing modes improves the system's flexibility because the surgeon can choose the appropriate visualization mode based on the current surgical conditions.

AR is not only used for the visualization of the final 3D Freehand SPECT reconstruction, it is also applied for acquisition guidance during the scanning phase. As previously mentioned in section 3.5, the scanning pattern has a major influence on the quality of the

resulting reconstructions. The scanning person should pay attention to cover the region of interest fully from at least two (preferably orthogonal) directions, which is pretty difficult to assure in operating room conditions. The surgeons tend to scan the area quickly without changing the orientation of the detector, so proper guidance and feedback about the quality of the covered area is essential in order to generate reliable Freehand SPECT images.

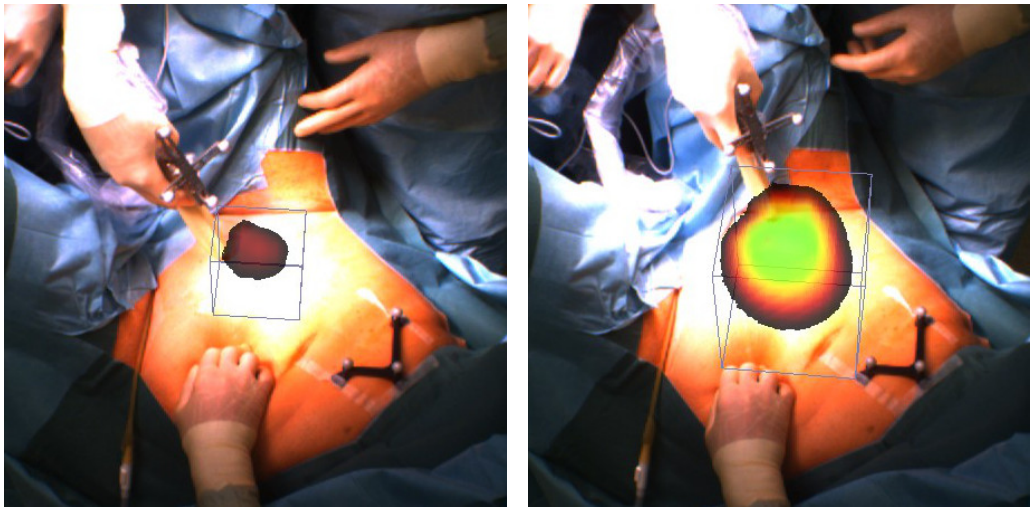

Figure 3.6.: AR visualization during a Freehand SPECT acquisition (declipseSPECT with gamma probe). Color augmented over the video image shows the amount of information collected on the region: green/yellow = sufficient information, red/black = insufficient information, white wireframe visualizes the computation volume whose size is adjusted on-the-fly during the acquisition.

In declipseSPECT, the AR acquisition guidance is realized by visualization of the surgical site as seen from the optical camera with an augmentation of the volume of interest as a wire frame in white and a color-indexed visualization of how much information each voxel in the volume received during the acquisition (Figure 3.6). As the scanning continues and as the user covers multiple angles and positions, the overlay grows bigger and turns from black/red to yellow/green, indicating the volume of interest is covered sufficiently.

In the latest version of declipseSPECT system, which is called *declipseSPECT Imaging Probe* system and which incorporates a optically tracked mini gamma camera as radiation detector instead of a gamma probe, a different AR acquisition guidance is implemented. Here, instead of a color-indexed coverage visualization, a simpler approach is followed. At the beginning of the scan, the whole volume of interest is overlaid in opaque white and as

the user scans the volume of interest, it gets slowly transparent. The user scans the region of interest from multiple directions and knows the collected data is sufficient, when he/she can see the targeted area on the camera image without an opaque overlay (Figure 3.7).

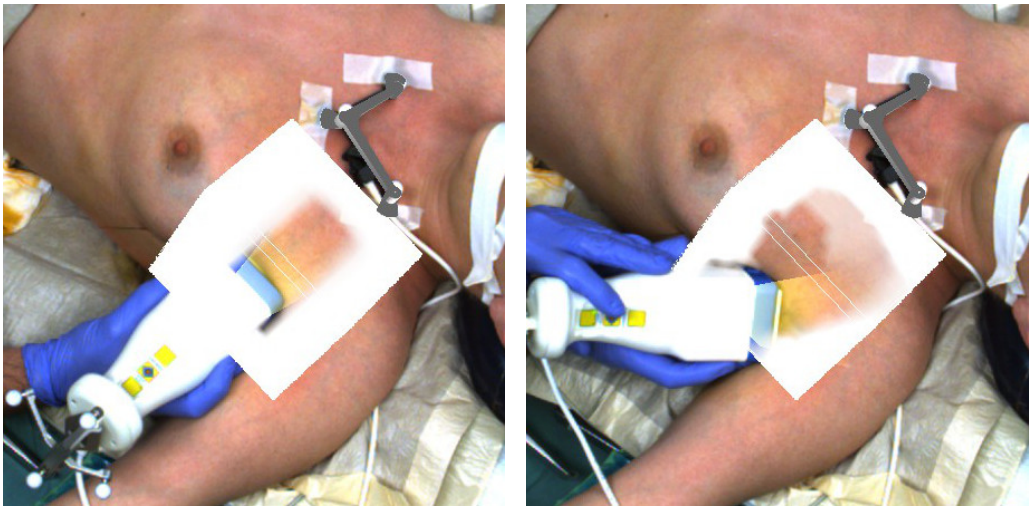

Figure 3.7.: AR visualization during a Freehand SPECT acquisition (declipseSPECT Imaging Probe with gamma camera). The size of the volume of interest is predefined depending on the indication. User places the gamma camera at the center of the area to be scanned and starts the acquisition. The augmentation gets transparent as the user scans the area.

Part II.

Contributions

CHAPTER 4

Human Component in Freehand SPECT Imaging

This chapter presents the contributions concerning post-operative *user* driven analysis and evaluations for Freehand SPECT imaging, which are based on the automatically generated performance log files by the system during the actual surgical procedure.

Due to its "freehand" nature, the Freehand SPECT experience is very much dependent on the *human* operator, so different users or user groups may benefit from this technology differently. In addition, since its first introduction, Freehand SPECT imaging technology brings Augmented and Virtual Reality concept into the operating room, as it incorporates monitor-based Mixed Reality visualization of the 3D reconstruction of the radiation distribution in the scanned region.

The analysis of the automatically generated performance log files gives the opportunity to investigate the usage characteristics of these augmented reality (AR) and virtual reality (VR) visualization modes by different user groups. In addition, these device and performance log files synchronized via timestamps can also be used to automatically detect major surgical workflow transitions if some features of the system are only available and used in specific workflow phases. Moreover, comparison of pre-incision and post-excision scan trajectories in patient target coordinate system as well as the amount of lost tracking signals during acquisition phase as recorded in these log files can be beneficial to identify some usage problems related to tracking and handling of the system.

This chapter is organized as follows: Section 4.1 introduces the advancements in the field of medical augmented reality and outlines the motivation behind our work. Thereafter, the necessary materials and methods for the studies performed are explained in section 4.2 in detail. Following that, the results are presented in section 4.3 and discussed in section 4.4.

Substantial parts of this chapter have already been published in the following article and are partially quoted verbatim (especially sections 4.1, 4.2.1, 4.2.4, 4.3.1, 4.3.2, 4.4):

[83] **A. Okur**, S.-A. Ahmadi, A. Bigdelou, T. Wendler, and N. Navab. MR in OR: First analysis of AR/VR visualization in 100 intra-operative Freehand SPECT acquisitions. In *Proceedings of the 10th IEEE International Symposium on Mixed and Augmented Reality (ISMAR)*, pages 211–218, Basel, Switzerland, 2011.

4.1. Introduction

Medical Augmented Reality (AR) is a much researched field, with numerous publications on hardware and technology [33, 122, 87, 123], visualization [99, 55, 56, 101], usability studies [57, 21, 81, 35] and experimental work [80, 107]. While many previous publications created excellent insight for the community on how to achieve realistic blending of real-world information with virtual data, the actual application of these technologies has often been limited to laboratory setups [122, 115] or limited real-life studies, e.g. on very few selected cases [80] or cadaver and phantom studies [114].

In the first study included in this chapter, observations and data analysis are presented for the first time in the AR community concerning the usage of a commercially developed and clinically approved surgical navigation system, which incorporates monitor-based Mixed Reality (MR) visualization during real-life surgeries. The usage of interchangeable Augmented and Virtual Reality (VR) visualization modes by the surgical team are analyzed and observations in over 100 Freehand SPECT acquisitions within different phases of 52 sentinel lymph node biopsy surgeries are reported.

Perhaps the only comparable study in medical AR community prior to this work is the study of Wang et al., who reported on the usage of CamC [80], a prototype system used during a limited round of early clinical trials [114, 116]. In that study, approximately 40 cases in which a camera-augmented mobile C-arm X-ray system was used intraoperatively, were documented and analyzed. A workflow-oriented study was used to reveal that radiation exposure can be significantly reduced in specific workflow steps, due to the augmentation of the X-ray image with a real-time camera video stream. These steps, such as patient localization, skin incision placement or tool posture adaptation, are common to many surgical procedures. Thus, due to the study, very specific advantages of AR visualization modes were found, sometimes unexpectedly, for particularly common workflow steps.

Here, a similar approach is followed, where the usage of a different device is reported,

which shares the possibility to augment the real-world image with virtual information, visualized on a monitor. The Freehand SPECT system, allowing flexible 3D reconstructions of radioactive emissions from the tissue marked by specific tracer substances, combines a regular, hand-held radioactive counter, namely a gamma probe, with an optical tracking system (cf. chapter 3). The acquisition is performed in a freehand motion, i.e. without restricted or prescribed hand motion patterns, upon which an approximation of the emitting source is calculated in 3D. Two main view modes allow the users to interact with the Freehand SPECT system. One view, the augmented reality (AR) view, offers an overview of the surgical site to the user, by projecting the 3D reconstruction on the video image of the body. The second view, or virtual reality (VR) view, is a purely virtual visualization of the 3D reconstructed radiation distribution from the view of the gamma probe, without visual reference to the anatomy. The Freehand SPECT technology and its components as well as the two separate visualization modes, including their appearance and motivation were presented in more detail previously in chapter 3 and in section 3.7, respectively.

The first study for AR/VR usage presents the natural interaction of the surgical staff with the two view modes. *The particularity of the study and also one of the main contributions is that no individual interacting with the system was informed about the intent of creating this study, nor about the originally intended usage of the two view modes. The interaction with the system was left deliberately uninfluenced and thus inherently unbiased.* In fact, the purpose of the 13-month usage period was to investigate how users interacting naturally and in an unbiased manner with the system, would utilize the view modes and under which circumstances. In order to formalize the study, the observation is tied to a particular workflow step, namely the reconstruction of the radioactively labeled lymph nodes before incision and after excision of sentinel lymph nodes during sentinel lymph node biopsies.

In this particular study, the analysis of the log files provided by the Freehand SPECT system is limited to one feature of the system only, namely the visualization modes for the 3D reconstruction, especially since this is the component which makes the Freehand SPECT system highly relevant for the AR community. This analysis is not automatic, since it is based on manual counting of AR/VR screenshots by the human evaluators due to the lack of an automatic user interaction log file provided by the Freehand SPECT system. However, the Freehand SPECT system also provides additional files such as tracking or activity log files, which can be useful for development of algorithms to automate such an analysis for usage characteristics for different users or user groups. Thanks to the collaboration with the manufacturer, for a second study, the automatic logging of the Freehand SPECT system was improved so that other possibilities for further analysis via such device and performance log files could be demonstrated on another set of Freehand SPECT data

enclosing 19 sentinel lymph node biopsy surgeries for breast cancer.

The workflow steps and the difference between pre-incision and post-excision scans are explained in the following thoroughly in subsection 4.1.1. Subsections 4.2.1 and 4.2.2 highlight the specifications of the particular Freehand SPECT system used for both of the studies presented in this chapter and reveal the details about the automatic device and performance logging included. Furthermore, in subsection 4.2.3, precautions required and taken while working with personal information in medical records in general and with Freehand SPECT data including device and performance log files in particular are described and the importance of data anonymization is emphasized.

Due to the workflow-oriented analysis for AR/VR usage by the surgical crew introduced in subsection 4.2.4, we are able to report on observations and draw conclusions from them as presented in subsections 4.3.1 and 4.3.2, one of them being that with a significant tendency, that the users prefer one of the two view modes over the other for certain atomic sub-tasks. A first approach on the automation for similar user-driven analyses based on Freehand SPECT logging is introduced in subsection 4.2.5 and the associated results of this second study are presented in subsection 4.3.3. Finally, the results and observations are discussed in the subsection 4.4, especially in respect to the relevance of the findings for the medical AR community.

4.1.1. Surgical Workflow

The sentinel lymph node biopsy technique for radioguided surgery was previously introduced and explained in detail in subsection 2.6.1.

For sentinel lymph node biopsy (SLNB) procedures within our university hospital in general, gamma probe-guided localization is applied in routine using Technetium-99m-nanocolloid as the radiotracer and conventional gamma probes for radiation detection. Depending on the indication, injection of an additional coloring material before incision is also used in combination to assure a visual verification of the SLN and to achieve better SLN detection rates. A simplified workflow of the SLNB procedure only under gamma probe guidance is shown in Figure 4.1.

In the first clinical studies in our university hospital where Freehand SPECT was used intraoperatively [16, 75], the surgical workflow had to be modified (Figure 4.2). Before starting with the surgical procedure, a Freehand SPECT scan is done and the reconstruction is visualized on the monitor to be interpreted by the users. The incision is made based on the readings of the gamma probe as well as according to the reconstructed 3D Freehand SPECT image. After the incision, the sentinel lymph nodes are localized either only using

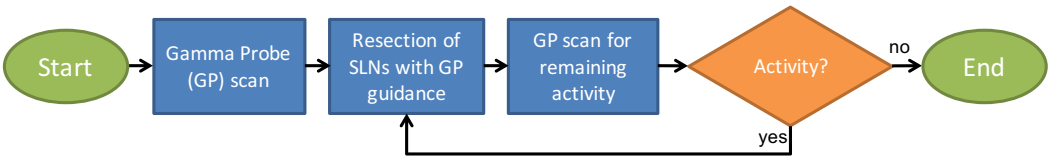

Figure 4.1.: Basic Workflow of a SLNB procedure without Freehand SPECT

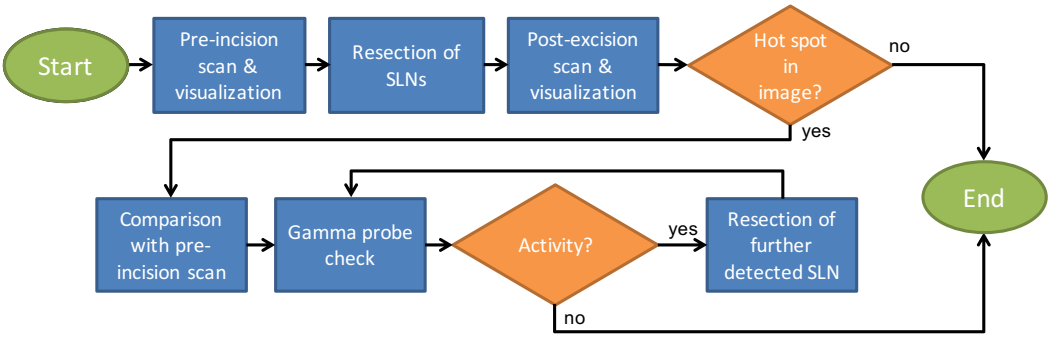

Figure 4.2.: Basic Workflow of a SLNB procedure with Freehand SPECT

the acoustic signal of the gamma probe or in combination with the 3D navigation Freehand SPECT system provides, if needed. After the sentinel lymph node(s) are removed, another Freehand SPECT scan is done for quality assurance of the surgery. If a further hot spot is detected, then the reconstruction is compared with the pre-incision image and the shown hot spot is also checked with the gamma probe to determine if it is another potential sentinel lymph node or just an artifact in the post-excision image. Further detected lymph nodes are also to be removed until the surgeon is sure that there is no relevant remaining activity in the volume of interest. In case of an additional but hard-to-resect lymph node, the surgeon might decide to leave it inside, if the sentinel lymph node(s) with major uptake were resected already.

4.2. Materials and Methods

4.2.1. System Description

Freehand SPECT system used in this work was an early prototype of the *declipseSPECT* cart system (SurgicEye GmbH, Germany), which includes a *Gamma-Probe System* gamma detector (Crystal Photonics, Germany) for radiation detection and a *Polaris Vicra*® infrared optical tracking system (Northern Digital, Canada) for spatial positioning. The sys-

tem presents an tracking accuracy of 0.25mm RMS within the tracking volume (approx. 50x50x50 cm^3). The tracking error at the tip of the instruments is below 1mm and the overall accuracy of the system including image reconstruction lies at 5mm. As previously described in section 3.1, the system also incorporates a touch-screen monitor for visualization and user-interaction as well as video camera for augmented reality visualization.

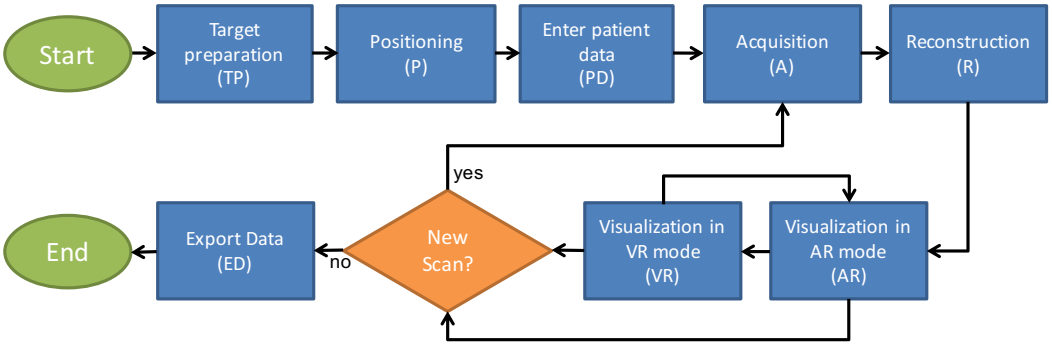

Figure 4.3.: Device workflow of the Freehand SPECT system.

Freehand SPECT device workflow stage	TP	P	PD	A	R	AR	VR	ED
AR view	no	no	no	yes	no	yes	no	no
VR view	no	no	no	no	no	no	yes	no
Probe target	yes	yes	no	yes	no	no	yes	no
Patient target	yes	yes	no	yes	no	yes	yes	no
Monitor interaction	no	no	yes	yes	no	yes	yes	yes
Positioning arm	no	yes	no	no	no	no	no	no

TP: Target preparation; P: Positioning; PD: Enter patient data; A: Acquisition; R: Reconstruction; AR: Visualization in AR mode; VR: Visualization in VR mode; ED: Export Data.

Table 4.1.: Key components involved in the particular device workflow stages.

The device workflow and the key components involved in the particular device workflow stages are shown in Figure 4.3 and Table 4.1 respectively. In *target preparation* phase, the gamma probe is covered with a sterile foil and a sterilized tracking target is attached to the probe. Disposable sterile tracking spheres are then attached to both the probe and the patient targets to assure the optical tracking. Later, in *positioning* phase, the Freehand SPECT system is positioned in such a way, that the camera head of the system has the best field of view with respect to the region to be scanned, i.e. with the least amount of occlusions and

without disturbing the sterile OR crew in their standard workflow. Furthermore, the patient target is placed on the patient in such a position so that it can be tracked by the camera head continuously. In *enter patient data* phase, the circulator or the Freehand SPECT technician enters the patient ID as well as the name and birthday of the patient to the system. After entering the patient data in the device database, the Freehand SPECT acquisition can be started. In this *acquisition* phase, only the AR visualization is available, which is used to guide the scanning person during the scanning process (Section 3.7, Figure 3.6). After acquiring enough measurements, which is approximately after 2 minutes of scanning from multiple positions and directions, the system switches to *reconstruction* phase, where the device computes the 3D reconstruction of the radiation distribution. This reconstruction is then visualized on the monitor first in AR mode. However, in the *visualization* phase, there are actually two different view modes available for the users (Figure 4.4). For easier and better interpretation of the reconstructed volume, the parameters such as threshold and filtering for the visualization can be adjusted in both viewing options. After the proper visualization, the users can either go back to *acquisition* phase and make another Freehand SPECT scan of the patient, e.g. the post-excision scan for quality assurance as mentioned in the previously (subsection 4.1.1), or they can switch to *export data* phase and export all the relevant data (subsection 4.2.2) to an external drive via USB and close the application.

4.2.2. Device and Performance Log Files

For each acquisition, the Freehand SPECT system (declipseSPECT cart system) used in our university hospital in Klinikum rechts der Isar, generates a folder with the following log files, which are synchronized via numerical timestamps.

- *activity.txt*: Radiation counts detected by the gamma detector.
- *tracking.txt*: Position and orientation of the reference targets used during surgery in infrared optical tracking camera coordinates.
- *settings.xml*: An XML file used by the system containing device information and all of its settings for the Freehand SPECT acquisition.
- *screenshotXXX.jpg*: Screenshots showing the surgical site from the view of the video camera overlaid with augmented reality information (XXX: three-digit counter). These are generated only one for every 5 seconds to save storage and computation resources.

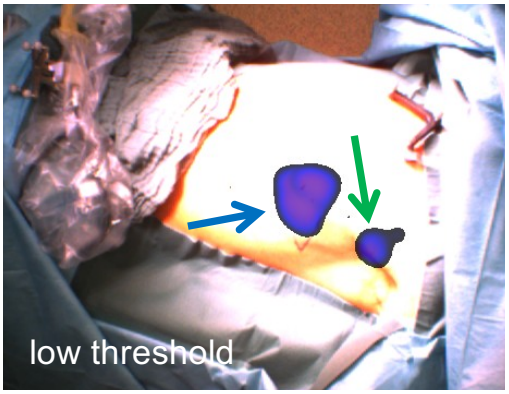

(a) Pre-incision reconstruction in AR view

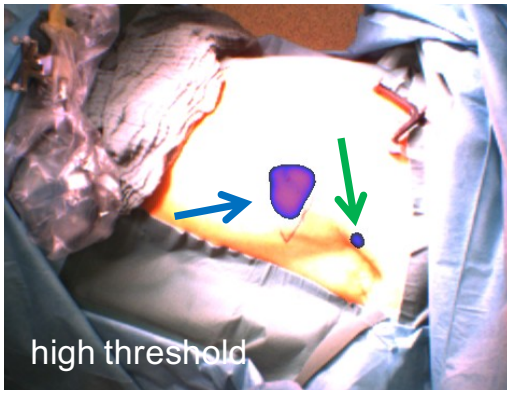

(b) Pre-incision reconstruction in AR view

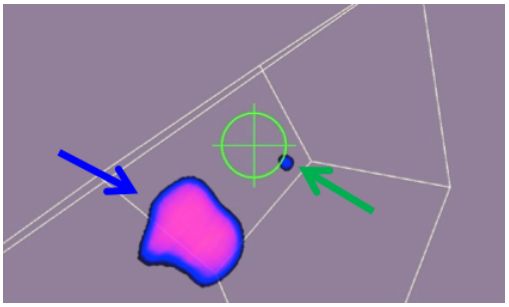

(c) 3D navigation in VR mode (pre-incision)

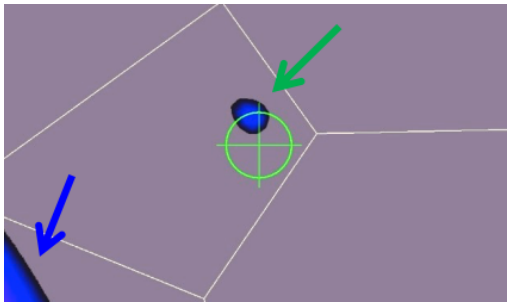

(d) 3D navigation in VR mode (pre-incision)

(e) Post-excision reconstruction showing homogeneous activity in the scanned area in AR view

(f) Thresholded post-excision reconstruction showing no major hot spot in AR view

Figure 4.4.: Freehand SPECT reconstructions in different surgical phases and view modes. Blue arrows: injection spot, green arrows: sentinel lymph node.

- *screenshots.xml*: Timestamp of each screenshot is saved in an additional XML file for synchronization with other logs.

- *userInteraction.txt*: A log file containing information about the user interface elements, button clicks, etc. Please note that this functionality was not available for the Freehand SPECT acquisitions in the first study of this chapter and is only included to the declipseSPECT cart system at a later point of time mainly due to our request.

In addition to these log files, the 3D reconstruction of the radiation distribution, the Freehand SPECT reconstruction itself, is also saved in this folder in DICOM format.

These automatically saved device and performance log files include almost all the information about how the users interact with the system, but they are not directly visible to the end users and they are hard to interpret without any further tools due to their sizes, the redundancy in the data and synchronization via numeric timestamps. However, they are very useful for research and development purposes, as they allow the developers and researchers to replay previous clinical Freehand SPECT scans offline, to investigate potential problems and to test new settings and parameters for improving the reconstruction quality. Furthermore, these log files can even be used for automatic detection of the phases of the surgical workflow and duration prediction (using data from previous scans). In addition, different freehand scan patterns and/or speeds can be identified and investigated for their influence on resulting images.

4.2.3. Anonymization / Pseudonymization of Patient Data

Patient data is very sensitive, therefore special care and attention is essential while working with it. Data protection regulations are getting stricter every day and as of General Data Protection Regulation (GDPR) effective of May 25th, 2018, every individual within European Union (EU) and European Economic Area (EEA) has the full control over all of their personal data [2], which also includes their medical records.

All clinical data acquired, stored and processed for the patient studies presented in this chapter as well as throughout this doctoral thesis are collected thanks to the successful collaboration with the medical faculty either in the scope of a pilot/feasibility study or a clinical study. Involved patients were informed about the Freehand SPECT technology, the advantages, the aim of the study and the potential risks by the responsible nuclear medicine physician and/or the responsible surgeon directly, and gave their voluntary consent to participate in the study directly to them. Freehand SPECT log files as described in the previous subsection are saved automatically on the local hard drive of the system.

To support usability evaluations of intraoperative imaging devices, we developed an extensible and flexible data gathering and evaluation framework called ORUse [10] in our institution. The first device modeled in ORUse framework is the declipseSPECT cart system. Since it automatically generates performance and log files for each acquisition, it is a perfect candidate for such usability evaluations. In addition to automatic *performance logging* via the device itself, ORUse also supports functionalities such as additional *video recordings* by additional video cameras and workflow and *annotations recording* via a mobile application, which is controlled by a usability engineer during surgery for synchronous documentation of the workflow stages as well as the feedback and comments of the OR staff. Furthermore, ORUse supports *configuration management*, which includes information about the software and hardware version of the device to be evaluated, test location and date as well as the information about the surgical team such as level of experience. In addition to that, ORUse is designed based on client-server architecture to serve as a data gathering platform for multi-center studies and cross-configuration tests. However, at the client side, several preprocessing steps are essential before transferring the data to the main server, especially in regard of patient data privacy. For more detailed information about ORUse framework please refer to [9] and [10].

The declipseSPECT cart system incorporating Freehand SPECT technology was initially not designed with any automatic functions to support anonymization or at least pseudonymization. It was not a requirement for the manufacturer during its initial design and development. On the contrary it was important for them to assure absolute identification of the saved data so the DICOM files and even screenshots generated by the system were designed to include the name and the birthdate of the patient, not only on file name or header, but also partially even as part of the image.

The Freehand SPECT system used clinically within our university hospital was not connected to the network of the hospital or to the internet during the course of this work. Only people who can physically access the device and have login credentials could export the data. As an additional data privacy measure, the medical data from the Freehand SPECT system were exported into an *encrypted* external hard drive for the post-operative processing and evaluations needed for the clinical studies. The encryption key was only given to involved researchers.

For many clinical publications, the findings in scintigraphy images and Freehand SPECT reconstructions need to be compared directly. Because of that, clinicians and researchers need to have access to both scintigraphy images and Freehand SPECT acquisitions of patients involved in the clinical study. In the scope of a supervised student group project (interdisciplinary project “Patient Data Privacy in ORUse Framework” by K. Bayer and

P. M. Hirschbeck) a standalone client side application called *MedNymizer* is developed to support clinicians in Klinikum rechts der Isar and researchers in Technische Universität München in Garching in their anonymization and pseudonymization efforts of the clinical data [8]. The non-anonymous medical data including scintigraphy and Freehand SPECT images of patients participating in the clinical studies are preprocessed with this tool before sharing with other researchers, using in publications and presentations or uploading to any other external servers such as the main server of ORUse framework.

The tool is developed in *C#* and using *Visual Studio 2010* and *Microsoft .NET* framework. Furthermore, *gdcm* library is used to handle DICOM file reading and manipulation. The application has two subprograms for handling scintigraphy data and Freehand SPECT data as both have different requirements and file directory structure. Scintigraphy images of the patients are saved into the picture archiving and communication system (PACS) of the Nuclear Medicine department of Klinikum rechts der Isar. These files only consist of DICOM files. Every scintigram results in individual DICOM images. These files only include patient name and birthdate in DICOM header but not in DICOM image itself. Therefore, the pseudonymization of these files is easy, as only manipulation of the header is necessary. However, in addition to these individual raw DICOM files, a thresholded summary image including all scintigrams is also saved as an additional DICOM file. This file does not only include the name and birthdate of the patient in the DICOM header, but it also includes it hardcoded in the image itself (Figure 4.5).

In nuclear medicine department of our university hospital, two different devices are used for the preoperative planar scintigraphy acquisitions of sentinel lymph node biopsy patients (FORTE and SKYlight gamma camera systems; Philips, The Netherlands). Depending on the device used for the scintigraphy, this overview image may have different properties and structure such as pixel-value encoding. For one scintigraphy device this overview image may be grayscale image whereas for another it may be a RGB colored JPEG either with 8 bit or 16 bit per value. For processing and also for displaying these different DICOM images properly inside the application, the pixel-value encoding type saved in a dedicated DICOM header tag needs to be taken into account. Furthermore, the size of the summary image may differ based on number of acquisitions and the location of the hardcoded name and birthdate of the patient may differ on the summary images generated by each device.

As previously mentioned, the automatically saved data for a Freehand SPECT examination may consist personal information on DICOM files as well as on screenshots. Therefore the preprocessing for pseudonymization of Freehand SPECT data has two parts: On the one hand, concerning the DICOM files for the resulting 3D Freehand SPECT reconstructions include the name and birthday information in dedicated DICOM header tags

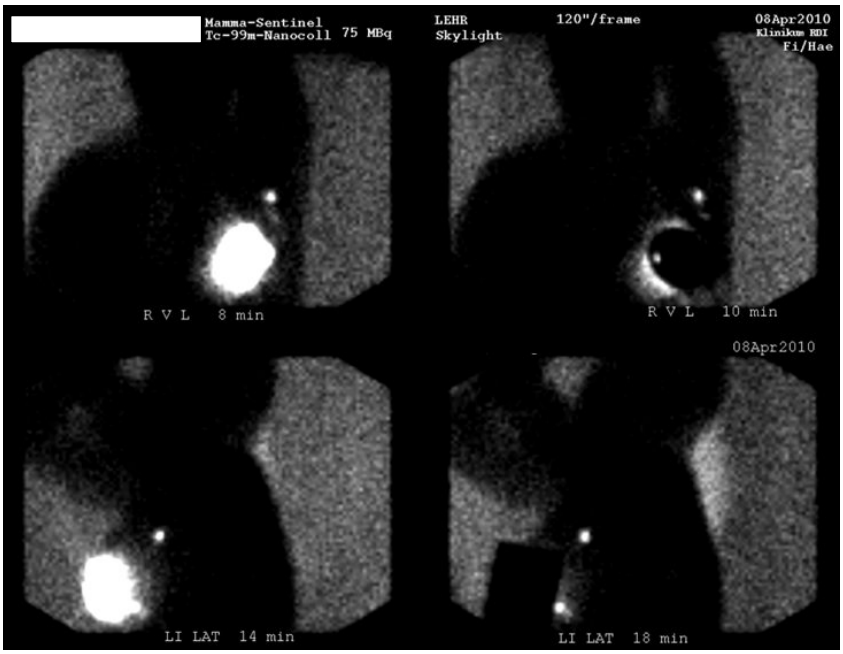

Figure 4.5.: Exemplary summary scintigraphy image of a patient. The white rectangle on the top left is added to protect the name and birthdate of the patient which is initially included in the image similar to the other information on the top such as examination date or injected activity.

which need to be replaced by user-defined pseudonyms. As the raw image data of the DICOM files do not contain any personal information of the patient (like name/birthday), no areas in the image needs to be manipulated as in scintigraphy images. On the other hand there are the screenshots generated every 5 seconds, which very often form a series like a flip-book. Therefore, a basic user-controlled blurring algorithm is implemented to be able to make critical parts of the succeeding screenshots not clearly identifiable (Figure 4.6). A typical example for the need of this functionality is the preoperative usage of Freehand SPECT. For instance for SLNB patients in breast cancer, the camera head is positioned in such a way that it has the perfect view from the top to cover the breast and the axilla of the patient to be scanned. This positioning is great for the acquisition, but it results in automatic screenshots sometimes showing the face of the patient clearly, especially if used preoperatively. In an intraoperative setting, this is commonly not as relevant, since the patient is covered with sterile surgical drapes and therefore the face is not clearly visible and recognizable. This functionality is also very useful for blurring faces of the personnel in these screenshots as well, regardless of preoperative or intraoperative usage.

Figure 4.6.: Exemplary Freehand SPECT screenshot of a test scan. The face of the person was clearly visible and therefore is blurred using the tool as shown here (yellow rectangle). The white box on the bottom of the screenshot includes information embedded into the image, the name and birthdate of the patient is always shown in the first line and needs to be removed if necessary (blackened).

4.2.4. Analysis of Freehand SPECT Acquisitions for Augmented and Mixed Reality Visualization

The surgical OR is a complex domain and there are several different actors involved depending on the procedure, the indications and the complexities [11, 53]. In the case of the sentinel lymph node biopsy cases included in the AR/VR visualization study, the *surgical team* within our university hospital can be basically defined as the team including the main surgeon, the assistant surgeon, the anesthetist, the sterile nurse, the unsterile nurse (circulator) and the Freehand SPECT technician (Figure 4.7).

The intraoperative usage of Freehand SPECT is mostly an interplay of the surgeons and the Freehand SPECT technician. Depending on the requests of the surgeons, the Freehand SPECT technician interacts with the touch-screen monitor of the device, since the surgeons

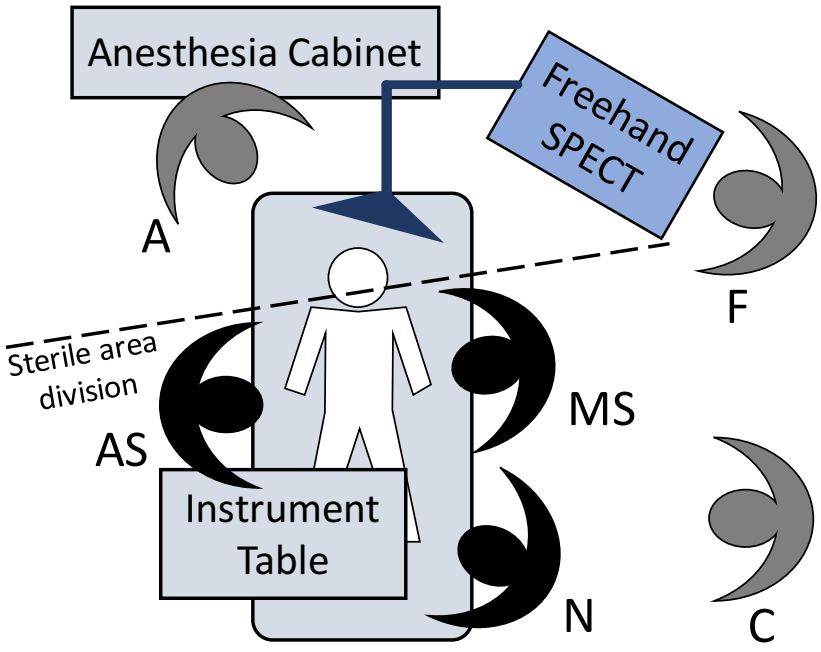

Figure 4.7.: An example OR setting for a SLNB procedure for the left breast under Freehand SPECT guidance in our university hospital: (MS) main surgeon, (AS) assistant surgeon, (N) sterile nurse, (C) circulator, (A) anesthetist, (F) Freehand SPECT technician

are sterile. He/she guides the surgeons on how to scan the region of interest and tries afterwards to find the optimal contrast parameters (thresholds). Therefore he/she actually is the person who interacts with the Freehand SPECT device most. However, the final decision on how long the device will actually be used and if any further depth measurement and 3D navigation is needed is made by the main surgeon. This is similar to the general user interactions in the OR as discussed in [92, 53].

Please note that during the observation period the system users were neither exposed to the plan to conduct this study report nor to technical terms such as *AR* and *VR*, which would have revealed the design goal of the respective view and consequently biased the system user. The two visualization modes were not presented as two particular user interface (UI) paradigms, but the surgical staff was only educated of both UI options and they chose to use different view modes serving best their needs. In order to minimize bias towards any of the UI options, all features of the system were explained for each of these options. The training was also performed according to a fixed content in order to avoid

variation from trainee to trainee. During the surgical procedure, the surgeon, the supporting staff and the Freehand SPECT technician were jointly selecting and switching the view modes, according to the current surgical workflow step and the view mode most suitable for each particular task, aiming only at optimal patient care. Therefore it is not differentiated between different actors and the surgical team is considered as a whole when talking about the *user* henceforth.

For this work, 46 patients who have undergone sentinel lymph node biopsy with intraoperative Freehand SPECT guidance are analyzed. The indications vary between early stage melanoma (13x), breast (31x) and vulvar cancer (2x). These patients were operated either in the Gynecology or in the Surgery Department of the Klinikum rechts der Isar, Munich, Germany. The time interval is between March 2010 and April 2011.

These 46 surgeries resulted in 52 pre-incision and 48 post-excision Freehand SPECT scans. This is due to the fact that some patients have undergone SLNB in more than one body region (e.g. bilateral breast cancer, vulvar cancer or some cases of melanoma). The different count of the pre-incision and post-excision scans are due to the time constraints in the OR and also due to the technical and practical problems encountered in between. Furthermore, in some cases the measurement with the gamma probe was enough for the surgeon to make sure that there is no more activity left in the region of interest and therefore the post-excision scan was not necessary.

For the analysis of the chosen visualization mode, the screenshots generated by the Freehand SPECT system are studied. Please note that the user interaction logs among automatic performance log files described in subsection 4.2.2 were not available for acquisition and evaluation period of this study. This logging is included to the declipseSPECT cart system by the manufacturer after completion of this analysis upon our request in a later software version, so that AR/VR usage comparison analysis in this particular study was only possible via manual analysis of the screenshots. These screenshots were automatically captured within the surgery at a frequency of 0.2Hz and saved as a sequence of JPEG images in separate folders dedicated for each acquisition as described in subsection 4.2.2. For calculation of the AR/VR ratios, the screenshots are reviewed twice, manually. In average the evaluation of a single acquisition took 5 minutes. Evaluation sessions of not more than 10 patients were enforced to avoid concentration errors. The usage has been documented by counting the screenshots for each of the visualization modes, for the time interval when the users were using the system explicitly. Since in the VR visualization of the system the users cannot relate to the anatomy of the patient directly, especially in cases where it is not easy to identify the SLN in the reconstructed image, it is also analyzed if the users switched back to AR mode in between while using VR for navigation. Moreover,

based on the screenshots, the adjustments of the thresholds in the displayed reconstruction are analyzed separately for the augmented reality (AR) and the virtual reality (VR) viewing modes, as described in section 3.7 in detail.

Pre-incision and post-excision datasets are analyzed separately, because they cannot be compared directly due to different requirements of the corresponding surgical stage. For the post-excision images it could also be determined if the users chose to compare the image with the previous one, namely the pre-incision image and if yes, in which of the viewing modes. The final screenshot counts are used to calculate the actual usage time and the ratio of AR vs. VR usage for each acquisition. The means and the standard deviations are calculated over the resulting ratios for each acquisition in both workflow stages.

4.2.5. Automatic Analysis of Freehand SPECT Acquisitions for Usage Characteristics and Surgical Phase Determination

In the previous subsection, the methodology for the evaluations in respect to usage characteristics of different user groups for augmented reality (AR) and virtual reality (VR) visualization modes of the Freehand SPECT system is presented, based on the manual analysis of the saved screenshots. However, this is a very time-consuming task for the evaluator. Since some user interface elements may be only available or used in some specific stages in the surgical workflow, the user interaction log, if available, can be very helpful to determine the transitions between the stages automatically. As mentioned previously in subsections 4.2.2 and 4.2.4, this user interaction log file was initially not part of the Freehand SPECT system and was included at a later point of time.

In the scope of a supervised interdisciplinary student project by R. Voigt, an application is developed to further investigate Freehand SPECT log files for usage characteristics and surgical phase determination by an automatic manner. This work is also presented in [86].

During the whole surgery the tracking information is recorded continuously which results in very large log files. It is not very easy for the study investigators to find the parts, which may be relevant for the resulting end reconstructions or usage characteristics. By an analysis of the tracking log in combination with the user interaction log, the tracking log can be limited to parts, which are related to the surgical phase of interest. Since the *scanning* phase is very user-dependent and affects the reconstructions tremendously, it is a major surgical phase of interest. Such an analysis allows for instance the identification and investigation of the problems with tracking or scanning speed and coverage.

In this second study, 19 breast cancer SLNB surgeries are analyzed, each consisting of two Freehand SPECT acquisitions, one pre-incision scan and one post-excision scan.

These 19 surgeries took place between January and September 2013. Freehand SPECT system used in these surgeries was again a declipseSPECT cart system, but this time with an updated software version, which generates the user interaction log file in addition to other performance log files as described in subsection 4.2.2.

For the preprocessing of the log files such as parsing and synchronization, a standalone application is developed in *C++* and using *Visual Studio 2010* as programming environment. The external dependencies for this application were the third-party C++ libraries called *RapidXML* and *Armadillo*, the former for the parsing of the XML files and the latter for the required linear algebra (matrix) operations.

By inspecting the surgical workflow (Figure 4.2), the device workflow (Figure 4.3) and the user interaction log in detail, specific entries (button clicks), which reflect major workflow phase transitions for *preparation*, *pre-incision scanning*, *pre-incision reconstruction*, *surgical act*, *post-excision scanning*, *post-excision reconstruction* and *end* phases, are identified as shown in Figure 4.8. Please note, that for this second set of breast cancer surgeries involved in this study, the visualization of the pre-incision scan was hidden from the surgeon on purpose, so that the added clinical value of Freehand SPECT could be investigated in the scope of a clinical study. The goal here was to find out if Freehand SPECT detects sentinel lymph nodes which would have been missed through the conventional sentinel lymph node biopsy. Pre-incision scan was only performed to be able to compare the post-excision scan and is only shown to the surgeon after the removal of the sentinel lymph node via gamma probe guidance only. Only after the surgeon is satisfied with the SLN removal via the conventional method, the post-excision scan is performed and both of the reconstructions are made available to surgeon to let him or her decide on the success of the procedure and eventually search for additional SLNs in the surgical cavity as shown in both pre-incision and post-excision Freehand SPECT reconstructions. For one patient in this clinical study in Klinikum rechts der Isar, the utilization of Freehand SPECT made a difference in the detection and staging of the cancer as reported in [15].

For clinical studies, it is often necessary to measure the additional surgery time required by the introduction and utilization of Freehand SPECT imaging for this particular clinical application field. Utilization of the user interaction log for this purpose allows even sublevel calculations of the time overhead for Freehand SPECT *scanning* and *reconstruction*, respectively. The duration of *preparation*, *surgical act* and *end* phases depend on many factors such as clinical indication and complexity as well as other unpredictable and non-standard circumstances inside the operating room, but the *scanning* and *reconstruction* phases are expected to be comparable for both pre-incision and post-excision scans. It is due to the fact that *scanning* is supposed to be performed according to a predefined

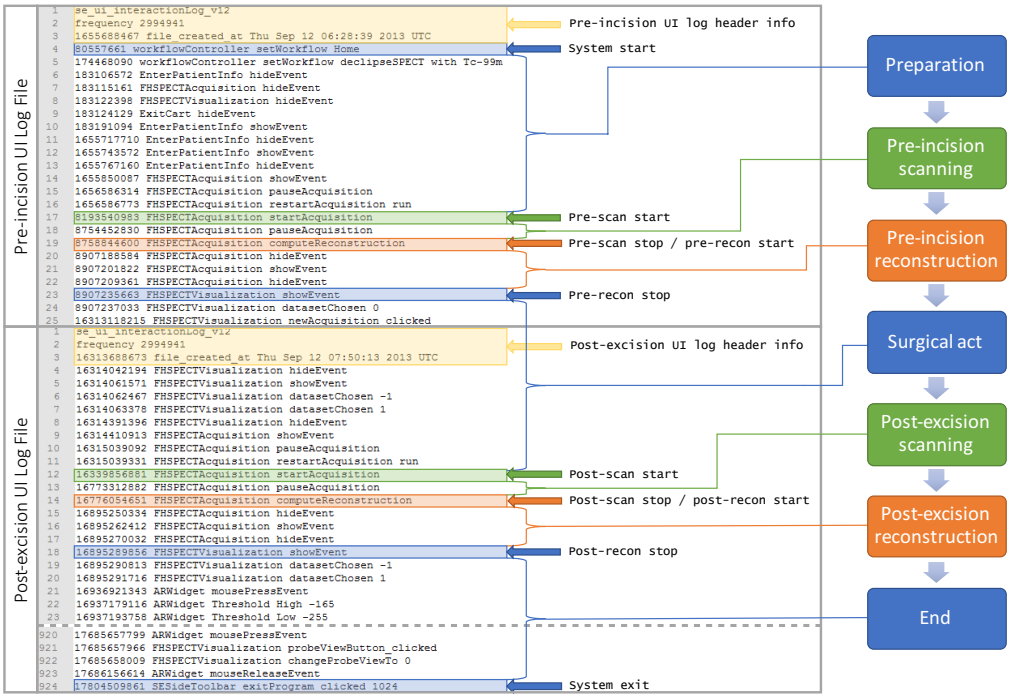

Figure 4.8.: User interaction log analysis of Freehand SPECT. Based on the presence of specific entries in the user interaction log files, the transition between major workflow phases can be determined automatically.

scanning protocol for the target anatomy and the *reconstruction* time is directly related to the scanning time and quality. Because of these reasons, the emphasis of the automatic detection of phase transitions in this second study is set on the *scanning* and *reconstruction* phases for both pre-incision and post-excision datasets.

The automatic *activity.txt*, *tracking.txt* and *userInteraction.txt* log files provided by the declipseSPECT cart system have two parts. The header, which typically consists of the first line or first few lines of the text file, provides the information about the log version number as well as the system clock frequency. In the body of the file, each corresponding log entry is written linewise with the corresponding timestamp in form of system clock ticks of the processor since Windows operating system start. Therefore, the frequency (processor clocks per second) is very important for the conversion of these timestamps into Unix (epoch) time or even human readable time. However, this only allows relative calculation of the timestamps in form of seconds or minutes in respect to the first entry in the file body. Even though this is sufficient for many of the calculations such as the

duration of the phases, a specific entry in the header part of the *UserInteraction.txt* file (version 12) allows the mapping of these timestamps to the exact date and time, as well. Here is an example:

```
1  se_ui_interactionLog_v12
2  frequency 3026455
3  693211762 file_created_at Wed Jan 9 09:31:53 2013 UTC
```

Excerpt 4.1: Header of user interaction log file, showing version number, frequency and base timestamp with the corresponding date and time.

This particular third line of the user interaction log in version 12 provides an accurate base timestamp for all the log files, if parsed and converted into Unix time or DATETIME format properly. The manufacturer most probably chose to use the clock ticks of the system over Unix time or DATETIME format for better performance and accuracy. Even extension of Unix time or DATETIME format by milliseconds would not allow the same sensitivity as the clock ticks (compare to the frequency in example above).

The body part of the tracking log file has a different structure than other log files provided by declipseSPECT. The number of the tracking log entries for each timestamp depends on the system settings and defined tracking targets, so the logging here is not linewise, but blockwise. Please note that the *settings.xml* file also includes the names of the design files of these defined tracking targets as shown below, which refer to the ROM files needed for the Polaris Vicra® tracking camera included in declipseSPECT cart system:

```
<DeviceFramework>
    <AVHTracker>
        <DeviceClass>NDITracker</DeviceClass>
        <Targets>
            <ChessboardTarget>SECalibrationBoard</ChessboardTarget>
            <PatientTarget>SEPatientTargetWhite</PatientTarget>
            <ProbeCalibratorTarget>SEGammaProbeCalibrator</
    ProbeCalibratorTarget>
            <ProbeTarget>SEProbeTargetSlide</ProbeTarget>
        </Targets>
        <UpdateRate>50</UpdateRate>
    </AVHTracker>
</DeviceFramework>
```

Excerpt 4.2: Tracker parameters in *settings.xml* referring to the respective ROM filenames for each of the defined tracking targets.

To make it clear, let us have a look in an example excerpt from such a tracking log file (numeric values are rounded to two decimal places to fit the line in the textspace below):

```
    1  se_tracker_v_12
    2  frequency 3026455
  ...
30048  1552812461    4       0
30049  chessboardTarget 0 0 0 0 1 0 0 0 0
30050  patientTarget -28.42 -59.57 -847.70 -0.55 -0.17 0.00 0.82 0.27 1
30051  probeCalibrator 0 0 0 0 1 0 0 0 0
30052  probeTarget -187.30 207.92 -957.14 0.94 -0.31 0.16 -0.01 0.18 1
  ...
```

Excerpt 4.3: Tracking log: First two lines show the header information, the blocksize for each tracking reading depends on the number of tracked objects.

The first line of the entry block includes the timestamp and the number of known tracking targets, in this particular example 4. This means, that the following 4 lines are related to this particular timestamp. For each of the targets, the tracking information is logged in the form below with the delimiter SPACE character:

$$\texttt{TargetName} \quad p_x \quad p_y \quad p_z \quad q_w \quad q_x \quad q_y \quad q_z \quad error \quad status$$

The position (translation) of the tracked object `TargetName` in tracker coordinate system is given here in form of (p_x, p_y, p_z) and the orientation (rotation) in form of unit quaternions (q_w, q_x, q_y, q_z). The tracking error $error$ provided by the Polaris Vicra® tracking camera and the tracking $status$ bit indicating the presence of the tracked object in the tracking volume is also appended to the log entry. For each of the tracked objects, the transformation matrix can be computed from these parameters using the following formula:

$$ {}^{camera}\mathbf{T}_{obj} = \begin{bmatrix} 1-2(q_y^2+q_z^2) & 2(q_xq_y-q_zq_w) & 2(q_xq_z+q_yq_w) & p_x \\ 2(q_xq_y+q_zq_w) & 1-2(q_x^2+q_z^2) & 2(q_yq_z-q_xq_w) & p_y \\ 2(q_xq_z-q_yq_w) & 2(q_yq_z+q_xq_w) & 1-2(q_x^2+q_y^2) & p_z \\ 0 & 0 & 0 & 1 \end{bmatrix} $$

For the reconstruction of the Freehand SPECT acquisition, the radiation counts at the tip of the detector should be mapped to its relative position and orientation in the reconstruction volume, as previously explained in chapter 3 and section 3.6 in particular. This volume is defined in the coordinate system of the patient tracking target, since the camera head of the Freehand SPECT system as well as the patient can be moved or repositioned

by the OR crew during the surgery, if required. Because of that, both patient and probe targets should be present in the tracking volume of the optical tracking system without any occlusions. The 4x4 transformation matrix for the so-called probe tip calibration ${}^{probe}\mathbf{T}_{tip}$ is stored in *settings.xml* file as shown in an example below:

```
<DeviceFramework>
    <CSSGammaProbe>
        <DeviceClass>PicoscopeClient</DeviceClass>
        <HardwareProcessingDelayInMicroseconds>0</
    HardwareProcessingDelayInMicroseconds>
        <ProbeTipCalibration>[0.592689504221846 -0.15054590860751
    0.791236447686206 140.988654130441;0.795834009130719
    -0.0417377707411006 -0.604074729094398
    -97.307096712022;0.123965384912375 0.987721609473582
    0.0950719918724134 -50.3756165257393;0 0 0 1]</ProbeTipCalibration>
        <TipAngleError>0.14581600841871</TipAngleError>
        <TipCalibratorTransformation>[0 0 1 30.0; 1 0 0 0; 0 1 0 -33.91;
     0 0 0 1]</TipCalibratorTransformation>
        <TipPositionError>2.66376828007399</TipPositionError>
        <UpdateRate>50</UpdateRate>
    </CSSGammaProbe>
</DeviceFramework>
```

Excerpt 4.4: Gamma probe related parameters in *settings.xml* file. The transformation matrix required for the calculation of the position and orientation of the tip of the detector in respect to the probe target can be found under the XML tag `<ProbeTipCalibration>`

The gamma probe utilized in declipseSPECT cart system, which is used in the surgeries in this study, is a straight gamma probe with a single detector crystal (Crystal Photonics, HiSens, 40^o collimator). By its construction and collimation, the detector field of view can be considered as a cone which is of course symmetrical in x and y direction. The probe tip calibration provided by declipseSPECT cart system in *settings.xml* transforms the origin of the probe target coordinate system to the tip of the probe and aligns its z axis with the direction of the probe.

In order to calculate the the position and orientation of the probe tip in respect to the patient target coordinate system (Figure 4.9), the following chain of matrix calculations are required:

$$ {}^{patient}\mathbf{T}_{tip} = ({}^{camera}\mathbf{T}_{patient})^{-1} \cdot {}^{camera}\mathbf{T}_{probe} \cdot {}^{probe}\mathbf{T}_{tip} $$

For the computation of the Freehand SPECT reconstruction, the transformation of the probe tip coordinates into the patient target coordinate system with the formula above is

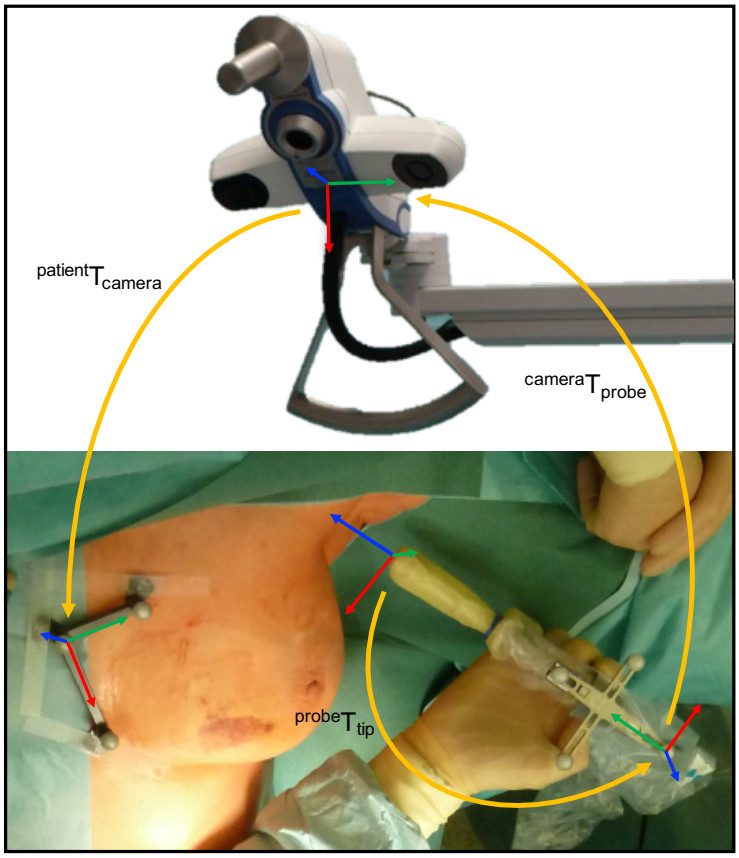

Figure 4.9.: Transformation chain from probe tip to patient target coordinate system. The third and fourth columns of the calculated transformation matrix ${}^{patient}T_{tip}$ is representing the orientation and position of the gamma probe in patient target coordinate system, respectively.

essential. First, the activity and tracking log entries with timestamps outside of the start and stop times of the scanning phase as determined from the user interaction log file, are not required and therefore discarded. Secondly, for each timestamp between start and stop acquisition button clicks in UI log, the status bit is checked in tracking log for both patient and probe tracking targets and the transformation above is calculated, if both of them are visible to the tracking camera. For this calculated detector position in patient target coordinate system, the associated radiation readings by the gamma probe is found in the activity log file by searching the log entry with the corresponding timestamp. Here is an example excerpt from an activity log file:

```
   1  se_probeLog_v_12
   2  frequency 3026455
 ...
5683  1552773410   0.000000        55205
5684  1552964972   71.657875       69776
5685  1553117274   17.291166       57833
5686  1553259179   0.000000        51708
5687  1553438587   0.000000        65023
 ...
```

Excerpt 4.5: Activity log: First two lines show the header information, the following lines in the body include the timestamp, the average radioactivity counts over the exposure duration in nanoseconds.

The log entries in the activity log file is structured as the following:

$$timestamp \quad \overline{counts} \quad exposure$$

Please note that here the value $\overline{counts}$ has decimals because it represents the average of the detected photons by the gamma probe radiation detector over $exposure$ duration given in nanoseconds. To calculate the corresponding radiation counts (detected photons) per timestamp, the following formula can be used:

$$counts = \frac{\overline{counts} \cdot exposure}{1000000}$$

By the combination of the information provided from three different log files, the developed C++ application computes automatically a *measurements.txt* file for a Freehand SPECT acquisition folder provided by the declipseSPECT cart system. This output file includes only the measurements in the scanning phase and can be processed by different tools such as *Matlab* or the freehand reconstruction standalone software library *NaNuLib* developed in our institution [62]. The entries in this file is structured as the following:

$$p_x \quad p_y \quad p_z \quad o_x \quad o_y \quad o_z \quad counts \quad timestamp$$

where $\vec{p} = (p_x, p_y, p_z)$ is the position and $\vec{o} = (o_x, o_y, o_z)$ is the orientation of the probe tip in patient target coordinates and the $counts$ are the photons detected by the gamma probe at time indicated with $timestamp$.

For each of the 19 surgeries included in this second study, the folder containing the pre-incision and post-excision scans are automatically processed by the C++ application and four files are generated for further evaluation with external tools, if needed:

- *LogSummaryPre.xml*: XML file containing the important entries such as VOI size, probe and nuclide information, probe tip calibration matrix in *settings.xml* file of the pre-incision scan as well as calculated values for the phases, reconstruction duration, speed, length, tracking problems, frequency and base timestamp.
- *LogSummaryPost.xml*: XML file containing the important entries such as VOI size, probe and nuclide information, probe tip calibration matrix in *settings.xml* file of the post-excision scan as well as calculated values for the phases, reconstruction duration, speed, length, tracking problems, frequency and base timestamp.
- *PreMeasurements.txt*: Text output file containing the measurements during scanning phase of the pre-incision acquisition, each line in form of position of the probe tip in patient coordinate system and orientation of the probe (z-axis), the radioactivity counts and the timestamp.
- *PostMeasurements.txt*: Text output file containing the measurements during scanning phase of the post-excision acquisition, each line in form of position of the probe tip in patient coordinate system and orientation of the probe (z-axis), the radioactivity counts and the timestamp.

The scanning trajectory and characteristics such as speed can also be investigated post-operatively offline by analysis of these files. In this study, Matlab is chosen for the offline visualizations of the scanning trajectories as it will be shown below in the results section (Subsection 4.3.3). If information about the users or OR crew present in surgery is also known, a similar study as the AR/VR visualization study in this chapter for different user groups can be performed in an automatic and evaluator independent manner using the methodology presented in this subsection.

4.3. Results

4.3.1. Data Analysis for AR/VR Visualization Modes

In the observed usage scenario in our AR/VR visualization study (subsection 4.2.4), it is important to distinguish between the pre-incision and the post-excision Freehand SPECT scans, since they occur in two different workflow stages and are aiming at different goals. The former is mostly used to localize the activity region, which can be used for navigation and the latter is mainly used for checking the quality of the removal procedure and possibly detecting the remaining activities.

In the pre-incision data, the AR/VR ratio is 64.0% to 36.0% with standard deviation 25.8% whereas in the post-excision data it is 86.4% to 13.6% with standard deviation 23.0%. The average system usage time during the pre-incision and the post-excision visualization stages were 3.15 and 1.56 minutes, respectively.

In 51 of 52 pre-incision scans (98.1%) the AR was the choice of visualization for setting the proper threshold values. The only acquisition (1.9%) for which this is not the case is a second pre-incision scan of the same patient in a different region of interest. Therefore, a new adjustment of the threshold values was not needed, due to the fact that the values from the first scan assured a proper visualization.

Although threshold adjustment is also available in the VR mode, the surgical team interacting with the device used this functionality additionally only in 3 of 52 pre-incision acquisitions (5.77%) whereas the threshold sliders remained untouched in the VR mode in 38 of 52 acquisitions (73.1%). In 11 of 52 pre-incision scans (21.2%), the surgical team chose not to use VR mode at all.

In those 41 of 52 acquisitions where they used VR with the pre-incision image, the surgical team switched back to AR at least once in 35 acquisitions (67.3% of total, 85.4% of VR cases).

For the post-excision acquisitions, the statistics are a little different. In 32 of 48 datasets (66.7%), the VR is not chosen at all. This is not surprising with regard to the surgical workflow. Post-excision scans are done for quality assurance of the surgical procedure, which means that the goal is to make sure that there is no remaining activity in the volume of interest. In most of the cases, the AR view of the reconstructed image was enough for the surgical team to decide that no further resection is needed. In such cases, the VR or 3D navigation in the volume becomes unnecessary.

In 12 of 48 post-excision images (25.0%), readjustment of the threshold sliders was not needed, whereas in 36 cases (75.0%), the users tried to find better threshold values for the newly acquired image. The usage here very much depends on the people involved: For some teams, it was enough to compare the pre-incision and post-excision images with the same threshold values (Figure 4.4(b) and 4.4(f)) whereas some users did not rely on the values from the first scan and wanted to adjust them again for the newly acquired image so that they would not oversee a radioactive (*hot*) spot with lower radioactive uptake which could be possibly a further SLN. Setting the lower threshold to a lower value would include more background activity in the visualized Freehand SPECT reconstruction. In such a case, a homogeneous distribution with no particular uptake should be interpreted as residual activity and not as a further SLN (Figure 4.4(e)). In 2 of 16 (12.5%) cases where VR is used in the post-excision images (4.2% in total), the thresholds were also adjusted

in the VR mode.

Again in 13 of those 16 cases (81.3%, 27.1% in total), the surgical team chose to switch back to the AR visualization at least once during the interaction with the device after choosing VR for 3D navigation in the reconstructed volume.

To assure that no further SLN is remaining in the scanned area, a comparison of the post-excision scan with the pre-incision image can be done. By checking the hot spots shown in the pre-incision image with the post-excision image and the acoustic sound of the gamma probe in real-time, the surgical team can be sure that there is no remaining hot spot in the region of interest. In the 48 post-excision scans analyzed, this functionality is used only in 29 cases (60.4%), whereas it is waived in 13 cases (27.1%). Unfortunately, in 6 of 48 cases, the pre-incision image was not available during the post-excision usage (12.5%). Furthermore, in 27 of the remaining 29 cases, the comparison is done in the AR mode (93.1%, 56.3% of total), while in one case only the VR mode (3.5%, 2.1% of total) and in one case both modes were utilized (3.5%, 2.2% of total).

As mentioned in section 4.2.4, the actors in the OR were considered as a whole during this study. However, the actual usage is very much dependent on the main surgeon involved, since he/she plays the role of decision maker for how effectively and how long the Freehand SPECT system will be used. Therefore it is interesting to investigate the usage time and the AR/VR ratio based on different main surgeons involved for their tendencies.

The 52 surgical procedures on 46 patients analyzed for this work were led by 14 different main surgeons, some of them encountered the system for the first time and therefore had limited experience with it whereas some had the opportunity to use the system intensely several times. For the three main breast surgeons who have used the system most, the usage over time in both the pre-incision and the post-excision data (Figure 4.10) is analyzed. The average usage time and the average AR/VR usage ratio for the teams of these three main surgeons are plotted in Figure 4.11.

Based on these graphs, different characteristics of the main surgeons can be identified. The statistics for the surgeon 3 differs from the other two surgeons both in the usage time and in the AR/VR ratio. As emphasized in Figure 4.11, surgeon 1 and surgeon 2 had a tendency to use the Freehand SPECT imaging system during both the pre-incision and the post-excision phases ca. 2 minutes long in average whereas surgeon 3 used the device in the pre-incision phase more intensely (4.5 minutes on average) and in the post-excision phase more briefly (1.5 minutes on average). The higher usage time and VR percentage in the pre-incision phase as well as the lower usage time and VR percentage in the post-excision phase for surgeon 3 could indicate that the teams led by the surgeon 3 used the Freehand SPECT device more likely for intraoperative 3D navigation during the excision

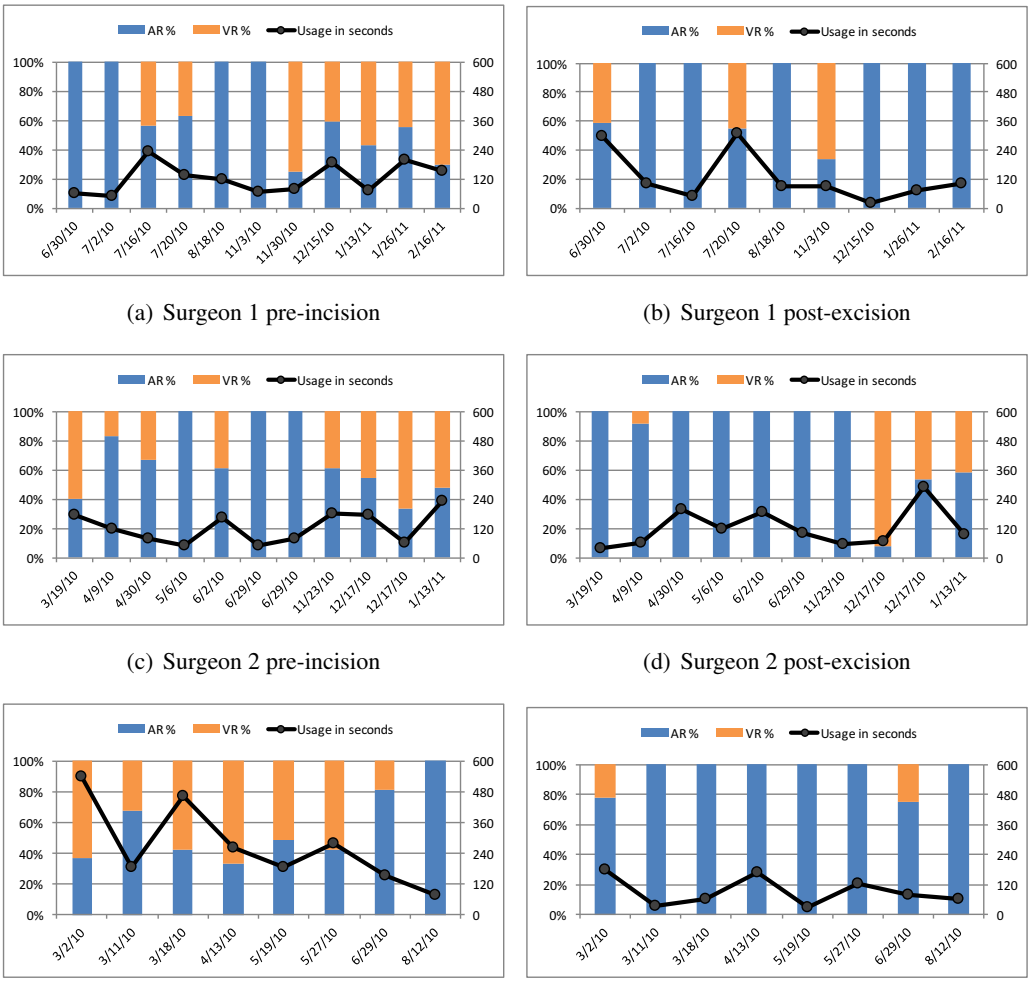

(a) Surgeon 1 pre-incision

(b) Surgeon 1 post-excision

(c) Surgeon 2 pre-incision

(d) Surgeon 2 post-excision

(e) Surgeon 3 pre-incision

(f) Surgeon 3 post-excision

Figure 4.10.: The average usage of the surgical teams led by three different main surgeons for pre-incision and post-excision images.

procedure. Based on this comparison, in contrast to surgeon 3, the other two surgeons used Freehand SPECT more likely to confirm the radioactivity in the volume of interest for the incision, but not for image-guided excision.

4.3.2. Additional Observations for AR/VR Visualization Study

As mentioned previously, in order to avoid any influence of our AR/VR visualization study on the normal usage pattern and the user interaction with the target system, the OR crew

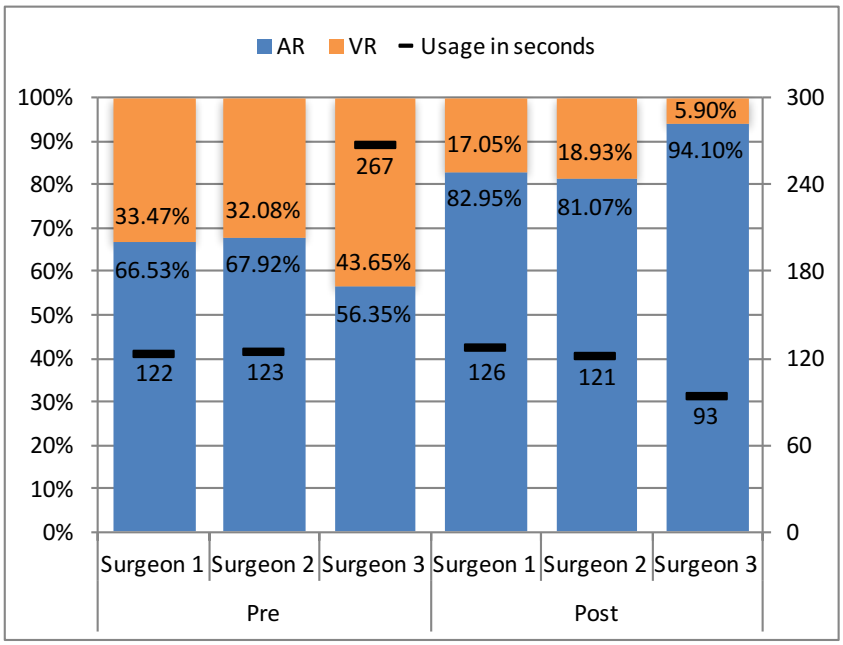

Figure 4.11.: Analysis of the surgical teams of three different main surgeons. The surgical teams of Surgeon 1 and Surgeon 2 have similar usage characteristics in contrast to the teams of Surgeon 3.

was not informed about the study plans within 13 months of observation period. Some of the surgical team members were frequently present during different surgical sessions. After the completion of the data collection period, series of discussion sessions with main members of the surgical teams, who were mostly exposed to the system and interacted with the device, are performed, in order to get further qualitative feedback on the usability of the system within their surgical procedure. In this subsection the main issues mentioned in regard to the usage of this MR-based system within the OR context are presented.

Similar to many other AR applications, the declipseSPECT cart system overlays co-registered and tracked virtual and real objects on the video images thanks to real-time tracking. A pair of calibrated infrared cameras is used to track retro-reflective tracking targets. The tracking accuracy strongly depends on the positioning of the Freehand SPECT device, which usually takes place during the *preparation* phase. The quality of the reconstructed model and the generated AR and VR images also depends on tracking accuracy. Moreover, due to the presence of the OR crew and other intraoperative equipment, repositioning the device is only possible in a limited manner, moving the camera head. This emphasizes the importance of the positioning of the device before the surgery starts, which

should be done by an experienced and trained person. Unsuitable placement of the device may further lead to improper and unreliable AR visualization.

An example for such a case is shown in Figure 4.12. In preoperative scintigraphy imaging (Figure 4.12(a)) and also in intraoperative pre-incision Freehand SPECT imaging, one sentinel lymph node was clearly identified. However, due to inappropriate positioning of the camera head of the declipseSPECT cart system during surgery, the right axilla of the

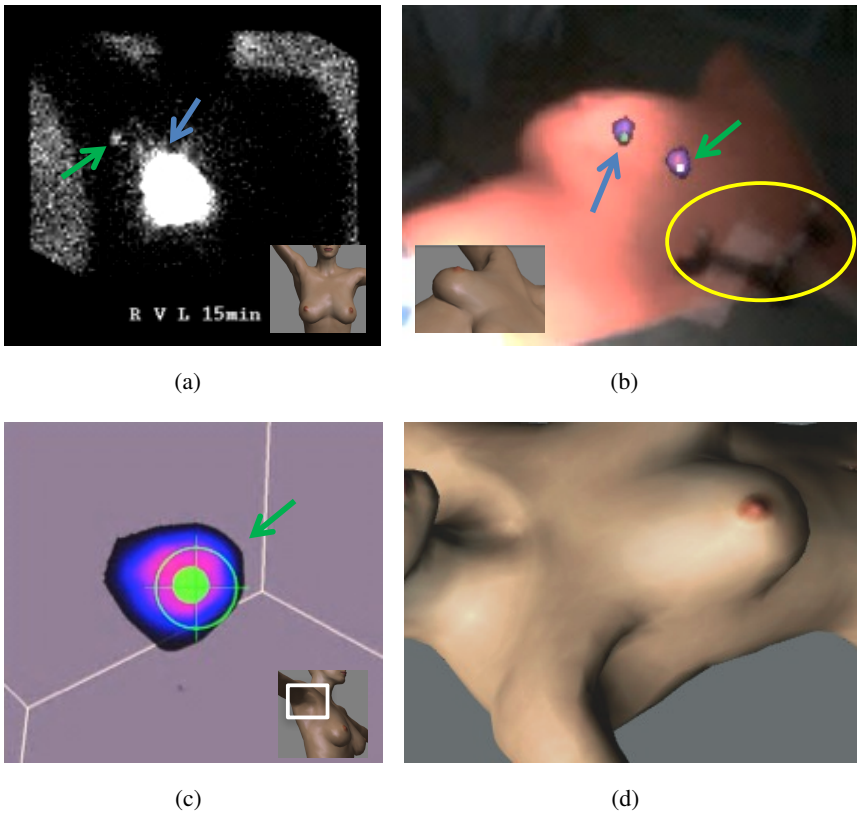

(a) (b)

(c) (d)

Figure 4.12.: Example case for bad AR visualization due to positioning problems. Blue arrows indicate the position of the injection spot, green arrows mark the SLN. (a) Scintigraphy image of the patient showing one SLN in the frontal view. (b) Confusing AR image during surgery. The patient target (circle) is placed on the sternum. The SLN is actually deep in the axilla, but seems to be on top of the breast in the AR view. (c) Visualization of the SLN using VR and depth measurement. (d) Illustration for a better camera position for proper AR visualization.

patient is not visible in the camera view. Because of that, even though the reconstructed SLN is actually located deep in the axilla, it seems to be on top of the breast due to the misleading AR overlay (Figure 4.12(b)). In order to overcome this issue, the OR team of course had to switch to the VR mode (Figure 4.12(c)) and navigate in the reconstruction volume by moving the probe over the axilla. Prior surgery, if the camera head of the declipseSPECT cart system would have been placed in such a way so that the right axilla of the patient is clearly visible by the camera (Figure 4.12(d)), the AR visualization would have been more accurate. This particular surgery corresponds to the seventh surgery of the teams lead by surgeon 1 in the study (Figure 4.10(a)), where the VR percentage is much higher than other surgeries of the same surgeon as well as the other two main surgeons, although the system is used less than average.

In order to have proper visualization in the VR mode, both tracking targets have to be in the field of view of the optical tracking head of the Freehand SPECT system. Furthermore, the presence of many people around the patient in the sterile field increases the chance of occlusion. Thanks to the flexible design of the camera head of declipseSPECT cart system, its placement and orientation can be changed to overcome these issues. However, in the VR view mode this can be more challenging, compared to AR, due to the necessity to track both targets.

Other mentioned aspects could be categorized under the human-machine interaction. In the OR domain, due to the setup used in our hospital, the surgeon, who is the main user of the system, cannot directly touch the device and should forward his commands to a technician or nurse standing next to the device. Although the voice-based control may be useful for interacting with discrete functionalities, it has shown limited applicability for parametric features, where the user should modify a numeric value, such as threshold [53, 11]. In some situations this can slow down the interaction process where there are too many parameters to set during the operation. For the Freehand SPECT device there are few parameters which mostly can be initialized automatically. Furthermore, to achieve a proper camera image quality, suitable illumination and lighting condition should be considered. The proper distance of the visualization screen to the target user, the main surgeon in the case of the SLNB, plays an important role in increasing the user satisfaction, based on the observations during this work.

As seen in section 4.2.4, AR was the choice of visualization more often compared to VR in the analyzed Freehand SPECT surgeries in this AR/VR visualization study. However, this does not imply that AR is superior to VR. The usage of AR and VR strongly depends on the requirements within the current surgical workflow stage. AR was generally used to obtain a big picture of the activity distribution over the patient anatomy, however the VR

mode was mostly preferred whenever more accurate measurement and localization was required. According to the users, having two complementary viewing modes improved the overall usefulness of the device.

The results presented in this AR/VR visualization study were not subject of an experimental design with fixed hypothesis and controlled boundary conditions in the OR, like device placement, OR team, lighting, patient characteristics, clinical indication, etc. Thus, a generalization cannot be made based on its statistics. However, it can provide as a "phase I" study sufficient data for the planning of a controlled "phase II" study capable of evaluating in details and with proper statistical significance and power the contribution of this technology to the clinical output. Such a study could be performed as a randomized or matched study comparing the procedure with the conventional non-MR-guided one. The age of the users, their knowledge of computers and the influence of the training could also be some further aspects that may be considered.

4.3.3. Analysis for Surgical Phase Determination and Usage Characteristics

This subsection presents the results of the second study, which is based on the *automatic* analysis of the device and performance log files provided by declipseSPECT cart system.

By searching automatically for the dedicated entries in the user interaction log files of the pre-incision and post-excision Freehand SPECT acquisitions as described in subsection 4.2.5 (Figure 4.8), the duration of the major workflow phases of the 19 breast cancer sentinel lymph node biopsy surgeries with Freehand SPECT system are determined. For each surgery, the durations are calculated automatically for all seven phases and the means and standard deviations are calculated over all 19 surgeries for each individual phase as shown in Table 4.2.

In order to interpret the post-excision scan by comparing the radiation distribution in both of the reconstructed images, the surgeons need to make sure that they place the patient target on the patient during the *preparation* phase and leave it on the same position throughout the whole surgery. For breast cancer patients, the suggested position for the patient target is on top of the sternum, but this is not a must. As long as it is inside the tracking volume of the camera head and its location does not disturb the surgeons during the surgical procedure, it can be placed basically anywhere on the patient. An important thing here is that it stays on the same position throughout the surgery since all calculations are based on this reference coordinate system instead of the coordinate system of the tracking camera, in order to be able to compensate for the movements of the patient or the camera head of the declipseSPECT cart system, which may be required during surgery. It

#Surgery	Preparation	Pre-Scan	Pre-Recon	Surgical Act	Post-Scan	Post-Recon	End
1	389	111	19	1639	98	17	333
2	2253	99	20	1764	**116**	13	57
3	1536	102	15	1799	78	11	260
4	674	**140**	**50**	2394	91	16	99
5	776	93	25	807	94	27	126
6	289	98	23	1670	**129**	30	133
7	102	**152**	**37**	1412	**72**	14	144
8	430	97	22	2174	105	33	69
9	1146	116	16	2944	75	13	78
10	704	97	28	2232	86	18	247
11	1862	85	21	2924	97	16	136
12	135	**79**	20	2362	**66**	14	128
13	1819	98	20	634	78	13	512
14	1414	89	**13**	1959	77	10	972
15	361	**144**	34	1550	81	**62**	170
16	121	95	23	1644	100	25	182
17	3674	91	16	1589	83	26	1077
18	1543	104	27	3154	96	17	182
19	2707	**187**	**49**	2532	**144**	**39**	344
Mean	1154.47	109.32	25.16	1957	92.95	21.79	276.26
Stdev	987.50	27.41	10.51	673.51	19.95	12.69	287.02

Table 4.2.: Duration of workflow phases in seconds calculated automatically based on dedicated entries in Freehand SPECT user interaction logs of 19 different breast cancer sentinel lymph node biopsy surgeries. Bold: Outliers via $mean \pm stdev$ for scanning and reconstruction phases.

is expected that the scan coverage of both acquisitions overlap in patient target coordinate system as the surgeon scans the same region of interest (axilla) in both scans. Comparison of scan trajectories in patient target coordinate system revealed that in 18 out of 19 surgeries, this was the case as anticipated (e.g. Fig. 4.13 (left)). However strangely, in one surgery, the post-excision scan coverage was not overlapping with the pre-incision scan (Fig. 4.13 (right)). This finding is an indication for a usage problem during this surgery. Further investigation via the screenshots clarifies the reasoning behind this: The patient target was initially not taped on the patient properly and was misplaced during the surgical act between the two acquisitions. The surgeons reattached the target on the patient before the second scan, but of course not on the exact same position, so that a proper spatial comparison of pre- and post-scans was not possible anymore (Fig. 4.14).

Tracking problems can occur during surgery due to various reasons such as occlu-

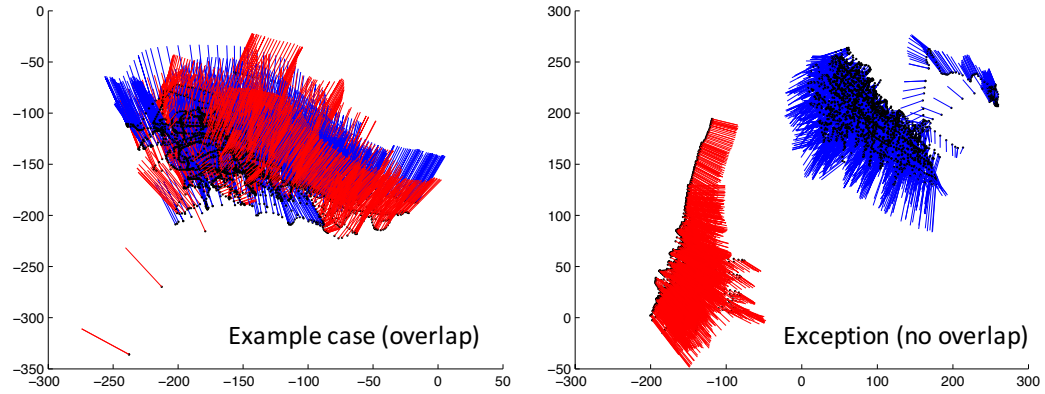

Figure 4.13.: Scan trajectories for two different surgeries in patient target coordinate system. Red: Pre-incision acquisition, Blue: Post-excision acquisition.

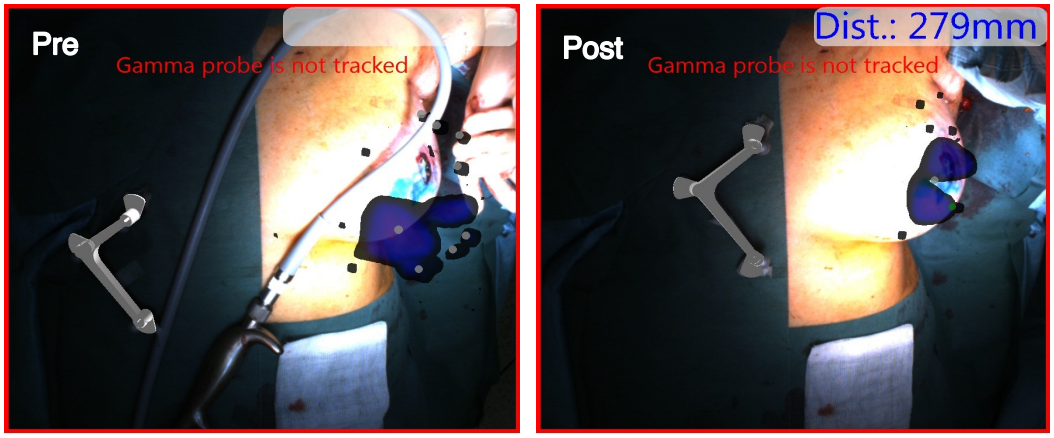

Figure 4.14.: AR view of non-overlapping Freehand SPECT reconstructions in one surgery. Left: Pre-incision reconstruction visualization before post-excision scan, patient target was initially taped on sternum but was shifted during surgical procedure so that the reconstruction is not visualized as expected. Right: Post-excision reconstruction, patient target repositioned on sternum.

sions, repositioning of the reference targets or the tracking camera as well as movement of tracked objects out of the tracking volume during scanning. If the declipseSPECT camera head and the reference patient target are positioned properly in *preparation* phase, both tracking targets should be in the field of view of the camera during the whole *scanning* phase. Missing tracking log values during *scanning* might indicate a usage problem which requires further attention. Table 4.3 shows the number of times tracking errors occurred

	Pre-Incision			Post-Excision		
#Surgery	Probe	Patient	Total	Probe	Patient	Total
1	1	0	1	**9**	1	**10**
2	1	3	4	3	**6**	**9**
3	5	0	5	2	0	2
4	**9**	1	**10**	0	0	0
5	1	0	1	0	0	0
6	0	0	0	0	0	0
7	1	0	1	0	0	0
8	3	1	4	**10**	0	**10**
9	3	1	4	3	0	3
10	1	0	1	0	0	0
11	3	0	3	**8**	2	**10**
12	1	0	1	1	0	1
13	1	0	1	2	0	2
14	**10**	0	**10**	3	0	3
15	4	0	4	1	0	1
16	0	2	2	1	1	2
17	3	1	4	2	**4**	6
18	1	0	1	0	0	0
19	3	**9**	**12**	2	0	2
Mean	2.68	0.95	3.63	2.47	0.74	3.21
Stdev	2.77	2.12	3.48	3.12	1.63	3.78

Table 4.3.: Lost tracking signals for both optical tracking targets. The values represent the number of times tracking errors occurred for patient and probe targets during *scanning* phase of pre-incision and post-excision acquisitions. Bold: High values indicating potential usage/handling problems during the *scanning* phase.

for both patient and probe targets during *scanning* phase of pre-incision and post-excision acquisitions. Via the comparison of the means and standard deviations for both tracking targets as shown in the table, it is clear that the surgeons experienced tracking problems more related to the probe than the patient reference target. This is not surprising since the operator needs to move the probe around in a freehand fashion for the acquisition. If not trained properly or if not paying too much attention, he or she may hold the probe in a wrong or tilted way while scanning so that the probe tracking target is not clearly visible by the camera head. Therefore, encountering some tracking related problems during the acquisition is common, but it is unusual to have a very high number of tracking problems especially since the declipseSPECT system warns the operator acoustically, if one of the objects are not tracked while scanning. If so, this clearly indicates there is a usage problem.

The automatic analysis of the log files for such tracking errors allows the identification of potential usage problems in a systematic and evaluator-independent manner.

4.4. Discussion

This chapter presented the methods and evaluations investigating the effect of the human component in Freehand SPECT imaging via two different sets of clinical data acquired during the intraoperative utilization of the Freehand SPECT in our university hospital. The first study focuses on the AR/VR visualization concept within 100 intraoperative acquisitions of the Freehand SPECT imaging by the manual analysis of the automatic screenshots generated by the system. By building on top of the experience and insights gained by this study, the methodology is extended in a following study by the inclusion and processing of further log files in a structured manner in order to determine the transitions of the surgical phases of interest as well as to identify potential usage problems, automatically.

Device and performance logging can be a very valuable asset for retrospective analyses of new technical solutions introduced to the surgical theater, especially in respect to the user experience and usage characteristics. The methods and studies presented in this chapter are based on manual analysis of the data or some basic automation approaches for the detection of surgical phase transitions and potential usage problems. This may be sufficient as a proof-of-concept, however, incorporation of machine learning algorithms can also be considered to further extend the capabilities.

Freehand SPECT is one of the first intraoperative devices, which makes full use of AR as well as VR visualization. Our analysis of the choice of user interface, mainly confirms the importance of the analysis of the surgical workflow and the need for adaptation of the user interface and visualization hardware and software to particular flow of subtasks within a surgical procedure. For each phase of the procedure, e.g. pre-incision or post-excision imaging, the OR team tends to prefer a particular mode of visualization. For some subtasks, e.g. setting proper threshold values for the reconstruction, AR has been the preferred visualization mode, while for other subtasks, e.g. image-guided resection of the lymph node, the preference goes to VR.

Based on our observations, we think that the final solutions would benefit by having alternate viewing modes, which may be more suited for different conditions. In fact, hybrid solutions may be the ones which will get accepted not only due to their flexibility but also because they offer wider ranges of customization. A surgical technique or a particular surgeon may opt for VR in a particular phase of the surgery because of need for precise measurement of the absolute size of an anatomical target; another one may prefer the AR

because of its ability of localizing the target within patient's anatomical context.

We believe that such flexibilities will also be needed both for the choices of tracking and display technology. Optical tracking for example could provide co-registered views of tracking targets and surgical site and therefore ease the generation of advantageous AR views, while other tracking technology may cope better with the limited space and crowdedness of OR within different phases of the procedures.

Hybrid display solutions may also offer different advantages for various subtasks of surgical procedures. In some phases, the surgeon prefers the surgical crew to share the information in order to provide further assistance and in other phases he or she may prefer direct in-situ visualization for better performing a particular task. Unfortunately, although the technology used in head-mounted displays is advancing every day, the available HMDs by the time of the initial development of the Freehand SPECT technology and its commercialization were not yet optimized in terms of size, weight, resolution, cabling and ease of use. Also, in this specific application, since AR is only needed for a short period of time and in fact more as a general guidance and confirmation rather than for precise localization and navigation, it is not justified both in terms of costs and in terms of efforts in adapting this technology.

One could also consider other possible AR display technologies, such as semi-transparent display [13], however in order to bring AR and VR techniques into the operating room, the smoothest path is to start with choices which do not introduce considerable changes to the surgical workflow and environment and require minimum training. Such considerations increase the chance of acceptance of the technology by surgeons.

The OR domain is complex. The study of this domain is fully required for the design and integration of AR and VR solutions, which can revolutionize the computer assisted interventions by providing the most valuable information, at the right time and in the right format within such interventions with the final goal of the improvement of outcome in terms of increasing success rate of surgical procedures and decreasing the morbidity.

Freehand SPECT is one of the first clear successes of mixed reality based visualization solutions as integrated parts of an intraoperative imaging device. Still there is place for further analysis on the impact of this solution on the clinical output. Such analyses if performed in a controlled way will provide hard numbers on the efficacy of mixed reality in terms of time saving, accuracy and errors in the procedure. The surgical theatre will most probably welcome more and more such solutions in the upcoming years as the medical community gets used to such interfaces over time and takes advantages of their capabilities as such solutions get adjusted to the complex and dynamic requirements of different phases of various surgical procedures.

CHAPTER 5

Freehand SPECT with High Energy Gamma Probes

The Freehand SPECT concept was initially introduced by Wendler et al. as an extension of the conventional gamma probes by attachment of optical spatial tracking technology and generation of 3D reconstructions based on non-uniform projections acquired by moving the detector probe in a freehand fashion in the volume of interest [119]. Even though Freehand SPECT was first applied for the radioguided surgery technique of sentinel lymph node biopsy with ^{99m}Tc [120], theoretically its application is not limited to conventional gamma probes and that particular radionuclide.

In this chapter, we aim to take one step further and investigate the applicability of 3D Freehand SPECT imaging using positron emitting radiotraces such as ^{18}F-FDG. The proposed system combines a high energy gamma detection probe with an optical tracking system. Detection of the 511 keV annihilation gammas from positron emitting radiotracers is modeled analytically. The algorithm iteratively reconstructs the radioactivity distribution within a localized volume of interest. Based on the PET/CT data of patients with tumors and lymph node metastases in the head and neck region, a neck phantom with ^{18}F-FDG-filled reservoirs representing tumors and lymph nodes is constructed to evaluate the limitations and capabilities of the approach.

This chapter is organized as follows: Section 5.1 introduces the clinical motivation as well as the challenges behind the proposed adaptation of Freehand SPECT imaging for high energy gamma radiation emitting radiotracers such as ^{18}F-FDG. Thereafter, the materials and methods required for the integration of high energy gamma radiation detectors into Freehand SPECT imaging are explained in section 5.2 in detail. Following that, the phantom experiments and the associated results investigating the capabilities of this methodology are presented in section 5.3 and discussed in section 5.4.

Substantial parts of this chapter have already been published in the following articles and are partially quoted verbatim:

[96] D.I. Shakir, **A. Okur**, A. Hartl, P. Matthies, S.I. Ziegler, M. Essler, T. Lasser, and N. Navab. Towards Intra-operative PET for Head and Neck Cancer: Lymph Node Localization Using High-Energy Probes In *Medical Image Computing and Computer-Assisted Intervention - MICCAI 2012*, volume 7510 of *Lecture Notes in Computer Science*, pages 430–437. Springer International Publishing, 2012.
Copyright Statement. ©2012 Springer International Publishing.

[85] **A. Okur**, D.I. Shakir, P. Matthies, A. Hartl, S.I. Ziegler, M. Essler, T. Lasser, and N. Navab. Freehand Tomographic Nuclear Imaging Using Tracked High-Energy Gamma Probes In *Bildverarbeitung für die Medizin 2013. Informatik aktuell*, pages 362–367. Springer Berlin Heidelberg, 2013.
Copyright Statement. ©2013 Springer Berlin Heidelberg.

5.1. Introduction

Patients diagnosed with head and neck squamous (epithelial) cell carcinoma (HNSCC) are mostly treated by a surgical procedure where the major aim is to resect the tumor and all lymph node metastases. Although the metastatic lymph nodes can be identified preoperatively with high sensitivity and specificity using ^{18}F-FDG-Positron-Emission-Tomography (PET) and Computed tomography (CT), in clinical practice *all* lymph nodes in the region of the suspicious one(s) are resected. Even though the tumor itself is mostly easily accessible for the surgeon, the intraoperative detection and resection of the few small *metastatic* lymph nodes is very difficult especially due to the presence of vital anatomic structures such as nerves and vessels in the neck region. In order to detect these metastatic lymph nodes intraoperatively, additional preoperative injection of PET imaging tracer ^{18}F-FDG (e.g. 1 hour before surgery) and intraoperative usage of dedicated high energy gamma radiation detectors would be required, since the metastatic lymph nodes with an increased glucose metabolism cannot be assessed visually, but only via radiation detection. Aesthetic concerns motivate minimally invasive interventions as well.

High energy gamma probes are used in clinical practice, for example in head and neck squamous cell carcinoma [74] and thyroid cancer applications [58], however without tracking and navigation capabilities. Intra-operative PET scanners [102, 66], combined intraoperative PET and transrectal ultrasound [51], or handheld PET imaging probes with an external detector ring for full tomographic data [52] have also been introduced in the scientific community. However, such high energy gamma probes are not commonly used for

radioguided surgery applications as discussed in chapter 2 (Table 2.7). Due to the challenges attached to the intraoperative high energy gamma radiation detection, conventional gamma probes and radiotracers suited for detection of the SPECT energy window dominate the clinical application field.

This chapter presents the contributions concerning Freehand SPECT imaging with high energy gamma radiation detection probes, a system to image and detect *PET-positive* lymph nodes intraoperatively. The iterative 3D reconstruction of the radiotracer distribution within the volume of interest (VOI) is based on analytical models of the detection physics [44, 43]. Please note, that even though this proposed Freehand SPECT system with high energy probes is also called shortly as Freehand PET in our prior publications due to its utilization with positron emitting radiotracers, in the remainder of this dissertation, this definition is not preferred, since the system is not based on coincidence detection as in positron emission tomography (PET).

5.1.1. Clinical Workflow

Typically, a cancer is diagnosed only after the appearance of symptoms, which affect the daily life of the patient. In the case of head and neck squamous cell carcinoma (HNSCC), the most common symptom is a swelling or sore throat which does not heal. However, there is a huge variety of symptoms like pain, persistent sore throat, change in voice, difficulty in breathing, frequent nose bleeds or unusual nasal discharge, which can be related specifically to the tumor site of the head and neck cancer [95, 20]. Nevertheless, one should note that sometimes patients diagnosed with head and neck cancer may not necessarily have any of such symptoms at all. Furthermore, the cause of such a symptom may also be a different medical condition that is not cancer so the proper diagnosis can be done only by an otolaryngologist - ear, nose and throat (ENT) specialist - with additional findings, tests and examinations.

An ultrasound scan of the region is the first essential step for the diagnosis of the cancer. Most of the time, the primary tumor is determined via ultrasound examination due to its suspicious presence and no further imaging modality may be required. A PET/CT examination may be requested in addition with intravenous ^{18}F-FDG injection (subsection 2.2.2) for further confirmation, if the physician suspects spread of the cancer to the lymphatic system due to the presence of enlarged lymph nodes in the area of the tumor in ultrasound examination.

Based on our discussions with an experienced nuclear medicine physician at Klinikum rechts der Isar, the proposed Freehand SPECT imaging approach with high energy gamma

probes and ^{18}F-FDG injection was assessed as especially beneficial for the intraoperative detection of metastatic lymph nodes of *recurring* head and neck squamous cell carcinoma. According to the specialist, if a surgical treatment is indicated for the patient including lymph node dissection, the primary tumor is excised desirably with a clean resection margin and preferably all the lymph nodes in the neck region are targeted for resection during the first surgery. Depending on the stage of the diagnosed cancer and the pathological results of the resected tissue and lymph nodes, the patient may receive postoperative radiotherapy or chemotherapy treatment in addition.

After such a treatment, the patients are subject to follow-up screenings for cancer recurrence. By such patients, enlarged lymph nodes in routine follow-up ultrasound scans are indicators for recurrence, so PET/CT examinations are indicated for further investigation, as such metastatic residual lymph nodes can be identified due to their increased ^{18}F-FDG uptake. Another surgical treatment may be considered in rare cases, if the recurring cancer is in an early stage, meaning it is focal and not widely spread yet. In such a follow up surgery, it is extremely challenging to identify the metastatic tissue or the very few metastatic PET-positive lymph nodes in the region, mainly due to the large tissue loss and the morbidity caused by the primary surgery [95]. Therefore, it is of high clinical relevance to intraoperatively guide the surgeon to these few metastatic lymph nodes in with the aid of an intraoperative nuclear imaging and navigation system such as Freehand SPECT.

5.2. Materials and Methods

5.2.1. System Description

The proposed solution combines a high energy gamma probe (NodeSeeker 800, Intra Medical Imaging LLC, CA, USA) with an optical tracking system (Polaris Vicra, Northern Digital Incorporated, ON, Canada). An application workstation (declipseSPECT, SurgicEye GmbH, Munich, Germany) is available for synchronisation of the data as well as the computation of the reconstruction and its augmented visualization. The software on this workstation is modified for supporting the detection model and the characteristics of this specific probe.

Although the introduced system is very similar to the Freehand SPECT technology, the accurate modeling of the high energy gamma rays and their detection result in some additional challenges. First of all, these annihilation gamma rays caused by positron-emitting radiotracers such as ^{18}F-FDG can penetrate through matter more than e.g. the gamma rays of ^{99m}Tc due to their much higher energies. Even though the high energy probes are

constructed with much thicker shielding, it may be not sufficient enough to block all the background gammas. Furthermore, the ^{18}F-FDG is injected to the patient systematically, which is distributed via the blood vessels to the whole body, resulting in a non-zero background and causing also some unspecific ^{18}F-FDG uptake in tissue (subsections 2.2.2 and 2.3.2). In contrast, the radiotracers used in sentinel lymph node procedures are injected locally around or close to the tumor and are distributed via the lymphatic system, resulting in almost no unspecific uptake (subsections 2.2.1 and 2.3.1).

5.2.2. Freehand SPECT Imaging with High Energy Gamma Probes

Previously in chapter 3, Freehand SPECT imaging is presented in detail including different types of radiation detectors which can be used for Freehand SPECT imaging (section 3.3) and the mathematical foundations for the generation of 3D reconstructions out of readings provided by these gamma radiation detection systems (section 3.6). The major challenge in this work is the utilization of a different gamma radiation detection system for Freehand SPECT imaging, namely a high energy gamma radiation detection probe which is designed and calibrated for the detection of high energy photons instead.

A high energy gamma probe is a handheld radiation counter, typically with a thick shielding around the detector head, that can detect annihilation gamma rays (511keV) resulting from positrons emitted by the radiotracers. In contrast to regular diagnostic PET imaging systems with multiple detectors around the patient, which are based on coincidence detection and detect the two (almost) simultaneous annihilation gamma rays in opposite directions, a high energy gamma probe alone can only detect one of these annihilation gamma rays. Furthermore, since these annihilation gammas have a much higher energy (511keV) compared to the gamma rays emitted by SPECT tracers such as ^{99m}Tc (141keV), a much better and thicker collimation is required for the detector crystal of the high energy gamma probe to assure the desired field of view (FOV) and to block the scattering and the radiation from outside of the FOV accordingly (Figure 5.1). This requirement results in bulkier and heavier handheld gamma radiation detectors which are not as easy to handle as the regular gamma probes during a surgical procedure.

A gamma probe provides only a one dimensional signal which is proportional to the amount of detected radiation in the field of view. It is by itself not sufficient for generation of 3D images. Therefore, a model of the physical factors affecting the detection of the radiation is required. Also it needs to be combined with a spatial positioning system so that the acquired probe signals during the scanning phase are mapped to the positions and orientations of the probe with respect to the volume of interest (VOI) discretized into vox-

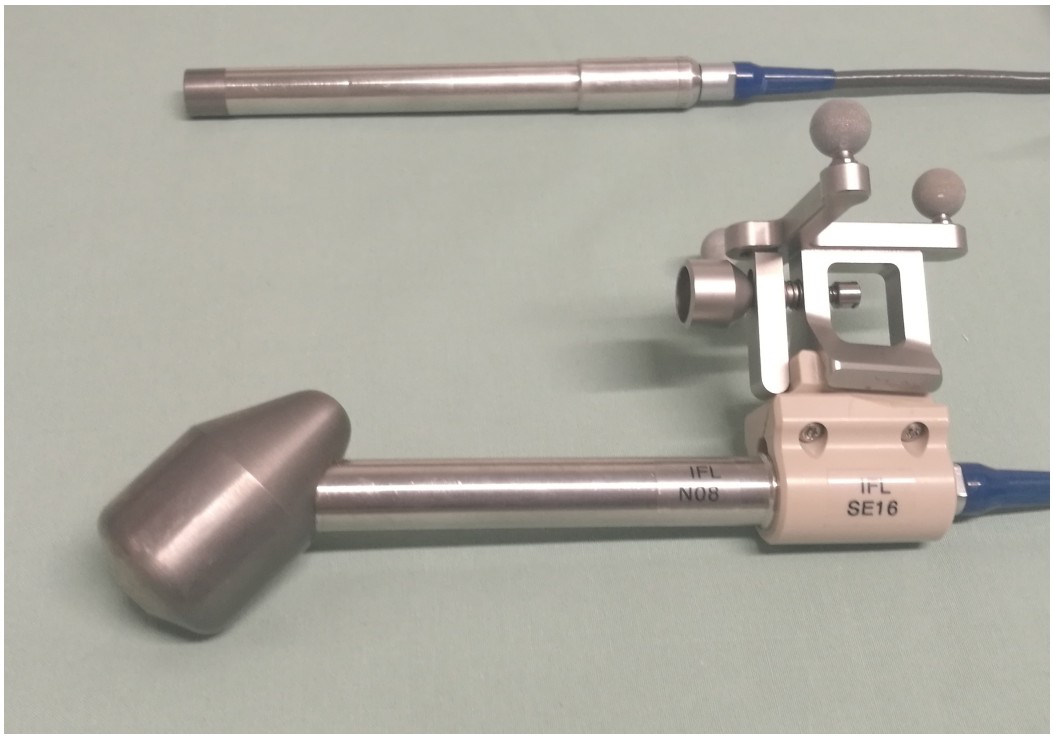

Figure 5.1.: Comparison of different gamma probes available for the NodeSeeker 800 gamma probe detection system. High energy gamma probe (bottom) is heavier, has a thicker collimation and has a tilted field of view in contrast to the low-energy gamma probe (top).

els. Each probe measurement y_j is modeled by a linear combination of the contributions a_{ji} of the unknown activity values x_i in all voxels:

$$y_j = \sum_i a_{ji} x_i$$

All the measurements within a scan can be stacked into a system of linear equations $\vec{y} = A\vec{x}$ using this model. The activity distribution in the VOI can be retrieved using an iterative solver like MLEM (Maximum Likelihood Expectation Maximization) [119]. The system matrix A with the contributions a_{ji} is needed for the inversion, so the contributions are computed on-the-fly using an ad-hoc model of the detection physics of the probe [44, 43], since the acquisition geometry is not fix.

(a) (b)

Figure 5.2.: Phantom construction. (a) The neck phantom was constructed by using a plastic cylinder (very close to the human neck in dimension) and three 2 ml laboratory reservoirs: two were rigidly glued to each other for simulating the tumor (blue arrow), and a third one was used for simulating the lymph node (red arrow). (b) A tracking target was attached on top of the phantom, and after preparation with ^{18}F-FDG, the phantom was scanned using our system.

5.2.3. Experiments

In order to demonstrate the capabilities of the proposed system, a phantom simulating a tumor and a lymph node in the neck region was prepared, using a plastic cylinder with 125 mm diameter and three rigidly fixed plastic lab reservoirs with 2 ml volume each (Figure 5.2 (a) and (b)). Using this phantom, three sets of experiments were conducted in total to evaluate the Freehand SPECT imaging using high energy gamma probes for the the identification and localization lymph node metastases in head and neck cancer and in particular HNSCC. For the first set of experiments, PET/CT images from 7 patients (mean age: 53, 6m/1f) were analyzed. Each patient had one or two PET-positive lymph nodes. Based on these data sets, the radioactivity distributions were calculated for the reservoirs representing the lymph node and the tumor in the realistic experiments with ^{18}F-FDG (Table 5.1). The plastic cylinder was then filled with water to simulate human tissue.

In order to determine the limits of the system, the activity proportions in the second set of experiments were increased, where the aim was to determine the required activity level which the system can reconstruct both the tumor and the lymph node.

For comparison of the system with the images of the commercially available Freehand

SPECT system, a third set of experiments were conducted, where the same radioactivity proportions were used as in the second set, but this time the experiments were conducted with ^{99m}Tc as radionuclide and a conventional gamma probe instead of ^{18}F-FDG and the high energy gamma probe.

In all these experiments, two operators scanned each phantom configuration either two or three times each, with an angular coverage of about 120 degrees and with 3000 measurements. In each case the resulting system of linear equations was inverted using MLEM with 20 iterations. On the obtained reconstructions a 4 or 6 mm Gaussian filter was applied to reduce noise due to the highly under-sampled acquisition with insufficient statistics as in Freehand SPECT.

5.3. Results

To evaluate the experiments qualitatively, the visibility of the tumor and the lymph node in the individual reconstructions were analysed. In the first set of experiments, the lymph node could be identified in 3 of the 6 reconstructions. On the other hand, the tumor could not be distinguished visually in any of these 6 reconstructions with realistic activity concentrations.

The lymph node could be identified in all of the 16 reconstructions in the second set of experiments (Figure 5.3(a)). Furthermore, the tumor could be seen in 6 reconstructions where 3 out of 6 were even with background radioactivity. In one of the reconstructions, the two individual reservoirs next to each other simulating the deeply seated tumor could even be identified visually in probe-view (VR) visualization provided by the declipseSPECT cart system (Figure 5.3(b)).

In the third set of experiments using ^{99m}Tc and a regular gamma probe, the lymph node

	Mean $\pm$ standard deviation
tumor depth from the surface:	5.3 $\pm$ 1.06 cm
lymph node depth from the surface:	2.6 $\pm$ 0.99 cm
tumor-to-background (T/BG) uptake ratio:	3.3 $\pm$ 1.17
tumor-to-lymph node (T/LN) uptake ratio:	1.5 $\pm$ 0.97
tumor uptake:	23.8 $\pm$ 9.41 kBq/ml
lymph node uptake:	21.3 $\pm$ 12.75 kBq/ml

Table 5.1.: The geometrical and activity-related parameters calculated from clinical data.

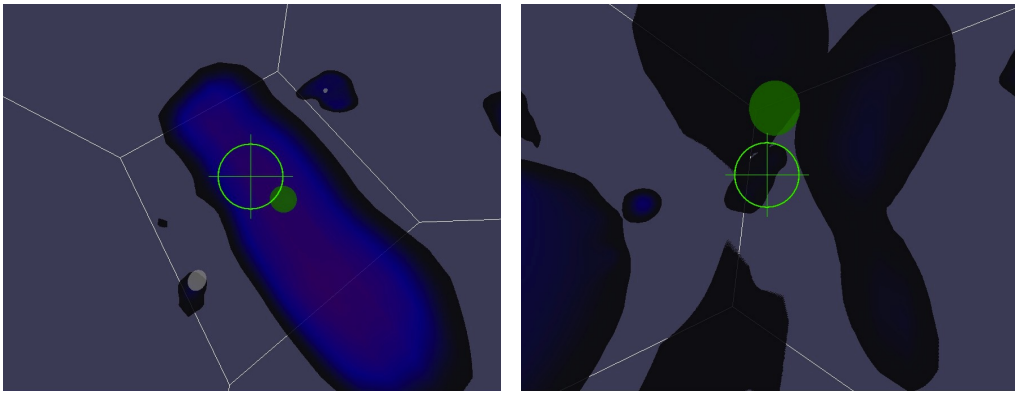

(a) (b)

Figure 5.3.: VR (probe-view) visualization of the reconstruction. (a) The shape of the reservoir representing the lymph node can be distinguished in the visualization of the reconstruction as seen from the probe tip. (b) The two reservoirs next to each other representing the tumor can be seen separately in one reconstruction although they are deeply seated.

could be determined in all of the 12 reconstructions. The tumor was also identified visually in 8 out of 12 reconstructions, 3 out of 6 being with background radioactivity.

For quantitative evaluation, a CT of the phantom was obtained as well to serve as the ground truth. CT data was then registered to Freehand SPECT reconstructions in all sets of experiments with both regular and high energy gamma probes using the phantom tracking target. The center of the lymph node and the tumor in the CT images were selected manually and used for the distance calculation to the centroids of the lymph node and the tumor in the registered images, for the cases where they were clearly identified and segmented (Figure 5.4).

Experiment setup	BG:T:LN	LN localization error	Tumor localization error
1. ^{18}F-FDG low	0:17:10	12.67 $\pm$ 2.48 mm	NA
2. ^{18}F-FDG high	0:20:20	13.57 $\pm$ 4.22 mm	34.79 $\pm$ 6.20 mm
	1:20:20	14.41 $\pm$ 5.75 mm	47.39 $\pm$ 22.28 mm
3. ^{99m}Tc high	0:20:20	11.35 $\pm$ 4.26 mm	39.39 $\pm$ 10.60 mm
	1:20:20	10.85 $\pm$ 4.07 mm	20.42 $\pm$ 2.55 mm

Table 5.2.: Accuracies achieved in experiments with different configurations.

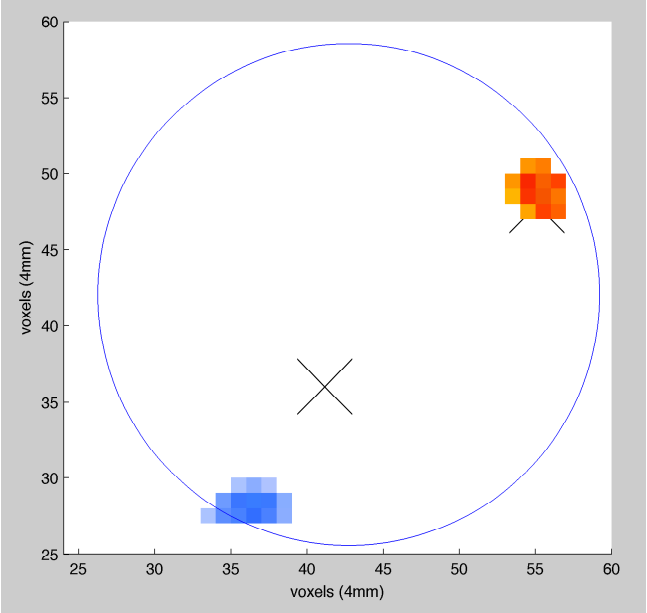

Figure 5.4.: Visualization of localization errors via a transverse slice of one segmented reconstruction. Red: Reconstructed lymph node. Blue: Reconstructed tumor. Circle: Outline of the phantom. Crosses: Positions obtained from the ground truth.

5.4. Discussion

The reservoir filled with ^{18}F-FDG representing the lymph node was reconstructed in all cases, however with a localization error between 12.7 and 14.4mm (Table 5.2). At the experiments with realistic activity concentrations based on the PET/CT data of patients, the tumor site could not be identified in the reconstructions at all. At the second set of experiments with increased activities, the tumor site was identified visually but unfortunately with very high localization errors. Although the detection of the tumor itself is not the primary focus of this clinical application, this finding still indicates that some improvements are required. The sub-optimal collimation in the currently available high energy gamma probes may be a limiting factor for the accuracy of the detection. Placing an additional detector block under the patient and detecting the coincidences can be considered to overcome this issue with detection accuracy. However, this would require major modification inside the operating room, so the proposed system would be more feasible for the surgery, if it can meet the accuracy requirements of the intervention.

A better physical model of the detection process or inclusion of attenuation correction and scatter effects could further improve the image quality of the proposed Freehand SPECT system with high energy gamma radiation probes. Registration of preoperative PET/CT data could be beneficial to provide attenuation correction information for better reconstructions as well. This could also lead to acquisition guidance and artifact reduction using prior information. Furthermore, utilization of intraoperative ultrasound in addition to Freehand SPECT imaging can be considered for the registration of such preoperative clinical data inside the operating room.

CHAPTER 6

Towards Non-Surgical SLNB for Breast Cancer

Ultrasound guided core needle biopsy of sonographically suspicious axillary lymph nodes has been introduced for cancer staging of early stage breast cancer [3]. However, core needle biopsy of the axillary *sentinel* lymph nodes is not established, as ultrasound images alone do not suffice to differentiate the sentinel from other lymph nodes in the same region. A proper combination of functional and anatomical information is required for being able to perform core needle biopsies of axillary sentinel lymph nodes.

In this chapter the first feasibility study for fully 3D Freehand SPECT - ultrasound fusion combining the advantages of both modalities is presented. By using spatial positioning either with optical or with electromagnetic tracking for the ultrasound probe, and a mini gamma camera as radiation detector for Freehand SPECT reconstructions, the capability of the introduced multi-model imaging system is investigated, where both 3D Freehand SPECT and 3D ultrasound are compared to ground truth for a realistic breast mimicking phantom and the effect of tissue deformation by ultrasound is investigated. Finally, its application in a real clinical setting is also demonstrated.

This chapter is organized as follows: In section 6.1, the clinical motivation behind the proposed 3D Freehand SPECT and ultrasound fusion is introduced and prior works in literature and our contributions in the field are summarized. Thereafter, section 6.2 establishes the necessary materials and methods behind the fully 3D Freehand SPECT and ultrasound fusion in detail. Associated experiments and their results are presented in section 6.3 and thoroughly discussed in section 6.4.

Substantial parts of this chapter have already been published in the following article and are partially quoted verbatim:

[84] **A. Okur**, C. Hennersperger, B. Runyan, J. Gardiazabal, M. Keicher, S. Paepke, T. Wendler, and N. Navab. fhSPECT-US Guided Needle Biopsy of Sentinel Lymph Nodes in the Axilla: Is it Feasible? In *Medical Image Computing and Computer-Assisted Intervention - MICCAI 2014*, volume 8673 of *Lecture Notes in Computer Science*, pages 577–584. Springer International Publishing, 2014.

6.1. Introduction

Sentinel Lymph Node Biopsy (SLNB) is a standard surgical procedure in early breast cancer for determination of the cancer stage [112]. By injecting dedicated radiotracers (commonly a Technetium-99m-radiocolloid) close to the tumor, and using appropriate imaging techniques with dedicated gamma radiation detectors, such as scintigraphy or SPECT, it is possible to visualize the sentinel lymph node(s) (SLN(s)), which is/are the first node on the lymphatic drainage way and is/are most likely to have (micro-)metastasis in case the tumor has progressed.

During surgery, the breast surgeon can differentiate between the radioactive SLNs and non-radioactive lymph nodes (LNs) with small handheld gamma radiation detectors, typically conventional gamma probes. However, this is not an easy task, especially in patients where the sentinel lymph node is too close to the actual injection site due to the collimation and sensitivity of the gamma probe as well as the shine-through and shadowing effect of the injection. It has been shown that Freehand SPECT (fhSPECT) [120], an intraoperative 3D nuclear imaging technique based on tracked gamma probes, can improve the discrimination for breast cancer patients [16]. Furthermore, mini gamma cameras, providing real-time 2D images of the axilla, recently also have found their way into the operating room [18].

Until now, these solutions made the localization of the SLNs much more convenient for the surgeon, however, the excision of the SLN still takes place inside the operating room under surgical conditions including general anesthesia. The reason for this fact is that such nuclear images alone do only provide *functional*, but no anatomical information.

In contrast to this, ultrasound (US) imaging is providing *anatomical* information and is also common practice for staging of lymph nodes. However, ultrasound can only detect metastatic lymph nodes since these lymph nodes are typically comparably bigger and appear conspicuous in ultrasound images. In early stage breast cancer where the SLNB is indicated, metastatic and healthy lymph nodes in axilla cannot be differentiated in ultrasound. Thus, only few experienced sonographers are currently doing ultrasound-

guided core needle biopsies on suspicious lymph nodes to enable proper, patient-specific chemotherapy planning for the patient. However, this minimal invasive procedure is still a challenging task due to deforming tissue and major veins adjacent to the nodes to biopsy.

In order to be able to perform ultrasound-guided core needle biopsies of the radioactively labeled *sentinel* lymph nodes, one needs to combine the advantages of both modalities. The fusion of Freehand SPECT with ultrasound could thus help the physician to identify the SLNs on ultrasound images and eventually to perform core needle biopsies during ultrasound examination by using only local anesthesia.

In general, combination of ultrasound with nuclear information has been proposed by [118], where optically tracked gamma probes were used, but did not include 3D SPECT-like reconstructions. Nowadays, there are solutions available, which allow quasi real-time fusion of 3D nuclear functional images with the ultrasound. Freesmeyer et al. [32] published their first clinical experience and results with such a system on thyroid patients. However, this work lacks on quantitative evaluation of the quality of the 3D reconstructions and uses a non-diagnostic version of Freehand SPECT (lower image resolution and sensitivity).

In this work, the 3D fusion of the Freehand SPECT and ultrasound data for the application in breast cancer is investigated for the first time. To do so, a system is proposed which is based on optically tracked 3D Freehand SPECT using mini gamma cameras instead of gamma probes for increased radiation detection and image quality, as well as on 3D freehand ultrasound data acquired either with optical (OP) or electromagnetic (EM) tracking. Both technologies are then compared to ground truth SPECT/CT obtained for a realistic breast mimicking phantom and the effect of the tissue deformation by the pressure applied during ultrasound acquisition is evaluated. Finally, results on real clinical cased with such a system are presented.

6.2. Materials and Methods

6.2.1. Hardware Setup

For this study, a Sonix RP ultrasound system (Ultrasonix, MA, USA) is used with a linear ultrasound probe (L14-5 GPS) (Figure 6.1), which incorporates a sensor for the electromagnetic tracking system (3D Guidance driveBAY 2, Ascension Technology Corporation, VT, USA). To compare the accuracy of the electromagnetic to the optical tracking for ultrasound, a reference target is mounted on the probe (Figure 6.2(a)).

The Freehand SPECT images are generated using a declipseSPECT Imaging Probe sys-

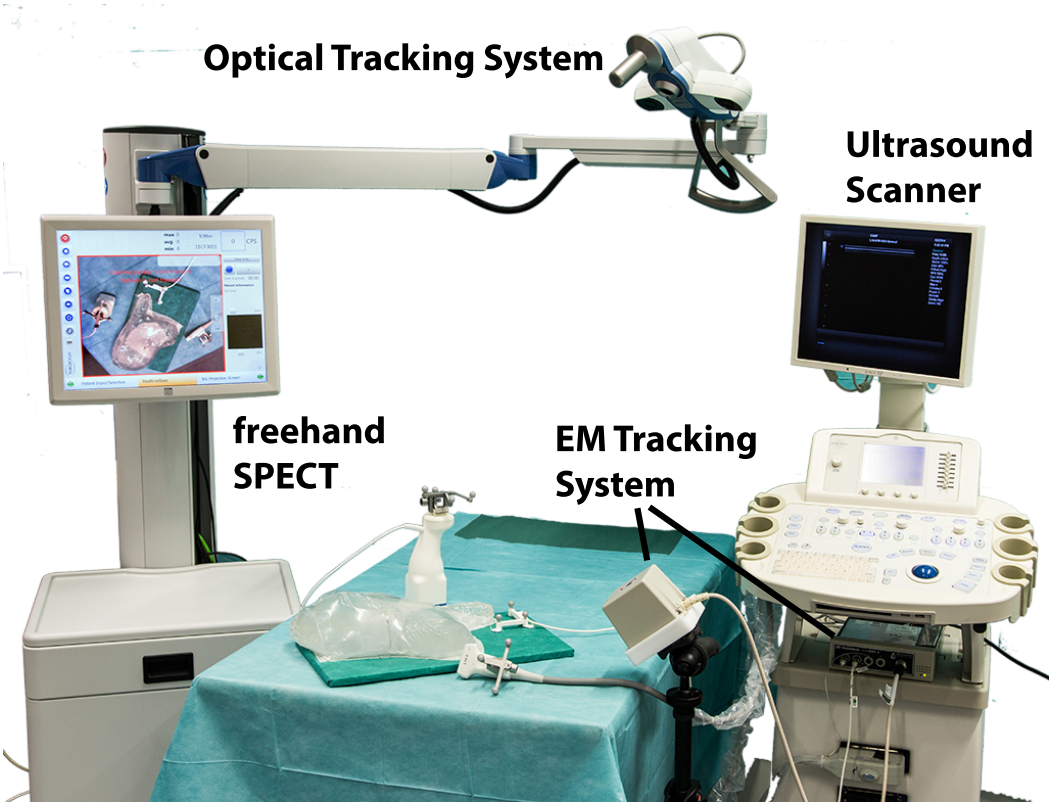

Figure 6.1.: Hardware setup. For Freehand SPECT imaging the declipseSPECT Imaging Probe system which includes Polaris Vicra optical tracking system and for ultrasound imaging the Sonix RP ultrasound system which includes the 3D Guidance driveBAY 2 EM tracking system are used in the experiments.

tem (SurgicEye GmbH, Munich, Germany), which uses a 2D mini gamma camera (Crystal Photonics, Berlin, Germany) for radiation detection (Figure 6.2(b)) and an infrared optical tracking system (Polaris Vicra, Northern Digital Inc., Ontario, Canada) for spatial positioning. The 3D Freehand SPECT images are reconstructed using the declipseSPECT software. The ultrasound images and the meta data with the ultrasound settings are saved synchronized with the tracking information from both of the localization systems.

6.2.2. Freehand SPECT Reconstruction

The Freehand SPECT system uses position information from the optical tracking system in addition to nuclear information from the attached radiation detector, in this particular study a handheld mini gamma camera. This information is then combined with calibration data

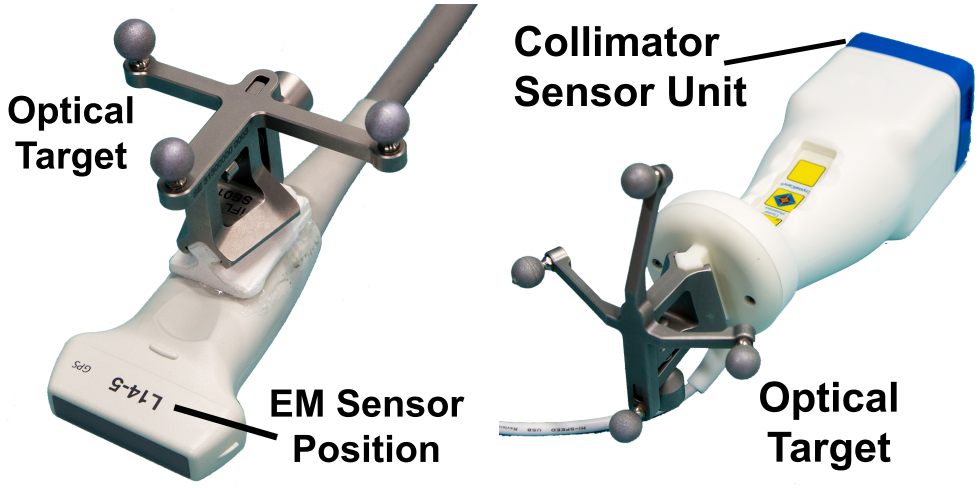

(a) (b)

Figure 6.2.: Close-up images of the tracked instruments for 3D imaging. (a) Ultrasound transducer with both EM sensor and optical reference target. (b) CrystalCam mini handheld gamma camera with optical reference target

specific for the detector to produce an input data set. The input data set is then processed using a standard Maximum Likelihood Expectation Maximization (MLEM) solver. Post processing options can include Gaussian filtering, if desired.

Details about Freehand SPECT imaging in general as well as the mathematical background on the iterative reconstruction algorithm employed in Freehand SPECT were given previously in chapter 3 and section 3.6 in particular.

6.2.3. Ultrasound Calibration

To calibrate the ultrasound probe for both tracking systems, a calibration phantom similar to the one in [64], is constructed. It consists of a pyramidal aluminum frame, where its three faces are covered with a thin nylon layer. In contrast to [64], the three faces all join at the same vertex with face angles of $90°$, resulting in a trirectangular tetrahedron, whose three edges form a local coordinate system. For calibration, an ultrasound sequence of the pyramid is acquired such that the intersection of the ultrasound image plane and the pyramid forms a triangle. Based on the pyramid coordinate system, direct point correspondences from 2D image points in the ultrasound plane to the corresponding positions in 3D space can be established, and used to obtain the transformation from the ultrasound plane

to the coordinates of the tracking system, cf. [108].

6.2.4. Ultrasound Compounding

As visualization is of crucial importance for the fusion of Freehand SPECT to 3D ultrasound data, a volume compounding step is employed, i.e. an interpolation of the acquired, irregularly sampled ultrasound data on a rectangular grid, yielding a 3D volume. Compounding is applied as a backward-warping normalized convolution directly on the ultrasound scanlines, following the approach of Hennersperger et al. in [49]. As this system provides fast compounding and resulting volumes of high quality, it is suitable for direct fusion with Freehand SPECT images.

6.2.5. Freehand SPECT / Ultrasound Fusion

The fusion of the final images for both Freehand SPECT and ultrasound data is assured with the aid of a reference target, which is tracked both optically and electromagnetically. This reference target can be seen on Figure 6.3(a).

The final DICOM files generated by the Freehand SPECT system are saved in the coordinate system of the optical reference target on the patient. Therefore, this coordinate system is used as the base for all the calculations. For a point in ultrasound plane, in the case of dual tracking, the following transformation chain is applied to get its positions in the reference frame of the optical reference target

$$^{refOP}\mathbf{T}_{US} = {}^{refOP}\mathbf{T}_{refEM} \cdot {}^{refEM}\mathbf{T}_{worldEM} \cdot {}^{worldEM}\mathbf{T}_{probeEM} \cdot {}^{probeEM}\mathbf{T}_{US}$$

In the case of optical tracking only, the sequence shortens to

$$^{refOP}\mathbf{T}_{US} = {}^{refOP}\mathbf{T}_{worldOP} \cdot {}^{worldOP}\mathbf{T}_{probeOP} \cdot {}^{probeOP}\mathbf{T}_{US}$$

where the transformations from the ultrasound plane to the optical target $^{probeOP}\mathbf{T}_{US}$, as well as to the EM sensor on the ultrasound probe $^{probeEM}\mathbf{T}_{US}$ are calculated as mentioned before. Furthermore, the transformation between the optical tracking target, serving as a reference for the patient, and the electromagnetic sensor rigidly attached to it, is known from precision manufactured target construction files. Alternatively, a calibration of the reference target with respect to EM and optical tracking system can be achieved by hand-eye calibration [108].

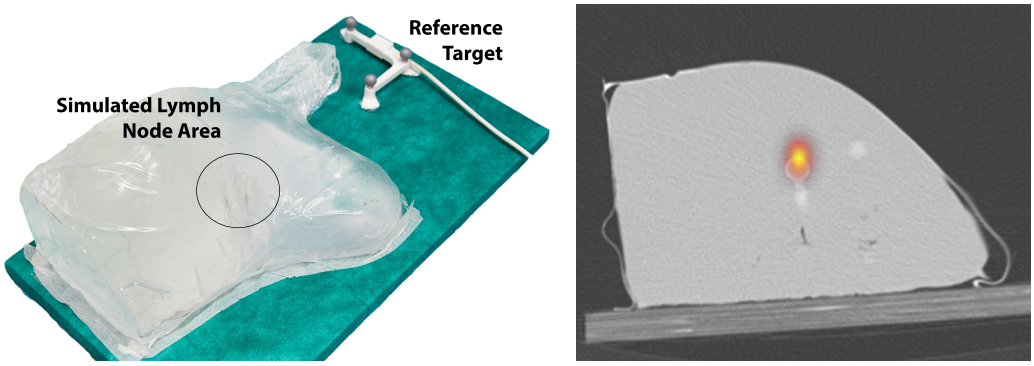

(a) (b)

Figure 6.3.: Phantom used in experiments. (a) Tissue mimicking breast phantom, where the spheres represent lymph nodes. (b) SPECT/CT fusion of the radioactive sphere in the phantom (ground truth).

6.3. Experiments and Results

6.3.1. Phantom Design

In order to demonstrate the technical feasibility of the system, possible phantom designs were discussed with experienced breast surgeons and nuclear medicine physicians to model the clinical scenario in the best possible way. With the goal of a realistic biopsy phantom for the axilla region, a plastic female torso mannequin is cut at the region of one breast and the axilla, which is then used as a mold for a phantom. As tissue mimicking material, Ceraflex N530 gel (C Tromm GmbH, Germany) is used, as it is well suited for ultrasound, SPECT and CT imaging, and additionally deforms in a realistic way when pressure is applied to the surface (Figure 6.3(a)). Thus, the phantom does not only allow for an evaluation of the US-SPECT fusion by itself, but it also makes an analysis of the changes in accuracies due to tissue deformation possible.

To evaluate the fusion scenario with the goal of finding the sentinel lymph nodes to biopsy, 4 spheres with similar sizes as the lymph nodes (240-300 µl) are placed in the phantom. One of spheres is filled with 1.1 MBq of Tc-99m before insertion into the phantom to represent a sentinel lymph node, while the others are filled with water representing non-radioactive lymph nodes in the same region.

6.3.2. Data Acquisition

The phantom is scanned with both the Freehand SPECT and the 3D ultrasound systems in 5 different configurations with varying positions and orientations of one or both tracking systems with respect to the breast phantom (cf. Figure 6.1). In each configuration, the phantom is scanned at least once with the Freehand SPECT system for about 2 minutes. Furthermore, at least 2 sweeps are acquired with the 3D ultrasound system for each configuration, trying to cover all spheres. To evaluate the quality of the 3D ultrasound system on its own, both EM and optical tracking systems are used simultaneously for the acquisitions, enabling a direct comparison of the resulting accuracies for both systems. Furthermore, the impact of deformation changes are evaluated separately using 4 ultrasound acquisitions with varying pressure applied to the breast phantom surface.

All phantom acquisitions for both Freehand SPECT and ultrasound are performed by the same person to avoid user-dependent variation. Finally, a SPECT/CT (Siemens Symbia T6) of the phantom was acquired to serve as ground truth image data for the evaluations of the acquired data with both Freehand SPECT and ultrasound systems (Figure 6.3(b)).

6.3.3. Offline Evaluation

Freehand SPECT and ultrasound images are evaluated against the ground truth CT images separately, by comparing the centroids of the spheres placed in the phantom with respect to the optical reference target. First, the transformation from CT coordinates to the reference target coordinates is calculated by the means of point based registration. This is achieved by using the coordinates of the centers of the retroreflective spheres on the reference target in the CT image and their corresponding known coordinates based on its computer-aided design (CAD) files. The root mean square (RMS) registration error for the transformation is calculated as 0.8 mm.

For each of the Freehand SPECT reconstructions the hotspot is segmented with an automatic region growing algorithm using the global maximum as the seedpoint and 50% as threshold. Later, the centroid of the segmented hotspot is computed and its coordinates with respect to the patient reference frame is calculated using the meta information of the DICOM tags of the Freehand SPECT reconstruction provided by the declipseSPECT cart system.

The online reconstructions with 3 mm voxelsize resulted in 2.17 mm average localization error (ALE) (standard deviation: 1.04 mm) for Freehand SPECT reconstructions. To improve the Freehand SPECT reconstruction quality, same acquisitions are reconstructed additionally for the same reconstruction volume, but with 1 mm voxelsize instead. These

achieved an average error of 1.73 mm (standard deviation: 0.67 mm). As a reference for Freehand SPECT quality, the fusion error between ground truth SPECT and CT centroids is calculated as 3.5 mm, cf. Fig 6.3(b).

For all ultrasound scans, the spheres in the acquired 3D ultrasound scans are segmented manually for both optical and EM tracking data. Average localization errors of the sphere centroids from 3D ultrasound to ground truth CT yielded 5.36 mm (standard deviation: 1.56 mm) for optical and 5.22 mm (standard deviation: 1.49 mm) for EM tracking, respectively. Results for the average errors to the 4 individual spheres are given in Table 6.1.

	EM		**Optical**	
	Mean	**Std**	**Mean**	**Std**
Sphere1	4.95	1.21	5.88	1.74
Sphere2	5.20	1.51	5.24	1.23
Sphere3	5.75	1.67	5.23	1.52
Sphere4	3.88	0.73	3.97	1.66

Table 6.1.: Localization errors in mm calculated for ultrasound and ground truth (CT).

From the 3D visualization, a systematic error of both tracking systems in direction of the US probe orientation can be observed, as shown in Figure 6.4. In addition, the deviations from ground truth regarding varying pressure applied during acquisition are also evaluated. Exactly this *pressure* is found to be the main cause for localization errors, as with increased pressure, the errors increase similarly for both tracking systems due to higher deformation (mean ALE 5.16 mm for normal pressure, 10.46 mm for high pressure), cf. Figure 6.5 and Figure 6.6.

6.3.4. Patient Studies

In addition to the phantom experiments, we also had the opportunity to scan 7 patients preoperatively right after radiotracer injection and scintigraphy imaging in nuclear medicine department of Klinikum rechts der Isar. Since the system used in the phantom experiments with optical tracking of the ultrasound probe is a research prototype and therefore not clinically approved, a GE Logiq E9 US system (GE Milwaukee, USA) is used for these patient scans with built-in EM tracking instead. This built-in EM tracking system is the exact same one as the one used in phantom experiments above. This ultrasound system can also visualize on-site the imported 3D Freehand SPECT DICOM images provided by the declipseSPECT cart system fused on the 2D image plane of the tracked ultrasound probe.

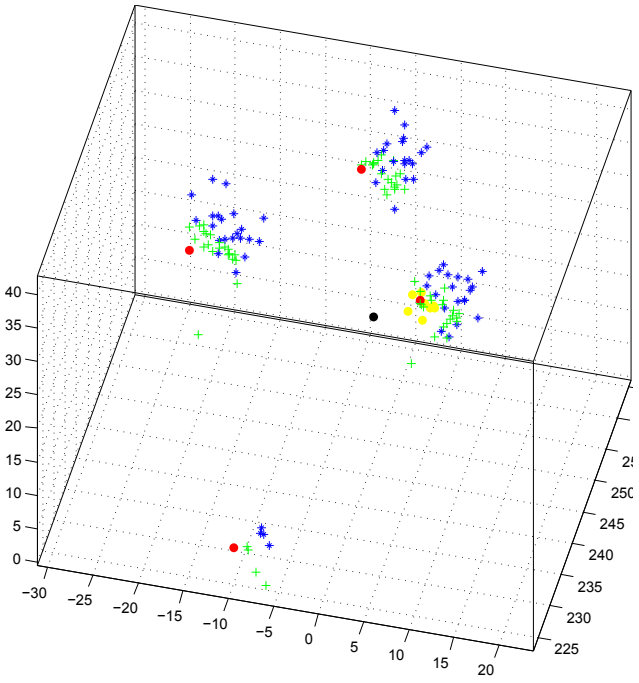

Figure 6.4.: Visualization of the centroids in 3D. Segmented sphere centroids compared for ground truth CT (red), SPECT (black), Freehand SPECT (yellow), ultrasound EM (blue) and ultrasound optical (green) tracking data.

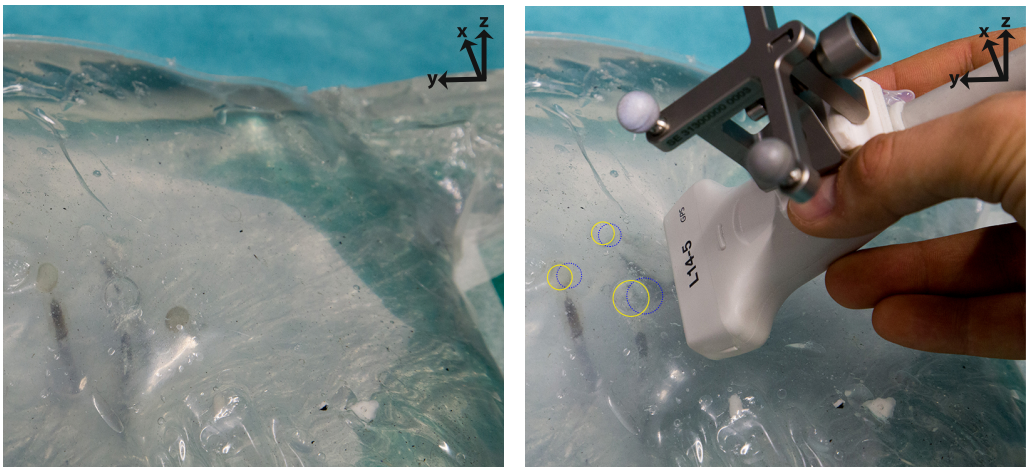

Figure 6.5.: Deformation on phantom during an ultrasound scan. Phantom position as used for Freehand SPECT and ultrasound show noticeable deformation (cf. marked circles on right image).

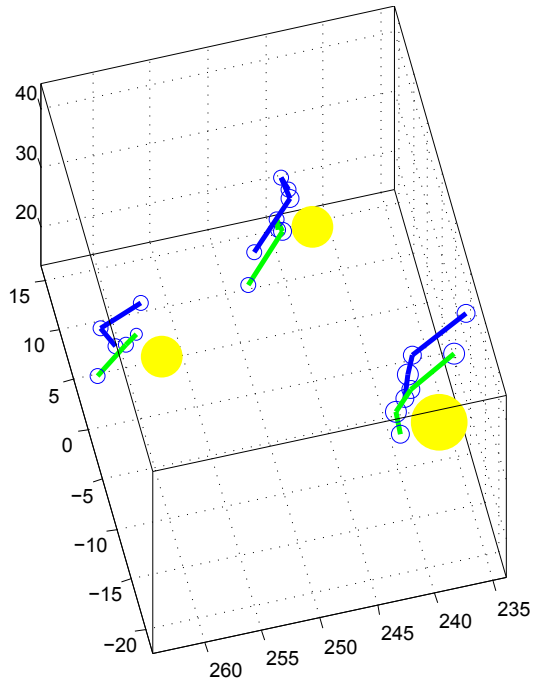

Figure 6.6.: Evaluation of the deformation on phantom during ultrasound scan. Extracted centroids for trajectories with increasing pressure for ultrasound EM (blue) and ultrasound optical (green) in relation to the ground truth CT (yellow).

In order to experience the clinical challenges posed by an interventional usage of such a fused Freehand SPECT and ultrasound system, one patient is scanned additionally once more before surgery inside the operating room (Figure 6.7 and 6.8). The accuracy was enough for the surgeon to determine the sentinel lymph node on ultrasound images. He was confident that he would be even able to perform a non-surgical Freehand SPECT and ultrasound guided core needle biopsy of the sentinel lymph node, if approved.

6.4. Discussion

Although Freehand SPECT has much smaller detector sizes than the conventional SPECT, it achieved better localization scores. This can be due to smaller distances between the actual radiation source and the detector and therefore provides better detection statistics with the mini gamma camera. Another reason could be its smaller voxel size (1 mm for Freehand SPECT, 4.8 mm for SPECT).

The localization error for ultrasound is considered to be mainly due to the deformation

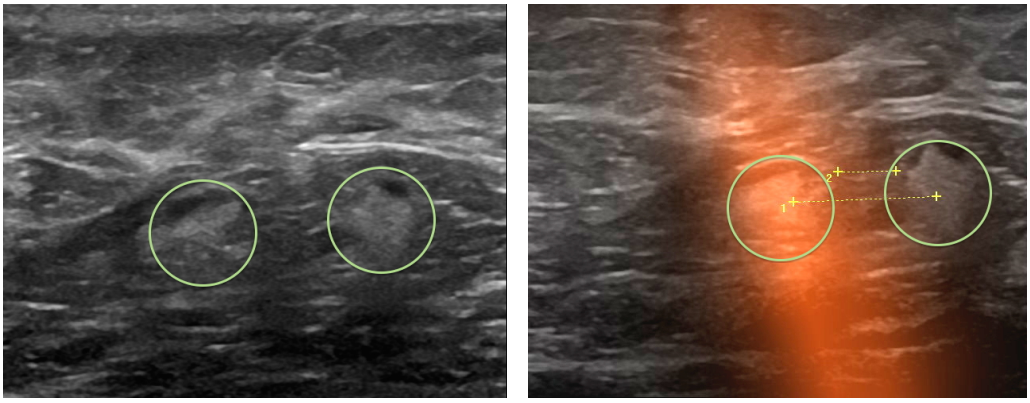

(a) (b)

Figure 6.7.: Freehand SPECT / ultrasound fusion for a patient inside the operating room. (a) Ultrasound image of two lymph nodes in the axilla. (b) Fused image of Freehand SPECT and ultrasound. Left lymph node is identified as the sentinel. The distance of the two lymph nodes is from centers 11.7 mm (1), from borders 4.7 mm (2).

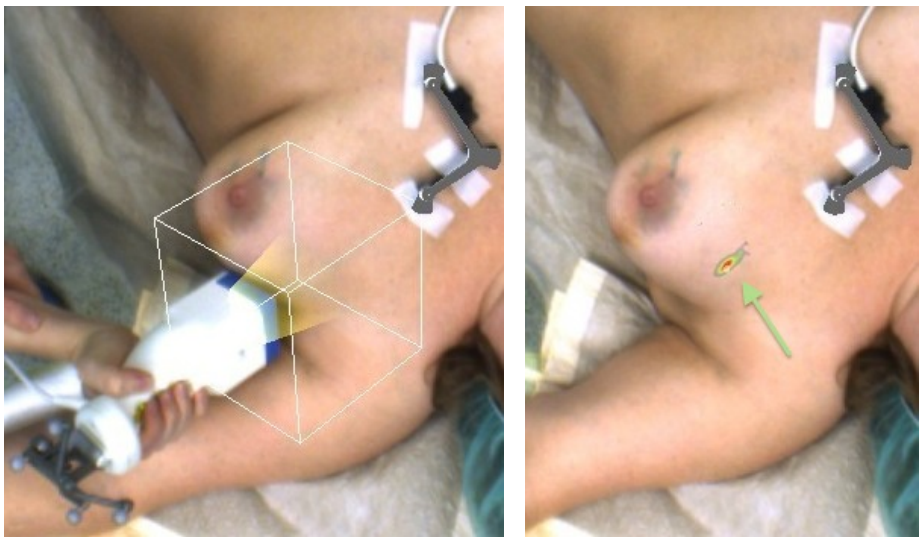

(a) (b)

Figure 6.8.: Patient scan inside the operating room. (a) Freehand SPECT acquisition and augmentation of the scanning volume (VOI). (b) Resulting Freehand SPECT reconstruction overlaid on the patient.

of the phantom during scanning. This is crucial for the fusion of the two images in real scenarios, as small movements of the patient might easily interfere with the reliability of the fusion. In an intervention using local anestesia this can easily happen between two scans and needs to be taken into account. However, new scanning protocols can be suggested for compensation of the deformation effect, such as a preceding scan without any pressure applied as reference, prior to the actual ultrasound scan.

For ultrasound, both tracking systems achieved comparable scores, where both have their own advantages and disadvantages. Electromagnetic tracking provides easier handling of the ultrasound probe than the optical tracking and therefore final solutions using electromagnetic tracking might ease the acceptance by the end users. However, since the Freehand SPECT system already uses optical tracking and integrated augmented reality visualization, optical tracking of the ultrasound probe might be beneficial in final Freehand SPECT / ultrasound solutions in terms of visualization and integration into one system.

Despite the deformation of soft tissue, results were satisfactory in regard to the clinical application towards Freehand SPECT and ultrasound guided core needle biopsies of sentinel lymph nodes. In our pilot patient study, one lymph node could be identified to be the sentinel lymph nodes on the fused images. However, to clinically approve this, an interventional study, investigating the patient outcome by comparison of radio-guided surgical sentinel lymph node biopsies and non-surgical Freehand SPECT and ultrasound guided core needle sentinel lymph node biopsies is essential.

Part III.

Conclusion

CHAPTER 7

Conclusion

7.1. Summary

This dissertation presented an extensive overview of radioguided surgery in chapter 2. Starting with a short summary of major historical milestones in literature, the chapter continued with the fundamental basics of radionuclides, radiotracers and radiation detectors used in radioguided surgery. Afterwards, the importance of radiation safety was highlighted, required definitions were introduced and recommendations for monitoring radiation exposure were presented. The chapter ended with the introduction of different radioguided surgery techniques in literature followed by an overview of their various clinical application domains.

After a general introduction to radioguided surgery, the thesis continued with the detailed introduction of Freehand SPECT in chapter 3, an invention bringing 3D SPECT-like imaging capabilities into the operating room via radiation measurements by tracked handheld gamma detectors and their non-uniform freehand scan coverage. The chapter presented the individual components of Freehand SPECT imaging on the basis of the commercial product declipseSPECT, including the tracking and radiation detection technologies incorporated as well as their synchronisation. Following that, the cruciality of the acquisition step was discussed and the mathematical background for the iterative reconstruction algorithm employed in Freehand SPECT technology were given. The chapter concluded with the details about the visualization aspects of Freehand SPECT imaging, not only covering the augmented reality and virtual reality visualization modes for the resulting 3D reconstructions, but also the different visual scan guidance approches employed in declipseSPECT to support and improve the acquisition procedure.

Chapter 4 presented the first contribution of this thesis, being the postoperative *user* driven analysis and evaluations for Freehand SPECT imaging, especially in respect to the medical augmented reality. The methodology was based on the analysis of the automatically generated log files by the system during actual surgical procedures. First, the major surgical phase transitions were determined related to the intraoperative utilization of Freehand SPECT for sentinel lymph node biopsy procedures in our university hospital. Then, the components and the device workflow of the declipseSPECT cart system as well as its device and performance logging were studied in detail. As these files included personal information about the patient such as name or birthday, as well as screenshots of the procedure, where the patient or the operating room personnel could be identified, a specialized application called *MedNymzier* was implemented, to support anonymization/pseudonymization efforts by preprocessing these log files and any additional clinical data containing personal information of the patient before using it for our research activities. In a first study, the focus was set on one device feature in one workflow stage of the system only, namely the augmented reality and virtual reality visualization modes for the 3D reconstruction. Here, the usage characteristics for the surgical team were analyzed manually by human evaluators and observations in over 100 Freehand SPECT acquisitions within different phases of 52 sentinel lymph node biopsy surgeries were reported. In a following study, the analysis methodology was extended by automatic processing of further text log files, which was only possible after the improvement of the automatic logging by the manufacturer through the inclusion of an additional user interaction log file, essential for the identification of phase transitions. This addition opened new doors for the automation of such analysis which was demonstrated via the Freehand SPECT data of 19 sentinel lymph node biopsy surgeries for breast cancer. The work related to the human component in Freehand SPECT imaging presented in this particular chapter spawned a series of publications in the field of medical augmented reality and computer-aided interventions [83, 79, 10, 86].

Another contribution of this thesis was the proposed adaptation of Freehand SPECT imaging for *recurring* head and neck squamous cell carcinoma patients by the integration of a high energy gamma probe instead of the conventional gamma detection probe due to the administration of positron emitting radiotracer ^{18}F-FDG, as presented in chapter 5. This was achieved by an analytical 511 keV annihilation gamma detection model of the particular high energy gamma detection probe utilized in the study, which was then saved in a form of a look up table and imported into the declipseSPECT software as a custom probe specification. The probe tip calibration was also performed externally and then imported into the declipseSPECT settings file. These actions made it possible to use

the commercial declipseSPECT reconstruction software and user interface for the Freehand SPECT reconstructions in the experiments, even with nonstandard gamma detectors, which were not supported by the manufacturer by default. The experiments were designed to test the feasibility of the approach on phantoms constructed based on clinical data. Based on the PET/CT data of 7 patients with tumors and lymph node metastases in the head and neck region, a neck phantom was built, with ^{18}F-FDG-filled reservoirs representing tumors and lymph nodes. A CT scan of the phantom was acquired to serve as the ground truth for the evaluations. Using this phantom, the limitations and capabilities of the method were investigated, though three sets of experiments with different radionuclides and radiation detection probes as well as different radioactivity proportions. Finally, possible improvements and requirements needed were discussed, so that the approach becomes clinically applicable. The work related to Freehand SPECT imaging for head and neck cancer using high energy gamma probes presented in this chapter resulted in publications in the field of computer-aided interventions [96, 85].

The last contribution of this thesis was presented in chapter 6, proposing 3D Freehand SPECT and 3D ultrasound fusion for breast cancer patients with the motivation of making it possible to identify the non-palpable and sonographically not suspicious *sentinel* lymph nodes in the axillary region in *fused* ultrasound images. Via proper fusion of Freehand SPECT and ultrasound images, even core needle biopsy of the axillary *sentinel* lymph nodes could be practicable, which could be then performed in a *non-surgical* environment without general anesthesia, in contrast to the conventional sentinel lymph node biopsy as commonly applied in clinical practice. In order to evaluate the applicability of this approach, a first feasibility study was conducted. First a realistic and deformable breast mimicking phantom was designed and built, in which 4 spheres with similar sizes representing lymph nodes in axillary region were placed. One of these 4 spheres were filled with radioactive Tc-99m to represent the sentinel lymph node, whereas others were only filled with water. A SPECT/CT of this phantom was acquired to serve as ground truth for the evaluations. The phantom was then scanned with both Freehand SPECT and ultrasound systems in different configurations. In addition, to evaluate the impact of the deformation by ultrasound, additional ultrasound acquisitions with varying pressure were performed and analyzed separately. Finally, the clinical relevance of the approach was demonstrated through 7 preoperative and 1 intraoperative Freehand SPECT acquisitions of real patients, which were then fused onto the 2D ultrasound plane allowing the operator to differentiate the sentinel lymph node. Our evaluation showed that both optical and EM tracking systems are suitable for such multi-modal data fusion within clinical settings. The work related to 3D Freehand SPECT and ultrasound fusion for non-surgical sentinel lymph node biopsy

for breast cancer as shown in this last chapter, was presented in [84].

7.2. Challenges and Outlook

In addition to these contributions, the author also had the opportunity to contribute to several other technical and clinical studies as well. These include the specific applications of Freehand SPECT imaging in other clinical domains as well as advancements of the underlying technology to improve its overall success and acceptance. Some of the work were referenced in related sections of this document, some were not directly discussed in this dissertation. Some of the research efforts even remained unpublished. A full list of co-authored publications is given in Appendix C.

Key lessons drawn from the experience of the author through all collaborative technical Freehand SPECT related studies are stated below:

- Freehand SPECT concept not limited to conventional gamma radiation detection probes and the radionuclide Technetium-99m. If an appropriate model of *any gamma radiation detector* coming into question is analytically available or can be obtained via experiments or simulations, it can be saved in form of a *look up table* and then can be processed on-the-fly for the generation of the system matrix required for the computation of the iterative reconstruction algorithm. However, this does not necessarily mean, that this would suffice to obtain reliable solutions under realistic conditions. Our experience with the *high energy* probes for the detection of 511 keV annihilation gammas is an example for this. Even though the experiments showed promising results, the applicability of 3D Freehand SPECT seems to be still far away, at least for this particular clinical scenario, due to the high localization errors in our experiments with realistic activity concentrations. Better models of the available detector, utilization a different detector, inclusion of prior information into the reconstruction algorithm for attenuation correction or experiments with alternative target clinical uses cases may be considered in this regard.

- Another example for the applicability of Freehand SPECT is its adaptation for *low energy* gamma radiation detecting probes. The clinical motivation behind this is the radioguided seed localization technique described in chapter 2, subsection 2.6.3, which can be applied as an alternative for the wire-guided localization of impalpable breast cancer tumors. In this method, Iodine-125 titanium seeds (subsection 2.2.3) are placed into the tissue for the marking of the impalpable breast tumor preoperatively, which could then be imaged with a Freehand SPECT system tuned for

the detection of the low energy gammas emitted from these radioactive seeds (between 27 and 35 keV). This would allow intraoperative depth measurements for optimized incision planning and eventually lead to less morbidity for the patient. For a very short period of time, the author had access to a beta probe (CXS-OP-β) with a gamma detection range of 20-50 keV and compatible with the controlling unit (SG03) of the available gamma probe detection system Crystal Probe (manufactured by Crystal Photonics). A first experiment was performed as a proof of concept with declipseSPECT cart system which was manually tuned through a customized look up table for this particular detector thanks to the collaboration with the manufacturers. The initial results were visually promising, indicating that a proper study for Freehand SPECT in this clinical application domain using such gamma detection probes may be of relevance to the scientific community. Unfortunately, other radiation detection probes available in our research laboratory were not suited to detect the photons of this energy range, so no further studies could be performed.

- Freehand SPECT systems with handheld mini *gamma cameras* as radiation detectors instead of single pixel gamma probes can be advantageous for the operating room due to the timing constraints. The simultaneous measurements by individual detector pixels lead to more projections for the reconstruction algorithm, therefore increases the reconstruction quality. However, the overall handling of the Freehand SPECT system may suffer from the weight and bulkiness of the gamma camera and the operator still needs to pay proper attention to the angular scan coverage.

- *Robotic Freehand SPECT* may be useful for phantom studies in experimental setups, especially for reproducibility tests and evaluations of new reconstruction algorithms or trajectory optimization approaches; but as of now, its intraoperative applicability seems unrealistic in terms of logistics and timing contraints of the operating room.

- *Registration of prior volumetric data*, such as preoperative SPECT/CT or PET/CT, can be considered to provide attenuation correction information for better Freehand SPECT reconstructions as well as better acquisition guidance and artifact reduction using prior information. Furthermore, the readings of the tracked gamma detectors can also be used to register and update such preoperative volumetric SPECT images instead of computation of Freehand SPECT reconstructions, as presented in [111].

Throughout the years, the author worked closely with physicians and surgeons and spent a significant amount of time inside the operating room. Some of the major challenges

encountered while investigating the applicability of Freehand SPECT for different clinical domains will be given in the following:

- Sentinel lymph node biopsy for *breast cancer* and *melanoma* are well-established radioguided surgery techniques, which can be easily performed with high success rates even only using a single pixel gamma radiation detecting probe. Therefore, even in the scope of a clinical study with scientific motivation behind, the intraoperative acceptance of Freehand SPECT for these clinical indications may be very challenging, especially if some of the surgeons involved do not see a major clinical added value by its intraoperative utilization. Own experience shows that surgeons who initiated the study were more motivated in general and were perfectly aware of the technology and its components, and because of that also achieved better results. However, some surgeons and surgical teams performed the Freehand SPECT scans without any enthusiasm, only because it was required for the clinical study, resulting in low quality reconstructions decreasing the success of the technology as well as in an unpleasant atmosphere in the operating room. Therefore, the author suggests that Freehand SPECT should only be utilized by motivated operators, regardless if it is within or without the context of a clinical study. Of course this is a valid point for all new advanced radioguided surgery systems, especially in early phases.

- Sentinel lymph node biopsy for *vulvar* and *cervical gynecological malignancies* are less commonly applied SLNB procedures, the latter being surgically even more complex due to the typical lymphatic drainage resulting in deep seated *sentinel* lymph nodes. Because of that, the utilization of Freehand SPECT for these indications was a topic of interest for our gynecology department. The declipseSPECT cart system with its default gamma detection probe could be used as it is, since the applied radiotracer is again ^{99m}Tc-nanocolloid. Due to the complexity of the target anatomy, a SPECT/CT scan of the patient is also performed preoperatively, in addition to the 2D scintigraphy as commonly performed for SLNB in general. If the Freehand SPECT patient target is also placed on the patient prior the SPECT/CT scan and its position is properly marked on the skin for the surgery next day, the volumetric SPECT/CT data can be registered to the Freehand SPECT coordinate frame during surgery. This approach may allow intraoperative visualization of the preoperative 3D SPECT/CT data via the declipseSPECT cart system. This may be better perceived by the surgeons through navigation and depth measurement possibilities compared to 2D slice images. However, small errors in intraoperative placement of the patient target on the patient would affect the registration significantly, resulting

in unreliable intraoperative visualization and navigation. In addition, deformation is not taken into account as the patient may be positioned differently than during the SPECT/CT scan for the particular surgical procedure. Because of that, using of dedicated CT markers as reference points for the point based registration, which are then registered to the probe positions on these markers in the patient target frame during surgery or even consideration of deformable registration methods may be better suited approaches for this purpose.

- Freehand SPECT can also be applied for the intraoperative detection of *metastatic* lymph nodes in *prostate cancer* patients, thanks to the recent advancements in radiopharmaceutical production of prostate-specific membrane antigen (PSMA) inhibitors. Utilization of positron emitting Gallium-68 (^{68}Ga) labeled PSMA allows accurate preoperative diagnosis by identification of even very small *metastatic* lymph nodes in PET/CT images. However, intraoperative detection of such lymph nodes without radioguidance may not be easy due to their inconspicuous presence or unusual localization. Unfortunately, ^{68}Ga-labeled PSMA is not well suited for radioguided surgery from logistics and radiation safety perspective, due to its high emission energies (about 2-3 MeV) and short half-life (about 1 hour) as well as the challenges associated with the detection of 511 keV annihilation gammas via high energy gamma radiation detection probes as previously discussed. However, Indium-111 (^{111}In) or even Technetium-99m (^{99m}Tc) labeled PSMA agents have recently been introduced for PSMA guided radiosurgery in our university hospital [72, 71], making it possible to detect *metastatic* lymph nodes intraoperatively due to the *cancer specific* radiotracer. The advantage of these radionuclides over ^{68}Ga is the emission of gammas with energies within the best detection range of conventional gamma radiation detection probes. Therefore, Freehand SPECT technology could be easily utilized within this clinical domain as well, as demonstrated in the first patient studies using ^{111}In-labeled PSMA agents in our university hospital [72].

- The proposed Freehand SPECT and ultrasound fusion is currently the only available alternative for *non-surgical* core needle biopsy technique for sonographically not suspicious axillary sentinel lymph nodes of *breast cancer* patients. The approach has a big potential, not only due to the technology behind it as it is relevant to the scientific community, but also due to its high clinical relevance as its forthcoming successful applications may even revolutionize the standart technique for nodal staging of early stage breast cancer in the future by replacing the surgical sentinel biopsy technique.

The applicability and success of the case specific adaptation and utilization of Freehand SPECT depends on numerous factors. These are not only the technical aspects such as the physical and biological characteristics of applied radiotracers or the specifications of the utilized radiation detection systems. It also very much depends on other subjective factors such as the characteristics and motivations of the individuals involved. Because of that the author believes that the Freehand SPECT technology can reach a higher impact in the clinical community in the future, if it is utilized

1. in a completely new clinical use case, where radioguided surgery concept is only introduced recently or is only partially established, such as PSMA guided radiosurgery for prostate cancer

   or

2. as a new but obligatory component within a new clinical workflow in a well established radioguided surgery domain, such as the non-surgical core needle biopsy of sentinel lymph nodes for breast cancer patients

since the acceptance by the physicians would not be directly dependent on breaking habits related to the underlaying initial technique.

Appendix

Bibliography

[1] The 2007 Recommendations of the International Commission on Radiological Protection. ICRP publication 103. *Annals of the ICRP*, 37(2-4):1–332, 2007.

[2] Regulation (EU) 2016/679 of the European Parliament and of the Council of 27 April 2016 on the protection of natural persons with regard to the processing of personal data and on the free movement of such data, and repealing Directive 95/46/EC (General Data Protection Regulation). *Official Journal of the European Union*, L119:1–88, May 2016. URL: `https://eur-lex.europa.eu/eli/reg/2016/679/oj`.

[3] H. Abe, R. A. Schmidt, C. A. Sennett, A. Shimauchi, and G. M. Newstead. US-guided Core Needle Biopsy of Axillary Lymph Nodes in Patients with Breast Cancer: Why and How to Do It. *RadioGraphics*, 27(suppl_1):S91–S99, Oct. 2007.

[4] D. R. Aitken, G. H. Hinkle, M. O. Thurston, S. E. Tuttle, D. T. Martin, J. Olsen, D. E. Haagensen, D. Houchens, and E. W. Martin. A gamma-detecting probe for radioimmune detection of CEA-producing tumors. Successful experimental use and clinical case report. *Diseases of the Colon and Rectum*, 27(5):279–282, May 1984.

[5] D. R. Aitken, M. O. Thurston, G. H. Hinkle, D. T. Martin, D. E. Haagensen, D. Houchens, S. E. Tuttle, and E. W. Martin. Portable gamma probe for radioimmune localization of experimental colon tumor xenografts. *Journal of Surgical Research*, 36(5):480–489, May 1984.

[6] J. J. Albertini, G. H. Lyman, C. Cox, T. Yeatman, L. Balducci, N. Ku, S. Shivers, C. Berman, K. Wells, D. Rapaport, A. Shons, J. Horton, H. Greenberg, S. Nicosia, R. Clark, A. Cantor, and D. S. Reintgen. Lymphatic Mapping and Sentinel Node Biopsy in the Patient With Breast Cancer. *JAMA*, 276(22):1818–1822, 1996.

[7] J. C. Alex, D. L. Weaver, J. T. Fairbank, B. S. Rankin, and D. N. Krag. Gamma-

probe-guided lymph node localization in malignant melanoma. *Surgical Oncology*, 2(5):303–308, Oct. 1993.

[8] K. Bayer and P. M. Hirschbeck. Patient Data Privacy in ORUse Framework. Interdisciplinary project report, Technische Universität München, München, 2012. Chair for Computer Aided Medical Procedures.

[9] A. Bigdelou. *Operating Room Specific Domain Model for Usability Evaluations and HCI Design*. Dissertation, Technische Universität München, München, 2012.

[10] A. Bigdelou, A. Okur, M.-E. Hoffmann, B. Azizi, and N. Navab. Towards Systematic Usability Evaluations for the OR: An Introduction to OR-Use Framework. In *Information Processing in Computer-Assisted Interventions*, volume 7330 of *Lecture Notes in Computer Science*, pages 146–156. Springer Berlin / Heidelberg, 2012.

[11] A. Bigdelou, T. Sterner, S. Wiesner, T. Wendler, F. Matthes, and N. Navab. OR specific domain model for usability evaluations of intra-operative systems. In *Information Processing in Computer-Assisted Interventions*, volume 6689, pages 25–35. Springer Berlin Heidelberg, Berlin, Heidelberg, 2011.

[12] W. Birkfellner, J. Hummel, E. Wilson, and K. Cleary. Tracking Devices. In T. Peters and K. Cleary, editors, *Image-Guided Interventions: Technology and Applications*, pages 23–44. Springer US, Boston, MA, 2008.

[13] M. Blackwell, C. Nikou, A. M. DiGioia, and T. Kanade. An image overlay system for medical data visualization. In *Medical Image Computing and Computer-Assisted Interventation â MICCAIâ98*, volume 1496, pages 232–240. Springer-Verlag, Berlin/Heidelberg, 1998.

[14] C. Bluemel, P. Matthies, K. Herrmann, and S. P. Povoski. 3d scintigraphic imaging and navigation in radioguided surgery: freehand SPECT technology and its clinical applications. *Expert Review of Medical Devices*, 13(4):339–351, 2016.

[15] C. Bluemel, A. Schnelzer, A. Ehlerding, K. Scheidhauer, and M. Kiechle. Changing the Intraoperative Nodal Status of a Breast Cancer Patient Using Freehand SPECT for Sentinel Lymph Node Biopsy. *Clinical Nuclear Medicine*, 39(5):e313–e314, May 2014.

[16] C. Bluemel, A. Schnelzer, A. Okur, A. Ehlerding, S. Paepke, K. Scheidhauer, and M. Kiechle. Freehand SPECT for image-guided sentinel lymph node biopsy in breast cancer. *EJNMMI*, 40(11):1656–1661, 2013.

[17] T. J. Boal and M. Pinak. Dose limits to the lens of the eye: International Basic Safety Standards and related guidance. *Annals of the ICRP*, 44(1 Suppl):112–117, June 2015.

[18] A. Bricou, M.-A. Duval, Y. Charon, and E. Barranger. Mobile gamma cameras in breast cancer care -â a review. *EJSO*, 39(5):409–416, May 2013.

[19] A. Bunschoten, N. S. van den Berg, R. A. Valdés Olmos, J. A. K. Blokland, and F. W. B. van Leeuwen. Tracers applied in radioguided surgery. In K. Herrmann, O. E. Nieweg, and S. P. Povoski, editors, *Radioguided Surgery: Current Applications and Innovative Directions in Clinical Practice*, chapter 5, pages 75–101. Springer International Publishing, 2016.

[20] Cancer.Net. Head and Neck Cancer, June 2012. Accessed on: 16.12.2018. URL: `https://www.cancer.net/cancer-types/head-and-neck-cancer/`.

[21] S. Charfi, E. Dubois, and D. L. Scapin. Usability recommendations in the design of mixed interactive systems. In *Proceedings of the 1st ACM SIGCHI symposium on Engineering interactive computing systems*, EICS '09, pages 231–236, New York, NY, USA, 2009. ACM.

[22] H. S. Cody. Sentinel lymph node mapping in breast cancer. *Breast Cancer*, 6(1):13–22, 1999.

[23] B. K. Das. Positron emission tomography: An overview. In B. K. Das, editor, *Positron Emission Tomography: A Guide for Clinicians*, pages 1–6. Springer India, New Delhi, 2015.

[24] D. C. Desai, M. Arnold, S. Saha, G. Hinkle, D. Soble, J. Fry, L. R. DePalatis, J. Mantil, M. Satter, and E. W. Martin. Correlative Whole-Body FDG-PET and Intraoperative Gamma Detection of FDG Distribution in Colorectal Cancer. *Clinical Positron Imaging*, 3(5):189–196, Sept. 2000.

[25] M. Donker, M. E. Straver, J. Wesseling, C. E. Loo, M. Schot, C. A. Drukker, H. van Tinteren, G. S. Sonke, E. J. T. Rutgers, and M.-J. T. F. D. Vrancken Peeters. Marking Axillary Lymph Nodes With Radioactive Iodine Seeds for Axillary Staging After Neoadjuvant Systemic Treatment in Breast Cancer Patients: The MARI Procedure. *Annals of Surgery*, 261(2):378, Feb. 2015.

[26] W. A. N. Dorland. *Dorland's illustrated medical dictionary (32nd ed.)*. Dorland's Medical Dictionary. Elsevier Health Sciences, 2011.

[27] S. M. Dua, R. J. Gray, and M. Keshtgar. Strategies for localisation of impalpable breast lesions. *The Breast*, 20(3):246–253, June 2011.

[28] G. M. Duarte, C. Cabello, R. Z. Torresan, M. Alvarenga, G. H. Q. Telles, S. T. Bianchessi, N. Caserta, S. R. Segala, M. C. L. de Lima, E. C. S. C. Etchebehere, and E. E. Camargo. Radioguided Intraoperative Margins Evaluation (RIME): Preliminary results of a new technique to aid breast cancer resection. *European Journal of Surgical Oncology (EJSO)*, 33(10):1150–1157, Dec. 2007.

[29] C. Eberhardt. Photomultiplier tube, 2006. Licensed under "`https://creativecommons.org/publicdomain/mark/1.0/deed.en`". Retrieved 24.07.2017, from "`https://commons.wikimedia.org/wiki/File:Photomultipliertube.png`".

[30] S. Fanti, M. Farsad, and L. Mansi. Normal Distribution of FDG. In *Atlas of PET/CT - A Quick Guide to Image Interpretation*, pages 1–23. Springer Berlin Heidelberg, Berlin, Heidelberg, 2009.

[31] A. M. Franz, T. Haidegger, W. Birkfellner, K. Cleary, T. M. Peters, and L. Maier-Hein. Electromagnetic tracking in medicine–a review of technology, validation, and applications. *IEEE transactions on medical imaging*, 33(8):1702–1725, Aug. 2014.

[32] M. Freesmeyer, T. Opfermann, and T. Winkens. Hybrid integration of real-time US and freehand SPECT: proof of concept in patients with thyroid diseases. *Radiology*, page 132415, Jan. 2014.

[33] H. Fuchs, A. State, E. D. Pisano, W. F. Garrett, G. Hirota, M. Livingston, M. C. Whitton, and S. M. Pizer. Towards performing ultrasound-guided needle biopsies from within a head-mounted display. In *Visualization in Biomedical Computing*, volume 1131, pages 591–600. Springer-Verlag, Berlin/Heidelberg, 1996.

[34] B. Fuerst, J. Sprung, F. Pinto, B. Frisch, T. Wendler, H. Simon, L. Mengus, N. S. v. d. Berg, H. G. v. d. Poel, F. W. B. van Leeuwen, and N. Navab. First Robotic SPECT for Minimally Invasive Sentinel Lymph Node Mapping. *IEEE Transactions on Medical Imaging*, 35(3):830–838, Mar. 2016.

[35] J. L. Gabbard and J. E. Swan II. Usability Engineering for Augmented Reality: Employing User-Based Studies to Inform Design. *IEEE Transactions on Visualization and Computer Graphics*, 14:513–525, 2008.

[36] J. P. Gambini and T. P. Quinn. Hybrid tracers and devices for intraoperative imaging: the future for radioguided surgery? *Clinical and Translational Imaging*, 4(5):343–351, Oct. 2016.

[37] J. Gardiazabal, T. Reichl, A. Okur, T. Lasser, and N. Navab. First flexible robotic intra-operative nuclear imaging for image-guided surgery. In *Proceedings of the 4th international conference on Information Processing in Computer-Assisted Interventions*, IPCAI'13, pages 81–90, Berlin, Heidelberg, 2013. Springer-Verlag.

[38] J. F. Gardiazabal Schilling. *Robotic freehand SPECT Imaging*. Dissertation, Technische Universität München, München, 2017.

[39] B. Ghelman, F. M. Thompson, and W. D. Arnold. Intraoperative radioactive localization of an osteoid-osteoma. Case report. *Journal of Bone*, 63(5):826–827, June 1981.

[40] R. J. Gray, C. E. Cox, and E. L. Dauway. Radioguided surgery for non-palpable breast lesions: I-125 radioactive seed localization. In K. Herrmann, O. E. Nieweg, and S. P. Povoski, editors, *Radioguided Surgery: Current Applications and Innovative Directions in Clinical Practice*, chapter 8, pages 125–137. Springer International Publishing, 2016.

[41] R. J. Gray, C. Salud, K. Nguyen, E. Dauway, J. Friedland, C. Berman, E. Peltz, G. Whitehead, and C. E. Cox. Randomized prospective evaluation of a novel technique for biopsy or lumpectomy of nonpalpable breast lesions: radioactive seed versus wire localization. *Annals of Surgical Oncology*, 8(9):711–715, 2001.

[42] C. Harris, R. Bigelow, J. Francis, G. Kelley, and P. Bell. A CsI(Tl)-Crystal Surgical Scintillation Probe. *Nucleonics (U.S.) Ceased publication*.

[43] A. Hartl. *Computational modeling of detection physics for 3D intraoperative imaging with navigated nuclear probes*. Dissertation, Technische Universität München, München, 2015.

[44] A. Hartl, D. I. Shakir, T. Lasser, S. I. Ziegler, and N. Navab. Detection models for freehand SPECT reconstruction. *Physics in Medicine & Biology*, 60(3):1031, 2015.

[45] W. C. Harvey and J. L. Lancaster. Technical and Clinical Characteristics of a Surgical Biopsy Probe. *Journal of Nuclear Medicine*, 22(2):184–186, Feb. 1981.

[46] C. M. S. Hassing, T. F. Tvedskov, N. Kroman, T. L. Klausen, J. B. Drejøe, J. F. Tvedskov, T. L. Lambine, H. Kledal, G. Lelkaitis, and L. Langhans. Radioactive seed localisation of non-palpable lymph nodes - A feasibility study. *European Journal of Surgical Oncology*, 44(5):725–730, May 2018.

[47] S. Heller and P. Zanzonico. Nuclear Probes and Intraoperative Gamma Cameras. *Seminars in Nuclear Medicine*, 41(3):166–181, May 2011.

[48] D. Hellingman and V.-S. Sergi. The use of intraoperative small and large field of view gamma cameras for radioguided surgery. In K. Herrmann, O. E. Nieweg, and S. P. Povoski, editors, *Radioguided Surgery: Current Applications and Innovative Directions in Clinical Practice*, chapter 3, pages 35–56. Springer International Publishing, 2016.

[49] C. Hennersperger, A. Karamalis, and N. Navab. Vascular 3D+T freehand ultrasound using correlation of doppler and pulse-oximetry data. In D. Stoyanov, D. Collins, I. Sakuma, P. Abolmaesumi, and P. Jannin, editors, *IPCAI 2014*, volume 8498 of *LNCS*, pages 68–77. Springer International Publishing, 2014.

[50] K. Herrmann, O. E. Nieweg, and S. P. Povoski. *Radioguided surgery: current applications and innovative directions in clinical practice*. Springer, 2016.

[51] J. Huber, W. Moses, J. Pouliot, and I. Hsu. Dual-Modality PET/Ultrasound imaging of the prostate. *IEEE Nucl Sci Symp Conf Rec*, 4:2187–2190, Oct. 2005.

[52] S. S. Huh, W. L. Rogers, and N. H. Clinthorne. An investigation of an intra-operative PET imaging probe. *IEEE Nucl Sci Symp Conf Rec*, pages 552–555, Oct. 2007.

[53] R. Johnson, K. O'Hara, A. Sellen, C. Cousins, and A. Criminisi. Exploring the potential for touchless interaction in image-guided interventional radiology. In *Proceedings of the 2011 annual conference on Human factors in computing systems*, CHI '11, pages 3323–3332, New York, NY, USA, 2011. ACM.

[54] F. A. A. d. Jonge and E. K. J. Pauwels. Technetium, the missing element. *European Journal of Nuclear Medicine*, 23(3):336–344, Mar. 1996.

[55] D. Kalkofen, E. Mendez, and D. Schmalstieg. Interactive Focus and Context Visualization for Augmented Reality. In *Proceedings of the 2007 6th IEEE and ACM*

International Symposium on Mixed and Augmented Reality, ISMAR '07, pages 1–10, Washington, DC, USA, 2007. IEEE Computer Society.

[56] D. Kalkofen, E. Mendez, and D. Schmalstieg. Comprehensible Visualization for Augmented Reality. *Visualization and Computer Graphics, IEEE Transactions on*, 15(2):193 –204, march-april 2009.

[57] H. Kaufmann and A. Dünser. Summary of Usability Evaluations of an Educational Augmented Reality Application. In *Virtual Reality*, volume 4563 of *Lecture Notes in Computer Science*, pages 660–669. Springer Berlin / Heidelberg, 2007.

[58] W. W. Kim, J. S. Kim, S. M. Hur, S. H. Kim, S.-K. Lee, J. H. Choi, S. Kim, J. Y. Choi, J. E. Lee, J.-H. Kim, S. J. Nam, J.-H. Yang, and J.-H. Choe. Radioguided surgery using an intraoperative PET probe for tumor localization and verification of complete resection in differentiated thyroid cancer: a pilot study. *Surgery*, 149(3):416–424, Mar. 2011.

[59] G. H. KleinJan, A. Bunschoten, O. R. Brouwer, N. S. v. d. Berg, R. A. Valdés-Olmos, and F. W. B. van Leeuwen. Multimodal imaging in radioguided surgery. *Clinical and Translational Imaging*, 1(6):433–444, Dec. 2013.

[60] T. Koivukangas, J. P. Katisko, and J. P. Koivukangas. Technical accuracy of optical and the electromagnetic tracking systems. *SpringerPlus*, 2, Mar. 2013.

[61] D. Krag, D. Weaver, J. Alex, and J. Fairbank. Surgical resection and radiolocalization of the sentinel lymph node in breast cancer using a gamma probe. *Surgical Oncology*, 2(6):335 – 340, 1993.

[62] T. Lasser. *Tomographic Reconstruction Methods for Optical and Intra-operative Functional Imaging*. Dissertation, Technische Universität München, München, 2011.

[63] M. Lassmann and U. Eberlein. Radiation safety and dosimetry. In K. Herrmann, O. E. Nieweg, and S. P. Povoski, editors, *Radioguided Surgery: Current Applications and Innovative Directions in Clinical Practice*, chapter 6, pages 103–111. Springer International Publishing, 2016.

[64] J. Liu, X. Gao, Z. Zhang, S. Gao, and J. Zhou. A new calibration method in 3d ultrasonic imaging system. In *Engineering in Medicine and Biology Society, 1998. Proc. of the 20th Ann. Int. Conf. of the IEEE*, volume 2, pages 839–841. IEEE, 1998.

[65] A. Luini, S. Zurrida, V. Galimberti, and G. Paganelli. Radioguided surgery of occult breast lesions. *European Journal of Cancer (Oxford, England: 1990)*, 34(1):204–205, Jan. 1998.

[66] S. Majewski, A. Stolin, P. Martone, and R. Raylman. Dedicated mobile PET prostate imager. *J Nucl Med Meeting Abstracts*, 52(1):1945, 2011.

[67] D. A. Martinez, D. R. King, C. Romshe, R. A. Lozano, J. D. Morris, M. S. O'Dorisio, and E. Martin. Intraoperative identification of parathyroid gland pathology: A new approach. *Journal of Pediatric Surgery*, 30(9):1306–1309, Sept. 1995.

[68] A. Martino, L. Monaco, R. Golia, P. Miletto, P. Capasso, C. Lombardi, G. D. Chiara, C. Iannace, C. Basagni, and F. Caracciolo. A new radioguided procedure for localization and surgical treatment of neck node metastasis of papillary thyroid cancer. *Journal of Endocrinological Investigation*, 33(5):339–342, Mar. 2014.

[69] P. Matthies. Design and optimization of an intraoperative mini gamma camera for the use with Freehand SPECT. Diploma thesis, Technische Universität München, München, 2011. Chair for Computer Aided Medical Procedures.

[70] P. Matthies, J. Gardiazabal, A. Okur, J. Vogel, T. Lasser, and N. Navab. Mini gamma cameras for intra-operative nuclear tomographic reconstruction. *Medical Image Analysis*, 18(8):1329 – 1336, 2014. Special Issue on the 2013 Conference on Medical Image Computing and Computer Assisted Intervention.

[71] T. Maurer, S. Robu, M. Schottelius, K. Schwamborn, I. Rauscher, N. S. van den Berg, F. W. van Leeuwen, B. Haller, T. Horn, M. M. Heck, J. E. Gschwend, M. Schwaiger, H.-J. Wester, and M. Eiber. 99mTechnetium-based Prostate-specific Membrane Antigen-Radioguided Surgery in Recurrent Prostate Cancer. *European Urology*, 75(4):659 – 666, 2019.

[72] T. Maurer, G. Weirich, M. Schottelius, M. Weineisen, B. Frisch, A. Okur, H. Kübler, M. Thalgott, N. Navab, M. Schwaiger, H.-J. Wester, J. E. Gschwend, and M. Eiber. Prostate-specific Membrane Antigen-radioguided Surgery for Metastatic Lymph Nodes in Prostate Cancer. *European Urology*, 68(3):530 – 534, 2015.

[73] P. Meershoek, M. N. van Oosterom, H. Simon, L. Mengus, T. Maurer, P. J. van Leeuwen, E. M. K. Wit, H. G. van der Poel, and F. W. B. van Leeuwen. Robot-assisted laparoscopic surgery using DROP-IN radioguidance: first-in-human translation. *European Journal of Nuclear Medicine and Molecular Imaging*, 46(1):49–53, Jan. 2019.

[74] B. Meller, K. Sommer, J. Gerl, K. von Hof, A. Surowiec, E. Richter, B. Wollenberg, and M. Baehre. High energy probe for detecting lymph node metastases with 18F-FDG in patients with head and neck cancer. *Nuklearmedizin. Nuclear Medicine*, 45(4):153–159, 2006.

[75] A. L. Mihaljevic, A. Rieger, B. Belloni, R. Hein, A. Okur, K. Scheidhauer, T. Schuster, H. Friess, and M. E. Martignoni. Transferring innovative freehand SPECT to the operating room: First experiences with sentinel lymph node biopsy in malignant melanoma. *European Journal of Surgical Oncology (EJSO)*, 40(1):42–48, Jan. 2014.

[76] D. L. Morton, D.-R. Wen, J. H. Wong, J. S. Economou, L. A. Cagle, F. K. Storm, L. J. Foshag, and A. J. Cochran. Technical Details of Intraoperative Lymphatic Mapping for Early Stage Melanoma. *Archives of Surgery*, 127:392–399, 1992.

[77] M.R.S.Keshtgar, W.A.Waddington, S. Lakhani, and P. Ell. *The Sentinel Node in Surgical Oncology*. Springer, 1999.

[78] D. Murawa and K. Połom. Fluorescent tracers, hybrid tracers. In K. Herrmann, O. E. Nieweg, and S. P. Povoski, editors, *Radioguided Surgery: Current Applications and Innovative Directions in Clinical Practice*, pages 449–462. Springer International Publishing, 2016.

[79] N. Navab, T. Blum, L. Wang, A. Okur, and T. Wendler. First Deployments of Augmented Reality in Operating Rooms. *Computer*, 45(7):48–55, 2012.

[80] N. Navab, S.-M. Heining, and J. Traub. Camera Augmented Mobile C-Arm (CAMC): Calibration, Accuracy Study, and Clinical Applications. *IEEE Transactions on Medical Imaging*, 29(7):1412 –1423, july 2010.

[81] S. Nilsson and B. Johansson. Fun and usable: augmented reality instructions in a hospital setting. In *Proceedings of the 19th Australasian conference on Computer-Human Interaction: Entertaining User Interfaces*, OZCHI '07, pages 123–130, New York, NY, USA, 2007. ACM.

[82] J. Norman and H. Chheda. Minimally invasive parathyroidectomy facilitated by intraoperative nuclear mapping. *Surgery*, 122(6):998–1004, Dec. 1997.

[83] A. Okur, S.-A. Ahmadi, A. Bigdelou, T. Wendler, and N. Navab. MR in OR: First analysis of AR/VR visualization in 100 intra-operative Freehand SPECT acquisitions.

In *Proceedings of the 10th IEEE International Symposium on Mixed and Augmented Reality (ISMAR)*, pages 211–218, Basel, Switzerland, October 2011.

[84] A. Okur, C. Hennersperger, B. Runyan, J. Gardiazabal, M. Keicher, S. Paepke, T. Wendler, and N. Navab. fhSPECT-US Guided Needle Biopsy of Sentinel Lymph Nodes in the Axilla: Is it Feasible? In *Medical Image Computing and Computer-Assisted Intervention - MICCAI 2014*, volume 8673 of *Lecture Notes in Computer Science*, pages 577–584. Springer International Publishing, 2014.

[85] A. Okur, D. I. Shakir, P. Matthies, A. Hartl, S. I. Ziegler, M. Essler, T. Lasser, and N. Navab. Freehand tomographic nuclear imaging using tracked high-energy gamma probes. In *Bildverarbeitung für die Medizin 2013*, Informatik aktuell, pages 362–367. Springer Berlin Heidelberg, 2013.

[86] A. Okur, R. Voigt, R. Stauder, and N. Navab. Investigation of performance log files of freehand SPECT acquisitions for usage characteristics and surgical phase determination. In G.-Z. Yang and A. Darzi, editors, *The Hamlyn Symposium on Medical Robotics: Proceedings*, 2014.

[87] G. Papagiannakis, G. Singh, and N. Magnenat-Thalmann. A survey of mobile and wireless technologies for augmented reality systems. *Computer Animation and Virtual Worlds*, 19(1):3–22, 2008.

[88] B. Pouw, L. J. de Wit-van der Veen, M. P. M. Stokkel, C. E. Loo, M.-J. T. F. D. Vrancken Peeters, and R. A. Valdés Olmos. Heading toward radioactive seed localization in non-palpable breast cancer surgery? A meta-analysis. *Journal of Surgical Oncology*, 111(2):185–191, Feb. 2015.

[89] B. Pouw, M.-J. T. F. D. Vrancken Peeters, and R. A. Valdés Olmos. Radioguided Surgery of Non-palpable Breast Lesions: Radio Occult Lesion Localization (ROLL). In K. Herrmann, O. E. Nieweg, and S. P. Povoski, editors, *Radioguided Surgery: Current Applications and Innovative Directions in Clinical Practice*, pages 139–148. Springer International Publishing, 2016.

[90] S. P. Povoski. The history of radioguided surgery: Early historical milestones and the development of later innovative clinical applications. In K. Herrmann, O. E. Nieweg, and S. P. Povoski, editors, *Radioguided Surgery: Current Applications and Innovative Directions in Clinical Practice*, chapter 1, pages 3–12. Springer International Publishing, 2016.

[91] S. P. Povoski, R. L. Neff, C. M. Mojzisik, D. M. O'Malley, G. H. Hinkle, N. C. Hall, D. A. Murrey, M. V. Knopp, and E. W. Martin. A comprehensive overview of radioguided surgery using gamma detection probe technology. *World Journal of Surgical Oncology*, 7:11, Jan. 2009.

[92] L. Schwarz, A. Bigdelou, and N. Navab. Learning Gestures for Customizable Human-Computer Interaction in the Operating Room. In *International Conference on Medical Image Computing and Computer Assisted Intervention (MICCAI)*, 2011. To appear.

[93] F. Scopinaro and A. Soluri. Gamma Ray Imaging Probes for Radioguided Surgery and Site-Directed Biopsy. In G. Mariani, A. E. Giuliano, and H. W. Strauss, editors, *Radioguided Surgery: A Comprehensive Team Approach*, pages 29–36. Springer New York, New York, NY, 2008.

[94] B. Selverstone, W. H. Sweet, and C. V. Robinson. The clinical use of radioactive phosphorus in the surgery of brain tumors. *Annals of Surgery*, 130(4):643, 1949.

[95] D. I. Shakir. *Intra-operative Nuclear Imaging Based on Positron-emitting Radiotracers*. Dissertation, Technische Universität München, München, 2014.

[96] D. I. Shakir, A. Okur, A. Hartl, P. Matthies, S. I. Ziegler, M. Essler, T. Lasser, and N. Navab. Towards intra-operative PET for head and neck cancer: Lymph node localization using high-energy probes. In *Medical Image Computing and Computer-Assisted Intervention – MICCAI 2012*, number 7510 in Lecture Notes in Computer Science, pages 430–437. Springer Berlin Heidelberg, 2012.

[97] L. A. Shepp and Y. Vardi. Maximum Likelihood Reconstruction for Emission Tomography. *IEEE Transactions on Medical Imaging*, 1(2):113–122, Oct. 1982.

[98] A. K. Shukla and U. Kumar. Positron emission tomography: An overview. *Journal of Medical Physics / Association of Medical Physicists of India*, 31(1):13–21, 2006.

[99] T. Sielhorst, M. Feuerstein, and N. Navab. Advanced Medical Displays: A Literature Review of Augmented Reality. *Journal of Display Technology*, 4(4):451–467, 2008.

[100] A. Soluri et al. Italian national research council (cnr). miniaturized gamma camera with very high spatial resolution. italian patent rm97a000233. april 23, 1997. *US patent*, 6(242):744.

[101] B. Sousa Santos, P. Dias, A. Pimentel, J.-W. Baggerman, C. Ferreira, S. Silva, and J. Madeira. Head-mounted display versus desktop for 3D navigation in virtual reality: a user study. *Multimedia Tools and Applications*, 41:161–181, 2009.

[102] A. V. Stolin, S. Majewski, R. R. Raylman, and P. Martone. Hand-Held SiPM-Based PET imagers for surgical applications. *Proc IEEE NSS-MIC*, Oct. 2011.

[103] V. E. Strong, J. Humm, P. Russo, A. Jungbluth, W. D. Wong, F. Daghighian, L. Old, Y. Fong, and S. M. Larson. A novel method to localize antibody-targeted cancer deposits intraoperatively using handheld pet beta and gamma probes. *Surgical Endoscopy*, 22(2):386–391, Feb 2008.

[104] Y. Sun, W. Wei, H.-W. Yang, and J.-L. Liu. Clinical usefulness of breast-specific gamma imaging as an adjunct modality to mammography for diagnosis of breast cancer: a systemic review and meta-analysis. *European Journal of Nuclear Medicine and Molecular Imaging*, 40(3):450–463, Nov. 2012.

[105] A. Testori, M. Rastrelli, E. De Fiori, J. Soteldo, P. Della Vigna, G. Trifirò, G. Mazzarol, L. L. Travaini, F. Verrecchia, E. L. Ratto, and M. Bellomi. Radio-guided ultrasound lymph node localization: feasibility of a new technique for localizing and excising nonpalpable lymph nodes ultrasound suspicious for melanoma metastases. *Melanoma Research*, 20(3):197–202, June 2010.

[106] J. A. Thie. *Nuclear Medicine Imaging: An Encyclopedic Dictionary*. Springer, 2012.

[107] R. G. Thomas, N. William John, and J. M. Delieu. Augmented Reality for Anatomical Education. *Journal of Visual Communication in Medicine*, 33(1):6–15, 2010.

[108] R. Y. Tsai and R. K. Lenz. A new technique for fully autonomous and efficient 3D robotics hand/eye calibration. *IEEE Transactions on Robotics and Automation*, 5(3):345–358, 1989.

[109] C. S. Ubhi, J. G. Hardy, and C. A. S. Pegg. Mediastinal parathyroid adenoma: A new method of localization. *British Journal of Surgery*, 71(11):859–860, 1984.

[110] H. G. van der Poel, T. Buckle, O. R. Brouwer, R. A. Valdés Olmos, and F. W. B. van Leeuwen. Intraoperative Laparoscopic Fluorescence Guidance to the Sentinel Lymph Node in Prostate Cancer Patients: Clinical Proof of Concept of an Integrated Functional Imaging Approach Using a Multimodal Tracer. *European Urology*, 60(4):826–833, Oct. 2011.

[111] C. Vetter, T. Lasser, A. Okur, and N. Navab. 1D-3D Registration for Intra-operative Nuclear Imaging in Radio-guided Surgery. *IEEE Transactions on Medical Imaging*, 34:608–617, Feb 2015.

[112] S. Vidal-Sicart and R. Valdés Olmos. Sentinel node mapping for breast cancer: Current situation. *Journal of Oncology*, 2012:e361341, Aug. 2012.

[113] J. Vogel, T. Lasser, J. Gardiazabal, and N. Navab. Trajectory optimization for intra-operative nuclear tomographic imaging. *Medical Image Analysis*, 17(7):723–731, Oct. 2013.

[114] L. Wang, J. Landes, S. Weidert, T. Blum, A. Von Der Heide, E. Euler, and N. Navab. First animal cadaver study for interlocking of intramedullary nails under camera augmented mobile c-arm: a surgical workflow based preclinical evaluation. In *Proceedings of the First international conference on Information processing in computer-assisted interventions*, IPCAI'10, pages 56–66, Berlin, Heidelberg, 2010. Springer-Verlag.

[115] L. Wang, S. Weidert, J. Traub, S. M. Heining, C. Riquarts, E. Euler, and N. Navab. Camera Augmented Mobile C-arm: Towards Real Patient Study. In *Proceedings of Bildverarbeitung fuer die Medizin (BVM 2009)*, Heidelberg, Germany, March 2009.

[116] S. Weidert, L. Wang, J. Landes, A. Heide, N. Navab, and E. Euler. First Surgical Procedures under Camera-Augmented Mobile C-arm (CamC) guidance. In *The 3rd Hamlyn Symposium for Medical Robotics*, 2010.

[117] T. Wendler, U. Eberlein, and M. Lassmann. Physics of radioguided surgery: Basic principles and methods of radiation detection. In K. Herrmann, O. E. Nieweg, and S. P. Povoski, editors, *Radioguided Surgery: Current Applications and Innovative Directions in Clinical Practice*, chapter 2, pages 15–33. Springer International Publishing, 2016.

[118] T. Wendler, M. Feuerstein, J. Traub, T. Lasser, J. Vogel, F. Daghighian, S. I. Ziegler, and N. Navab. Real-time fusion of ultrasound and gamma probe for navigated localization of liver metastases. In N. Ayache, S. Ourselin, and A. Maeder, editors, *Medical Image Computing and Computer-Assisted Intervention – MICCAI 2007*, pages 252–260, Berlin, Heidelberg, 2007. Springer Berlin Heidelberg.

[119] T. Wendler, A. Hartl, T. Lasser, J. Traub, F. Daghighian, S. I. Ziegler, and N. Navab. Towards intra-operative 3d nuclear imaging: Reconstruction of 3d radioactive distri-

butions using tracked gamma probes. In N. Ayache, S. Ourselin, and A. Maeder, editors, *Medical Image Computing and Computer-Assisted Intervention – MICCAI 2007*, pages 909–917, Berlin, Heidelberg, 2007. Springer Berlin Heidelberg.

[120] T. Wendler, K. Herrmann, A. Schnelzer, T. Lasser, J. Traub, O. Kutter, A. Ehlerding, K. Scheidhauer, T. Schuster, M. Kiechle, M. Schwaiger, N. Navab, S. I. Ziegler, and A. K. Buck. First demonstration of 3-D lymphatic mapping in breast cancer using freehand SPECT. *European Journal of Nuclear Medicine and Molecular Imaging*, 37(8):1452–1461, Aug. 2010.

[121] T. Wendler Vidal. *3D intraoperative functional imaging with navigated probes*. Dissertation, Technische Universität München, München, 2010.

[122] D. Yu, J. S. Jin, S. Luo, W. Lai, and Q. Huang. A Useful Visualization Technique: A Literature Review for Augmented Reality and its Application, limitation & future direction. In *Visual Information Communication*, pages 311–337. Springer US, 2010.

[123] F. Zhou, H.-L. Duh, and M. Billinghurst. Trends in augmented reality tracking, interaction and display: A review of ten years of ISMAR. In *Mixed and Augmented Reality, 2008. ISMAR 2008. 7th IEEE/ACM International Symposium on*, pages 193 –202, sept. 2008.

APPENDIX A

Glossary

Activity. Parameter used to quantify radioactivity and represents radioactive source transformations per unit time for the source. Commonly used units are *becquerel* (SI) and *curie*. [106]

Annihilation. Radiation produced by the collision and annihilation of a particle and its antiparticle, especially the two 511 keV gamma ray *photons* travelling in opposite directions produced by the annihilation of a *positron* and an *electron*. [26]

Artifact. Any misleading or invalid feature in a reconstruction, which is actually not existing in the original imaged object.

Areola. A circular area of a different color, surrounding a central point, such as the pupil of the eye or the nipple of the breast. [26]

Atom. The smallest unit of matter that retains its properties. An atom consists of a nucleus, made up of *protons* and *neutrons*, surrounded by a number of *electrons*. [106]

Atomic number. The number of *protons* found in the nucleus of an *atom*, which uniquely identifies a chemical element. Also called *proton number*.

Axilla. Medical term for the human body part beneath the junction of the arm and shoulder, the armpit.

Becquerel. The SI unit of *activity* of a radionuclide per second (symbol Bq). Becquerel is now preferred over the historically used *curie* (1 Ci = 3.7 $\times$ 10^{10} Bq.) [106]

Beta particle. *Electron* or *positron* upon its emission from an *atom*. Beams of these are called beta rays. [106]

Brachytherapy. Radiation treatment of a patient using sealed or unsealed sources of radiation placed within the patient's body. [1]

Clearance. Used synonymously with washout, the process of a tracer leaving a tissue over time. [106]

Collimator. A diaphragm or system of diaphragms made of an absorbing material, designed to define and restrict the dimensions and direction of a beam of radiation. [26]

Controlled area. A defined area in which specific protection measures and safety provisions are required for controlling normal exposures or preventing the spread of contamination during normal working conditions, and preventing or limiting the extent of potential exposures. [1]

Crystal. A homogeneous angular solid formed from a chemical element, compound, or isomorphous mixture, having a definite form in which the ultimate units from which it is built up are systematically arranged. [26]

Curie. A non-SI unit of radioactivity (symbol Ci), defined as 3.7 $\times$ 10^{10} atomic disintegrations or other nuclear transformations per second (1/s). One curie is equal to 37 gigabecquerels (GBq). [106]

Decay. Disintegration of the nucleus of an unstable nuclide by the spontaneous emission of charged particles and/or photons; called also radioactive disintegration. [26]

DICOM. Digital Imaging and Communications in Medicine (DICOM) is a comprehensive set of standards for communications between medical imaging devices, including handling, storing and transmitting information in medical imaging. It includes a file format definition and a network communication protocol. The acronym DICOM represents digital imaging and communications in medicine. Patient information, device settings and data

acquisition details may also be permanently associated with the image as part of its file header. [106]

Dose. A quantity of an agent administered, taken or absorbed at one time. [106]

Dose limit. The value of the *effective dose* or the *equivalent dose* to individuals from planned exposure situations that shall not be exceeded. [1]

Dosimeter. In radiology, an instrument used to detect and measure exposure to radiation of either personnel or radiotherapy patients. [26]

Electron volt. The energy associated when an electron moves through an electrical potential of 1 V in a vacuum. It is equivalent to $1.602 \times 10^{-19} J$. Traditionally in nuclear physics, this unit is used to quantify the energy of single individual particles of various types of radiation. Acronym is eV. [106]

Energy. The capacity of a physical system to do work. For types of radiation encountered in imaging, energy signifies their ability to exert a force over a distance as they pass through and interact with matter. A fundamental concept of energy is its being describable by the product of a measure of force and a measure of distance. The SI unit for energy is joule. *Photons* and particles of radiation have an associated energy. For these it is common to employ the unit *electron volt*. [106]

Gantry. A spanning framework used to support machinery. In SPECT, the gantry supports the moving gamma camera. For PET, the gantry houses the detectors. [106]

Geiger-Müller counter. A radiation counter that uses a gas-filled tube to indicate the presence of ionizing particles; the type and energy of a particle cannot be determined because the degree of ionization produced is independent of them. [26]

Gray. The special name for the SI unit of absorbed dose: 1 Gy = 1 J/kg. [1]

Half-life. The time required for a substance to lose half of its initial pharmacologic, physiologic or radiologic value. [106]

Injected dose. The *activity* of a tracer injected at the beginning of a scan. Units are Bq and Ci. [106]

International System of Units. The modern form of the metric system, and is the most widely used system of measurement (abbreviated as SI), which comprises a coherent system of units of measurement built on seven base units (meter, kilogram, second, ampere, kelvin, mole, candela).

Intratumoral. Within a tumor.

JPEG. A commonly used digital file format for compressing images. It is named after the Joint Photographic Experts Group, creator of the format.

Neoadjuvant therapy. In combined modality therapy for cancer, initial use of one modality, such as chemotherapy or radiotherapy, to decrease the tumor burden prior to treatment by another modality, usually surgery. [26]

Neutrino. An elementary particle that has no electric charge and no mass, and that very rarely reacts with matter; it is a product of beta decay. [26].

Occult. Hidden, not revealed; in oncology: not detectable by clinical methods alone.

Periareolar. Around the areola.

Peritumoral. Around a tumor.

Phantom. A specially designed object that is imaged or scanned in the field of medical imaging for the evaluation and performance tuning of imaging devices.

Photon. The smallest observable single packet of light or other electromagnetic radiation, generally considered to be a discrete particle carrying energy proportional to the radiation frequency but having no mass or charge. [106]

Poisson distribution. A distribution function describing probabilities of the occurrences of a selected number of independently random events in a chosen time or space domain interval. The standard deviation of a Poisson process is expected to be the square root of the average number of events occurring in the given interval. [106]

Positron. Positive beta particle. It is the antiparticle of the *electron*, having the same mass but being positively rather negatively charged. Unlike the electron, it is not a naturally occurring particle, it appears sometimes in disintegrations of radioisotopes and its existence is short-lived because it collides with an electron found throughout matter resulting in mutual *annihilation* and concurrent emission of a pair of 511-keV *photons*. [106]

Post-excision. After the excision (surgical removal) of the targeted human tissue (e.g. tumor or sentinel lymph node).

Pre-incision. Before the surgical incision, meaning before the start of the surgical act.

Projection. Detector data acquired from a specified direction in respect to the object. It represents a view from a certain direction. [106]

Radiation weighting factor. A dimensionless factor by which the organ or tissue absorbed dose is multiplied to reflect the higher biological effectiveness of high radiations compared with low radiations. It is used to derive the equivalent dose from the absorbed dose averaged over a tissue or organ. [1]

Reconstruction. The process of generating an image from the raw detector data, or set of unprocessed measurements, made by an imaging system. [106]

Scintigram. The graphic record obtained by *scintigraphy*. [26]

Scintigraphy. The production of two-dimensional images of the distribution of radioactivity in tissues after the internal administration of radionuclide, the images being obtained by a scintillation camera. [26]

Scintillation crystal. A substance that emits a flash of light when contacted by high-energy particles, such as alpha, beta, or gamma rays. [26]

Sievert. The special name for the SI unit of equivalent dose, effective dose, and operational dose quantities. The unit is joule per kilogram (1 Sv = 1 J/kg). [1]

Sternum. Medical term for the breastbone, a long flat bone located in the center of the chest.

Subdermal. Just below the skin.

Tissue weighting factor. The factor by which the equivalent dose in a tissue or organ T is weighted to represent the relative contribution of that tissue or organ to the total health detriment resulting from uniform irradiation of the body. It is weighted such that their sum equals to 1. [1]

Unix time. The number of seconds that have elapsed since 00:00:00 Thursday, 1 January 1970, Coordinated Universal Time (UTC), minus leap seconds.

UTC. Coordinated Universal Time (abbreviated to UTC) is the primary time standard by which the world regulates clocks and time. It is within about 1 second of mean solar time at 0° longitude and is not adjusted for daylight saving time.

Uptake. The absorption of some substance (e.g. radiotracer) by tissue and its permanent or temporary retention. [106]

Voxel. The unit used for the discretization of the 3D space for reconstruction, similar to pixel in 2D.

APPENDIX B

Acronyms

2D Two Dimensional

3D Three Dimensional

ALE Average Localization Error

ALND Axillary Lymph Node Dissection

AR Augmented Reality

Bq Becquerel

BSGI Breast Specific Gamma Imaging

CAD Computer-aided design

CE Conformité Européenne, meaning European Conformity

Ci Curie

cps Counts per second

cpm Counts per minute

CT Computed Tomography

DICOM Digital Imaging and Communications in Medicine

EEA European Economic Area

EM Electromagnetic

EU European Union

eV Electron Volt

FDA Food and Drug Administration, United States

FDG ^{18}F-FDG

FDGDS ^{18}F-FDG Directed Surgery

fhSPECT Freehand SPECT

FOV Field of view

fps Frame per Second

GB Gigabyte

GDPR General Data Protection Regulation

GHz Gigahertz

Gy Gray

HMD Head Mounted Display

ICG Indocyanine Green

IR Infrared

ICRP International Commission on Radiological Protection

keV kiloelectron Volt

LN Lymph Node

LMEM List-Mode Expectation Maximization

LUT Look up table

MARI Marking the Axillary Lymph Node with Radioactive Iodine Seeds

MB Megabyte

MBq Megabecquerel

MLEM Maximum Likelihood Expectation Maximization

MRI Magnetic Resonance Imaging

MR Mixed Reality

OP Optical

OR Operating Room

PACS Picture Archiving and Communication System

PC Personal Computer

PD Photodiode

PET Positron Emission Tomography

PMT Photomultiplier Tube

PSMA Prostate-Specific Membrane Antigen

RGB Red-Green-Blue

RGS Radioguided Surgery

RGSLNB Radioguided Sentinel Lymph Node Biopsy

RIGS Radioimmunoguided Surgery

RIME Radioguided Intraoperative Margins Evaluation

RMS Root Mean Square

ROLL Radioguided Occult Lesion Localization

RULL Radioguided Ultrasound Lymph Node Localization

RSL Radioguided Seed Localization

SI International System of Units

SiPM Silicon Photomultiplier

SLN Sentinel Lymph Node

SLNB Sentinel Lymph Node Biopsy

SNOLL Sentinel Node Occult Lesion Localization

SPECT Single-Photon Emission Computed Tomography

Sv Sievert

UI User Interface

US Ultrasound

USB Universal Serial Bus

UTC Coordinated Universal Time

UV Ultraviolet

VOI Volume of interest

VR Virtual Reality

WGL Wire Guided Localization

XML eXtensible Mark-up Language

APPENDIX C

List of Publications

C.1. Journal Articles

[1] C. Vetter, T. Lasser, **A. Okur**, and N. Navab. 1D-3D Registration for Intra-operative Nuclear Imaging in Radio-guided Surgery. *IEEE Transactions on Medical Imaging*, 34:608–617, Feb 2015.

[2] P. Matthies, J. Gardiazabal, **A. Okur**, J. Vogel, T. Lasser, and N. Navab. Mini gamma cameras for intra-operative nuclear tomographic reconstruction. *Medical Image Analysis*, 18(8):1329 – 1336, 2014. Special Issue on the 2013 Conference on Medical Image Computing and Computer Assisted Intervention.

[3] N. Navab, T. Blum, L. Wang, **A. Okur**, and T. Wendler. First deployments of augmented reality in operating rooms. *Computer*, 99:48–55, 2012.

C.2. Conference Full Papers

[1] **A. Okur**, C. Hennersperger, B. Runyan, J. Gardiazabal, M. Keicher, S. Paepke, T. Wendler, and N. Navab. fhSPECT-US Guided Needle Biopsy of Sentinel Lymph Nodes in the Axilla: Is it Feasible? In *Medical Image Computing and Computer-Assisted Intervention - MICCAI 2014*, volume 8673 of *Lecture Notes in Computer Science*, pages 577–584. Springer International Publishing, 2014.

[2] R. Stauder, **A. Okur**, L. Peter, A. Schneider, M. Kranzfelder, H. Feussner, and N. Navab. Random Forests for Phase Detection in Surgical Workflow Analysis. In *The 5th International Conference on Information Processing in Computer-Assisted Interventions (IPCAI)*, Fukuoka, Japan, June 2014.

[3] J. Gardiazabal, M. Esposito, P. Matthies, **A. Okur**, J. Vogel, S. Kraft, B. Frisch, T. Lasser, and N. Navab. Towards Personalized Interventional SPECT-CT Imaging. In *Medical Image Computing and Computer-Assisted Intervention - MICCAI 2014*, volume 8673 of *Lecture Notes in Computer Science*, pages 504–511. Springer International Publishing, 2014.

[4] **A. Okur**, D. I. Shakir, P. Matthies, A. Hartl, S. I. Ziegler, M. Essler, T. Lasser, and N. Navab. Freehand tomographic nuclear imaging using tracked high-energy gamma probes. In *Bildverarbeitung für die Medizin 2013*, Informatik aktuell, pages 362–367. Springer Berlin Heidelberg, 2013.

[5] P. Matthies, **A. Okur**, T. Wendler, N. Navab, and M. Friebe. Combination of intra-operative freehand SPECT imaging with MR images for guidance and navigation. In *Engineering in Medicine and Biology Society (EMBC), 2013 35th Annual International Conference of the IEEE*, pages 3383–3386, 2013.

[6] P. Matthies, K. Sharma, **A. Okur**, J. Gardiazabal, J. Vogel, T. Lasser, and N. Navab. First Use of Mini Gamma Cameras for Intra-operative Robotic SPECT Reconstruction. In *Medical Image Computing and Computer-Assisted Intervention – MICCAI 2013*, volume 8149 of *Lecture Notes in Computer Science*, pages 163–170. Springer Berlin Heidelberg, 2013.

[7] J. Gardiazabal, T. Reichl, **A. Okur**, T. Lasser, and N. Navab. First flexible robotic intra-operative nuclear imaging for image-guided surgery. In *Proceedings of the 4th international conference on Information Processing in Computer-Assisted Interventions*, IPCAI'13, pages 81–90, Berlin, Heidelberg, 2013. Springer-Verlag.

[8] D. I. Shakir, **A. Okur**, A. Hartl, P. Matthies, S. I. Ziegler, M. Essler, T. Lasser, and N. Navab. Towards intra-operative PET for head and neck cancer: Lymph node localization using high-energy probes. In *Medical Image Computing and Computer-Assisted Intervention – MICCAI 2012*, number 7510 in Lecture Notes in Computer Science, pages 430–437. Springer Berlin Heidelberg, 2012.

[9] A. Bigdelou, **A. Okur**, M.-E. Hoffmann, B. Azizi, and N. Navab. Towards Systematic Usability Evaluations for the OR: An Introduction to OR-Use Framework. In *Information Processing in Computer-Assisted Interventions*, volume 7330 of *Lecture Notes in Computer Science*, pages 146–156. Springer Berlin / Heidelberg, 2012.

[10] A. Bigdelou, R. Stauder, T. Benz, **A. Okur**, T. Blum, R. Ghotbi, and N. Navab. HCI Design in the OR: A Gesturing Case-study. In *MICCAI Workshop on Modeling and Monitoring of Computer Assisted Interventions (M2CAI)*, Nice, France, October 2012.

[11] **A. Okur**, S.-A. Ahmadi, A. Bigdelou, T. Wendler, and N. Navab. MR in OR: First analysis of AR/VR visualization in 100 intra-operative Freehand SPECT acquisitions. In *Proceedings of the 10th International Symposium on Mixed and Augmented Reality (ISMAR)*, pages 211–218, Basel, Switzerland, October 2011.

C.3. Conference Short Papers

[1] **A. Okur**, R. Voigt, R. Stauder, and N. Navab. Investigation of performance log files of freehand SPECT acquisitions for usage characteristics and surgical phase determination. In G.-Z. Yang and A. Darzi, editors, *The Hamlyn Symposium on Medical Robotics: Proceedings*, 2014.

[2] R. Stauder, **A. Okur**, and N. Navab. Detecting and analyzing the surgical workflow to aid human and robotic scrub nurses. In G.-Z. Yang and A. Darzi, editors, *The Hamlyn Symposium on Medical Robotics: Proceedings*, 2014.

[3] P. Matthies, J. Gardiazabal, **A. Okur**, T. Lasser, and N. Navab. Accuracy evaluation of interventional nuclear tomographic reconstruction using mini gamma cameras. In G.-Z. Yang and A. Darzi, editors, *The Hamlyn Symposium on Medical Robotics: Proceedings*, 2014.

C.4. Editorials

[1] N. Navab, **A. Okur**, and R. Stauder. IJCARS MICCAI 2015 Special Issue. *International Journal of Computer Assisted Radiology and Surgery*, 11(9):1559, 2016.

C.5. Clinical Journal Articles

[1] T. Maurer, G. Weirich, M. Schottelius, M. Weineisen, B. Frisch, **A. Okur**, H. Kübler, M. Thalgott, N. Navab, M. Schwaiger, H.-J. Wester, J. E. Gschwend, and M. Eiber. Prostate-specific Membrane Antigen-Radioguided Surgery for Metastatic Lymph Nodes in Prostate Cancer. *European Urology*, 68(3):530–534, 2015.

[2] A. L. Mihaljevic, A. Rieger, B. Belloni, R. Hein, **A. Okur**, K. Scheidhauer, T. Schuster, H. Friess, and M. E. Martignoni. Transferring innovative freehand SPECT to the operating room: First experiences with sentinel lymph node biopsy in malignant melanoma. *European Journal of Surgical Oncology (EJSO)*, 40(1):42–48, Jan. 2014.

[3] I. Einspieler, A. Novotny, **A. Okur**, M. Essler, and M. E. Martignoni. First experience with image-guided resection of paraganglioma. *Clinical Nuclear Medicine August 2014*, 39(8), 2014.

[4] C. Blümel, A. Schnelzer, **A. Okur**, A. Ehlerding, S. Paepke, K. Scheidhauer, and M. Kiechle. Freehand SPECT for image-guided sentinel lymph node biopsy in breast cancer. *European Journal of Nuclear Medicine and Molecular Imaging (EJNMMI)*, 40(11):1656–1661, 2013.

[5] A. Schnelzer, A. Ehlerding, C. Blümel, **A. Okur**, K. Scheidhauer, S. Paepke, and M. Kiechle. Showcase of intraoperative 3D imaging of the sentinel lymph node in a breast cancer patient using the new freehand SPECT technology. *Breast Care*, 7(6):484–486, 2012.

[6] A. Rieger, J. Säckl, B. Belloni, R. Hein, **A. Okur**, K. Scheidhauer, T. Wendler, J. Traub, H. Friess, and M. Martignoni. First experiences with navigated Radio-Guided surgery using freehand SPECT. *Case Reports in Oncology*, 4:420–425, 2011.

C.6. Clinical Abstracts

[1] T. Maurer, M. Weineisen, H.-J. Wester, M. Schottelius, **A. Okur**, G. Weirich, H. Kübler, M. Schwaiger, J. E. Gschwend, B. Frisch, and M. Eiber. PSMA-radioguided surgery: Introducing molecular surgery in patients with recurrent prostate cancer. *The Journal of Urology*, 193(4S):e1040–e1041, 2015.

[2] T. Maurer, M. Weineisen, H.-J. Wester, M. Schottelius, **A. Okur**, G. Weirich, H. Kübler, M. Schwaiger, J. Gschwend, B. Frisch, and M. Eiber. Introduction of PSMA-radioguided surgery in patients with recurrent prostate cancer: Taking salvage lymphadenectomy to the next level? *European Urology Supplements*, 2(14):e675, 2015.

[3] B. Frisch, T. Maurer, **A. Okur**, M. Weineisen, M. Schottelius, H. Kübler, N. Navab, H. Wester, M. Schwaiger, and M. Eiber. Freehand SPECT for 111In-PSMA-I&T radioguided lymphadenectomy in prostate cancer patients. *Journal of Nuclear Medicine*, 56(Supplement 3):157–157, 2015.

[4] **A. Okur**, C. Gerngroß, A. Schnelzer, A. Ehlerding, M. Keicher, S. Wiesner, S. Paepke, K. Scheidhauer, and T. Wendler. First experience with fused ultrasound / freehand SPECT system for hybrid lymphatic mapping in breast cancer patients. In *52. Jahrestagung der Deutschen Gesellschaft fuer Nuklearmedizin*, March 2014.

[5] T. Maurer, G. Weirich, M. Weineisen, H. Wester, M. Schottelius, B. Frisch, **A. Okur**, H. Kübler, M. Schwaiger, J. Gschwend, and M. Eiber. Initial experience with PSMA-radioguided surgery in prostate cancer patients. *European Urology Supplements*, 13(5):170–171, 2014.

[6] M. E. Martignoni, A. Rieger, J. Saeckl, R. Hein, **A. Okur**, T. Wendler, K. Scheidhauer, T. Schuster, and H. Friess. Transferring innovative freehand SPECT to the operating room - First experiences with sentinel lymphonodectomy in malignant melanoma. *European Journal of Surgical Oncology*, 38(9):760, Sept. 2012.

[7] I. Einspieler, **A. Okur**, A. R. Novotny, M. E. Martignoni, and K. Scheidhauer. Case Report - Image-guided Resection of Paraganglioma. *European Journal of Surgical Oncology*, 38(9):866, Sept. 2012.

[8] C. Blümel, A. Schnelzer, A. Rieger, A. Ehlerding, **A. Okur**, C. Gerngroß, M. Martignoni, K. Scheidhauer, and M. Schwaiger. 3D navigated (radio-guided) sentinel

lymph node biopsy using freehand SPECT : final evaluation of Munich's pilot experience in the operating room. In *Abstracts der 50. DGN-Jahrestagung in Bremen*, page A51, Apr. 2012.

[9] **A. Okur**, C. Blümel, A. Ehlerding, K. Scheidhauer, and A. Schnelzer. Meme kanseri cerrahisinde freehandSPECT ile ilk tecrübe: Aksiller sentinel lenf nodu biyopsisinde üç boyutlu navigasyon ve kalite güvencesi. In *XI. Ulusal Meme Hastalıkları Kongresi, 2011*, Antalya, Turkey, October 2011.

[10] C. Lapa, J. Säckl, A. Rieger, C. Blümel, **A. Okur**, T. Wendler, M. Martignoni, and K. Scheidhauer. Investigating added value of freehand SPECT in sentinel node biopsy of melanomas. In *Proceedings of SNM 2011*, San Antonio, Texas, USA, Jun. 2011. Society of Nuclear Medicine.

[11] C. Blümel, A. Schnelzer, A. Ehlerding, **A. Okur**, K. Scheidhauer, M. Kiechle, and M. Schwaiger. Evaluation of freehand SPECT in sentinel lymph node biopsy of breast cancer. In *Proceedings of the EANM 2011*, Birmingham, UK, Oct. 2011. EANM.

[12] C. Blümel, A. Ehlerding, C. Lapa, **A. Okur**, T. Wendler, A. Schnelzer, and K. Scheidhauer. Improvements in sentinel node biopsy of breast cancer using freehand SPECT. In *Proceedings of SNM 2011*, San Antonio, Texas, USA, Jun. 2011. Society of Nuclear Medicine.

[13] M. C. Kreissl, **A. Okur**, M.-C. Chen, A. E. Bartel, T. Wendler, and K. Scheidhauer. Pilot study of freehand SPECT for lymphatic mapping in melanoma in upper body. In *Proceedings of SNM 2010*, volume 51 Supplement 2, page 1389, Salt Lake City, Utah, USA, Jun. 2010. Society of Nuclear Medicine.